FORCES ON A ROTARY TINE AERATOR UNDER NORMAL WORKING CONDITIONS

A Thesis Submitted to the

College of Graduate Studies and Research

in Partial Fulfilment of the Requirements

for a Degree of Masters of Science in the

Department of Agriculture and Bioresource Engineering

University of Saskatchewan

Saskatoon

By

Ryan Robert Georgison

Winter 2010

PERMISSION TO USE

In presenting this thesis in partial fulfilment of the requirements for a Postgraduate degree from the University of Saskatchewan, I agree that the Libraries of this University may make it freely available for inspection. I further agree that permission for copying of this thesis in any manner, in whole or in part, for scholarly purposes may be granted by the professor or professors who supervised my thesis work or, in their absence, by the Head of the Department or the Dean of the College in which my thesis work was done. It is understood that any copying or publication or use of this thesis or parts thereof for financial gain shall not be allowed without my written permission. It is also understood that due recognition shall be given to me and to the University of Saskatchewan in any scholarly use which may be made of any material in my thesis.

Requests for permission to copy or to make other use of material in this thesis in whole or part should be addressed to:

Head of the Department of Agricultural and Bioresource Engineering

University of Saskatchewan

Saskatoon, Saskatchewan, S7N 5A9

ABSTRACT

Emphasis on soil conservation in recent times has been brought about by the degradation of soils due to intensive tillage operations. A relatively new tillage philosophy, coined "conservation tillage", has opened up a new realm of tillage equipment design. The Rotary Tine Aerator (RTA) is new tillage tool that is starting to see commercial applications within the agriculture industry.

Being a new tillage tool, very little information has been gathered about the RTA and especially the variables that affect tool loading. For the purpose of improving the design of the soil engaging components of the RTA, an experiment was carried out investigating the effect various settings have on tool loading. A factorial experiment was set up with three factors and two levels. The variables examined were depth, velocity of the tool carriage and tine, and the tine gang angle, with soil density and moisture content maintained constant.

Draft and vertical forces on the frame were seen to increase with depth. Side loading on the bearing mounts was seen to be primarily affected by the angle of the tine gang, increasing as the gang angle increased. Tool shape was seen to affect the side loading of the bearing mounts causing the force to change directions when the tool was working and 20 cm depth and the tine gang was set a 0º. Forward velocity was not seen to be a significant factor affecting forces on the frame.

The loading in the X, Y and Z direction on the tine increased as depth increased from 10cm to 20 cm. A decrease in force on the tine in the X, Y and Z direction was seen with increasing tine velocity. It is suggested that an overlap in soil failure zones could be the cause of this relationship. Opening the gang angle from 0º to 10º increased

the force in the Z direction and decreased the force in the X direction. Tool shape was also seen to affect the direction of the load on the tine in the Z direction when the tine was tilling at a depth 20cm with a tine gang of 0º.

From the information gathered in this experiment, statistical models were developed for the loading on the tine and frame. The all possible regressors approach was used to formulate the statistical models. As each regressor was added, the new equation's fit was assessed using the coefficient of determination (R^2) and the sum of squared error (SSE). If there was a discrepancy as to whether an added regressor significantly contributed to the fit of the equation, a hypothesis test using the F-statistic was used to justify the regressors addition or removal. The models were then compared against the original data.

The models developed for the tine loading showed sufficient accuracy. The models for side loading of the bearing mounts and draft loading of the tool frame contained only one significant regressor. The lowest coefficient of correlation was R=0.63 for the model of side loading of the bearing mount. The statistical model for the vertical loading correlated well with the test data with a coefficient of correlation of R=0.95.

ACKNOWLEDGEMENTS

I would like to thank my family and friends for the encouragement and guidance throughout my life. I would like to thank my supervisor, Martin Roberge, for giving me the opportunity to read my Masters. I would like to thank the members of my graduate committee, Charles Maule and Trever Crowe, for the added support through this experience.

Special thanks to Ms. Toni Schleicher for her patience and assistance when setting up my instrumentation, and to the gentlemen in the machine shop, namely Henry Berg, for their expertise and advice when needed.

Finally, I would like to thank PMF Ltd. for the initial funding of this project and the Agricultural and Bioresource Department at the University of Saskatchewan for the use of their facilities.

TABLE OF CONTENTS

LIST OF FIGURES

LIST OF TABLES

CHAPTER 1: INTRODUCTION

The practice of tillage is about as old as agriculture itself and has changed dramatically over time. As our understanding of the soil medium and soil plant dynamics improves, the philosophies behind the design of tillage equipment changes.

Tillage is defined as the manipulation of soil for a desired purpose (ASAE 2005). The desired purpose, with respect to commercial agriculture, is to provide a suitable medium for plant growth. Variation in soil physical properties, such as density and particle size, affects germination and root growth directly (Guerif *et al*. 2001). As soil structure and density can be modified by tillage, tillage is an important component in commercial crop production.

Emphasis on soil conservation in recent times has been brought about by the degradation of soils due to intensive tillage operations. A new tillage philosophy, coined "conservation tillage", has opened up a new realm of tillage equipment design. The aim of conservation tillage tools is to modify the soil structure while minimising disturbance to the surface crop residue. Crop residue on the soil surface has been seen to help reduce soil erosion and conserve moisture (ANON 2002).

The Rotary Tine Aerator (RTA) is a tool that has been developed by various companies, most notably AerWay ® and HCC Inc., for the purpose of penetrating

compaction layers while minimizing crop residue disturbance. The unit uses rotating tines to cleave the soil to a depth of 20 cm (Figure 1.1). The vertical manner at which the RTA fractures the soil minimizes disturbance of the surface residue.

The RTA is also designed to be adjustable so that the aggressiveness of the tillage can be varied. The tine gang angle can be varied from zero to ten degrees in 2.5-degree increments, perpendicular to the direction of travel, causing more exposure of the broad flat side of the tine to the soil (Figure 1.1). Exposing the broad flat side of the tine increases the volume of soil displaced and creates some soil turning which has the effect of incorporating crop residue into the soil.

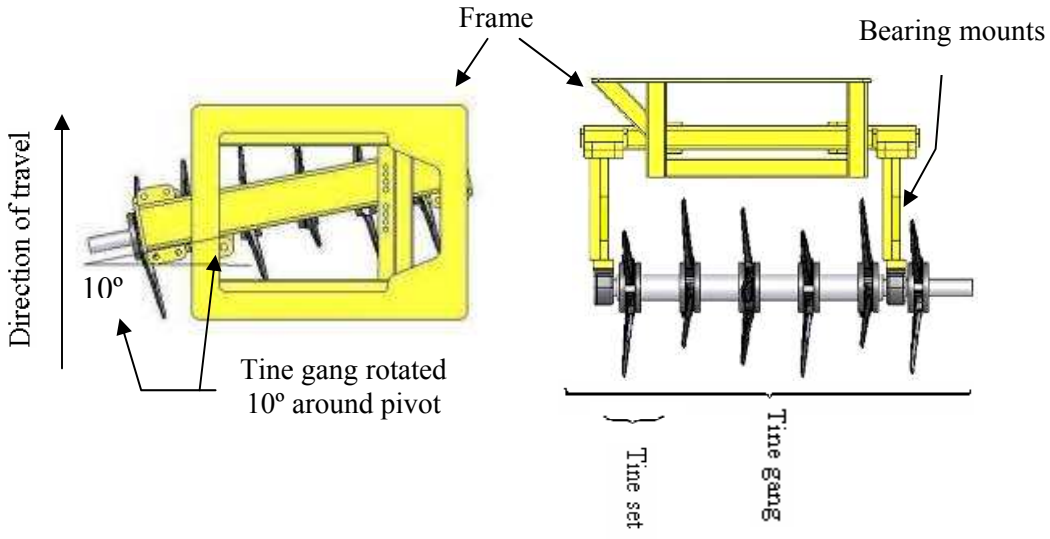

Figure 1.1: The RTA module used in the experiment, component naming conventions.

The tillage tool used in the experiment is a modular version of the production tool. The modular tools geometry and functionality is essentially the same as the production intent tool. To achieve the various widths required for the different markets, a number of tine gangs were used on a single frame. For example, PMF Inc. used two tine gangs for the 11ft version and four for the 22ft tillage tool.

Many studies have been carried out determining the agronomic benefits of the RTA in a range of agricultural applications. The original intention of the RTA was to rejuvenate perennial grass and alfalfa stands. Studies have been also carried out using the RTA in conjunction with a slurry application unit and recently as a pre-treatment in a novel seeding system coined “slurry-seeding”.

As the RTA is a relatively new tillage tool, research on the soil-tool interaction is limited. By carrying out a series of controlled tests, the loading of the tool frame and the soil engaging tine will be better understood. These forces will be analyzed as a function of velocity, tine depth and the attack angle of tine gang.

The objectives of this study are to; (1) measure the forces on the rotary tine aerator (RTA) while undergoing normal working conditions, and (2) develop a statistical model of the tool loading.

The variables of concern in the model are:

- tri-axial loading of the tine,
- side loading of the frame,
- vertical and draft forces on the frame,
- velocity of the tine and frame and
- the soil conditions.

CHAPTER 2: LITERATURE REVIEW

Tillage, as it applies to agriculture, has a long history and is constantly evolving along with our understanding of soil-plant dynamics and the soil ecosystem. As our needs change, so do our tools. The following sections will go through a brief history of tillage tools describing some of the classifications and changes in practices that have caused tillage tools to evolve. A background on the Rotary Tine Aerator, the tillage tool of focus in this study, will be given, outlining some of the literature published on the utilization of this tillage tool. Completing this chapter will be a discussion of the considerations made during the development of tillage tool models.

2.1 Tillage tool history, considerations and evolution

2.1.1 A brief history of tillage tools

Tillage is an ancient practice, with evidence dating back to 3000 B.C. in the valley of the Euphrates and Nile rivers. Early tillage tools were simple wooden tools used to perform initial break-up of the soil and cover up seed crops. Two thousand years ago, Romans and Chinese were using iron ploughs in combination with draft animals. Makeshift ploughs were also found in India; comprised of wedge-shaped hardwood blocks pulled by bullocks. However, modern-like mouldboard ploughs with cutting

coulters were not common until 1500 A.D. By the 1700s, tillage equipment similar to that which is used today began to appear (McKyes 1985).

Robert Ransome, in 1785, patented a cast-iron plough and, in 1803, a self-sharpening share. He also introduced standard parts that could be replaced in the field. In the 1830's, John Deere developed a steel one-piece share and mouldboard plough. In the 1860's, mechanized power in the form of steam engines began to replace draft animals. By 1892, draft power, in the form of the internal combustion engines, began replacing steam engines in the United States and in Europe soon after (McKyes 1985).

Tillage practices tend to vary from region to region and are almost cultural in practice. As technologies improved, tillage tools became more effective and specialized. Tillage is defined as the mechanical manipulation of soil for any desired purpose; however, in agriculture the term usually refers to the changing of soil conditions for the enhancement of crop production. Modern tillage tools are designed for a wide range of purposes such as improving the soil structure to provide a better seed bed and growing environment, burying weeds and weed seeds, managing crop residue and drying soil.

Tillage equipment is often grouped based on its function. Primary tillage equipment usually carries out the first pass and is designed for cutting and loosening the soil. This action is performed to a depth of 15 to 90 cm (McKyes 1985). Examples of primary tillage tools are mouldboard ploughs, chisel ploughs and subsoilers.

Secondary tillage tools are often used after the primary tillage equipment, usually for one or more passes. The aims of these tools are to improve seedbed levelness, structure, conserve moisture, bury weed seeds and crop residue (McKyes 1985).

In recent years, there has been much emphasis on soil conservation due to the degradation of soil fertility by intensive cultivation practices. Conservation tillage is defined as tillage operations that leave a minimum 30% of the soil surface covered in crop residue after planting. Therefore, conservation tillage does not necessarily mean "no" tillage. Certain regions prefer a certain level of tillage for the purpose of residue management and seed bed preparation. Conservation tillage has been adopted as a means of improving water conservation and the retention of organic matter, while reducing soil erosion. Additional benefits of conservation tillage include reduced fuel consumption, reduced compaction, planting and harvesting flexibility, reduced labour requirements, and improved soil tilth (ANON 2002).

Conservation tillage practices and tools are typically divided into three groups: zero till, strip tillage and vertical tillage. Zero-till practices attempt to minimize the total tillage operations with the attempt to maximize crop residue coverage. Strip tillage practices perform all tillage functions within a narrow band in which the seed will be placed, leaving the rest of the field untilled. Vertical tillage practices till the soil without inverting the soil, leaving much of the crop residue on the soil surface. Each tillage group within the conservation tillage family has resulted in very different tillage equipment for there application (Hayes 1985)

Zero tillage practices intent is to minimize the disturbance to the soil environment. Typically, the only time the soil is disturbed is during the seeding or planting of crops. The seeding and planting equipment is designed to manage high levels of crop residue during the planting process with the extensive use of disks and coulters. Some seeding

equipment manufactures have designed zero-till seeding equipment with narrow knife openers that require no disks or coulters to cut through crop residue (Hayes 1985).

Strip tillage practices perform all tillage functions within the narrow band in which the seed will be placed. The tillage operations usually disturbs about one-third of the distance between the rows. By maintaining undisturbed soil on two-thirds of the soil surface, strip tillage sees many of the benefits seen by zero tillage, such as moisture conservation and reduction in soil erosion. By tilling the seed bed and removing some of the crop residue from the soil surface around the seed row, strip tillage typically sees higher soil temperature earlier in the spring allowing for earlier seeding (Hayes 1985).

Vertical tillage practices modify the soil environment by tilling the soil in a way that maintains some level of crop residue on the soil surface and while burying the rest in the top eight to ten centimetres into the soil. This is typically done with the used of chisels and sweeps. Vertical tillage tools are used in areas that produce high levels of crop residue. By burying some of the crop residue, the crop residue breaks down quicker resulting in minimal residue build up; however, by maintaining some level of crop residue on the soil surface soil erosion is reduced (Hayes 1985).

2.1.2 Tillage, soil quality and plant growth

For healthy plant growth, a suitable soil medium is required. Tillage physically alters the soil environment directly affecting germination and root growth. The required soil environment for healthy plant growth is a complex multiphase environment which is sensitive to external influences.

When considering the structural change of soil due to tillage, it is important to make the distinction between textural and structural pores. Textural porosity results

from basic structure of the elementary particles (sand, silt and clay). Structural porosity consists of the voids formed by the arrangement of the aggregates and clods created during tillage, climatic and biological events. Structural pores largely determine the density of the soil because the pores between aggregates are much larger than the pore space between textural surfaces. Structural pores are critical in determining the rate of air and water movement through the soil. These structural pores are sensitive to soil management techniques such as tillage (Guerif *et al*. 2001).

Soil type and the moisture content of the soil during tillage affects the sizes of the fractured particles and distribution of soil aggregates. The size and organization of soil particles determines the soil-seed contact area. Contact surface area between the soil and seed determines the area in which the exchange of water, gas and nutrients will take place. A seed germinates when its water content reaches a critical level. By improving the transfer rates to the seed through the soil-seed contact area, by packing the soil in the immediate area around the seed, germination rates improve (Guerif *et al*. 2001).

Soil-root contact also encourages the transfer of water and nutrients to the root system. Compacted soil provides a high level of soil-root contact (Guerif *et al*. 2001); however, dense soils can impede root growth limiting the area to which the plant can extract water and nutrients. Furthermore, under drying conditions, the soil strength will typically increase, furthering the mechanical impedance of root growth through the soil (Bengough *et al*. 2006, Johnson and Bailey 2002). By aerating the soil, plant root systems are free to grow allowing for broader access to soil nutrients and water within the soil. Compaction usually occurs at the expense of structural pores resulting reduction in soil porosity. Decreased porosity limits the movement of air and water

within the soil limiting the availability of water and air solutes to the plant root system (Johnson and Bailey 2002).

2.1.3 Conservation tillage, crop residue and soil fertility

For tillage practices to be classified as conservation tillage, after planting, 30% of the soil surface is required to be covered in crop residue (ANON 2002). This minimum level of crop residue cover is important as it influences factors such as soil temperature, soil moisture content, erodability and the soil nutrient cycle.

Soil temperature is a major concern with producers as it has a direct effect on the rate of emergence and the final number of seedlings that emerge. Soil temperature is determined by two factors: available heat and heat transfer. Available heat is dependent on the radiant energy and the soil color. Heat transfer is dependent on the soil water content and the mulch from the crop residue (Lafond and Derksen 1995).

Crop residue has a strong involvement in water conservation. In the prairies, potential evaporation exceeds precipitation during the growing season. The layer of crop residue covering the soil helps to conserve moisture by trapping snow, improving water infiltration, reducing run-off and minimizing evaporation losses. By using management techniques that maximize surface residue, there is a potential to increase crop yield due to increases in available water (Lafond and Derksen 1995).

Maintaining a layer of crop residue on the soil surface has also been found to greatly reduce water erosion. Crop residue dissipates energy from water droplets and flowing water, reducing erosion. No-till plots have been shown to have lower concentrations of sediments in the runoff water when compared to the runoff collected

from conventionally tilled plots (King *et al*. 1995). A lower concentration of soil sediments in the runoff suggests that less soil erosion was taking place.

The placement of crop residue within the soil has an effect on the nutrient cycle. Buried residue decomposes faster because the residue is distributed over a larger area and is subject to high moisture contents. A study by Mrabet *et al*. (2001) comparing no-till systems to conventional tillage, found that organic carbon, total nitrogen, phosphorus and potassium were all found to be higher with the no-till system in the 0-70 mm depth range. The concentration of immobile nutrients such as potassium and phosphorus in surface layers was attributed to the elimination of soil mixing. Increases of organic carbon in no-till field plots were attributed to lower oxidation rates and less microbial activity acting on the residue due to minimized incorporation. Higher nitrogen levels within the 0-70 mm depth zone (seed zone) were attributed to the microbial biomass being near the surface, thus the nitrogen was less available for mineralization or leaching. The study concluded that by maintaining a crop residue on the surface of the soil, long term soil productivity can be improved.

The role of tillage in commercial agriculture is slowly changing as researchers identify the effects tillage has on soil-plant dynamics. As this understanding increases, tillage tools will change to meet the requirements sought out by the research and producers.

2.2 Previous research on the rotary tine aerator

2.2.1 Perennial grass and alfalfa rejuvenation

High levels of soil compaction may limit crop yields by restricting root growth and the movement of water and air through the soil. Forage harvesting and slurry spreading equipment with conventional tires (opposed to low ground pressure tires) have been shown to create deep soil compaction resulting in grass yield reductions. Animals treading on pasture lands can also cause shallow compaction, particularly in areas of high rainfall where intensive grazing systems are used, reducing forage yields (Fortune *et al.* 1999).

The traditional method of grassland rejuvenation has been to break the land and reseed (Malhi *et al*. 2000, Fortune *et al.* 1999). This method increases input costs and leaves the land out of production for a year. Aeration techniques have been used extensively to recondition sport turf grounds and have received some attention as a way to alleviate compaction in agricultural forage land in hope of improving yields.

Experiments have been carried out with varying compaction sources on perennial grass and pasture land to investigate the effects of aeration on grass yield. Davis *et al*. (1989) found a large improvement (approximately double) in forage yields in pasturelands in the United Kingdom. Davis *et al.* (1989) hypothesized that this was attributed to better drainage, increased surface for gas exchange, and increased mineralization of nitrogen from soil organic matter. Malhi *et al*. (2000) found no significant effect on yields in pasture land in five locations in Alberta, Canada.

Douglas *et al*. (1995) found that on forage lands south of Edinburgh, Scotland, subjected to compaction by conventional and reduced ground pressure forage

equipment, aeration increased the volume and number of macropores, but changes in yields due to aeration were insignificant. A study by Fortune *et al*. (1999) on forage land in Ireland concluded that routine aeration was unlikely to produce yield benefits and would not alleviate the effects of wheel compaction; however, stated that it may be beneficial where shallow compaction problems occur.

2.2.2 Slurry application

Mechanical aeration using a rotary tine aerator has been studied as a means of incorporating slurry manure into soil. Aeration causes increased depression storage and infiltration which would lead to the assumption of possible reduction in slurry runoff and a better nutrient distribution through the grass root zone when slurry was applied (Shah *et al*. 2004). Douglas *et al.* (1995) observed, while studying the effect aeration had on forage production, that the slots formed when the soil was aerated filled with slurry rapidly after slurry was applied.

Injection of slurry into grassland allows for greater access of available nutrients to the plants while reducing odour emissions and ammonia volatilization when compared to surface application (Chen *et al*. 2000). However, the soil disruption caused to the root zone by the injection tool can cause reductions in yields. As the RTA has been seen to be relatively benign, its application for the incorporation of liquid slurry has seen much interest.

Livestock manures are often used as a source of nutrients for perennial crops. Livestock operations which store liquid manure typically broadcast liquid manures over cropland using a splash plate applicator. Misselbrook *et al.* (2005) stated the main factors affecting ammonia volatilization from applied manure is dry matter content for

dairy manure and wind speed for both dairy and swine manure. The difference in effect moisture content had on swine and dairy manure was attributed to the difference in texture of the manures. Dairy manure tends to contain more fibrous material which increased the viscosity and water holding ability. Higher viscosity of dairy slurry may impede infiltration of the slurry into the soil leaving it exposed. Broadcast application of slurry coats the plant material, as well as the soil, in manure increasing the surface area exposed to the wind, which increases emissions. By reducing the surface area at which the manure is exposed, ammonia losses can be reduced.

The RTA has been studied in conjunction with a low pressure band applicator system for the application of slurry manures. This system has been compared to other injection systems such as the splash plate broadcast system, low pressure band applicators, and direct injection systems. Using the RTA in conjunction with the band applicator reduced ammonia losses by 70% when compared to splash plate broadcast application (Bittman *et al*. 2005). The reduction in ammonia losses was seen to be due to the application of the slurry below the crop canopy and the improved absorption due to the loosening and slotting of the soil (Bittman *et al.* 2005, Chen *et. al.* 2000).

The yield results, when using the RTA in conjunction with a manure application system, are mixed. Chen *et al.* (2000) found earlier yield response and increased grassland yields when liquid manure was incorporated using an RTA unit. Bittman *et al.* (2005) found an average grassland yield increase of 12.3% over the control when using the RTA unit in conjunction with a dribble bar applicator. However, Shah *et al.* (2004) found the RTA unit negatively impacted yields. When comparing the grassland yield of the plots that were aerated and applied with slurry and plots that were not

aerated, Shah *et al.* (2004) found over the three years of the study, a total forage yield reduction of 19%.

2.2.3 Slurry seeding and its application in the establishment of cover crops

Cover crops are crops that are grown outside of the normal cropping season to prevent soil degradation and nutrient loss. There also have been some additional benefits for growing cover crops such as weed suppression, carbon sequestration, and their use within an integrated pest management system (Dabney *et al*. 2001).

Despite the benefits of cover crops, their use in commercial agriculture has not been fully adopted. The establishment of winter cover crops competes for labour during harvest and use additional financial and management resources (Harrigan *et al.* 2007).

To alleviate some of the cost in establishing cover crops, Harrigan *et al*. (2007) combined the operation of slurry application with the seeding of the cover crops by mixing the seed in the slurry. The slurry application system used a RTA tillage tool with a dribble bar system in behind. The initial intent of the slurry-seeding method of seeding cover crops was to mimic a common method of seed distribution, via the digestion tract of grazing animals and subsequent deposition of the seeds in the feces. The tillage tool was used to create a fissure for the slurry to seep, and in doing so carrying the seed into a favorable environment for germination.

When comparing the crop potential of slurry-seeding to direct drilling, slurry seeding showed significant decreases in the number of plant stands. However, total biomass produced from the slurry-seeding was larger then the crops seeded with a direct drill. This was attributed to the total biomass per plant being up to six times larger in plots seeded using the slurry-seeding method compared to plots seeded by direct

drilling. Additional to the herbage yield benefits seen, there was also substantial reduction in the input costs of seeding the cover crops. When comparing to conventional seeding methods, there was a reduction in fuel usage of 18 liter ha^{-1} and a time savings of 0.85 h ha^{-1} (Harrigan *et al.* 2006).

2.3 Variables affecting soil-tool models

2.3.1 General tool model

When considering soil manipulation using tillage tools, there are a limited number of design factors such as: initial soil conditions, the shape of the tillage tool, and the manner of movement. These variables can be used to determine the forces on the tool and resultant soil condition. The forces and resultant soil conditions can be mathematically represented by two simplified equations:

$$F = f(T_S, T_M, S_i) \text{ and} \quad \textbf{[2.1]}$$

$$S_f = f(T_S, T_M, S_i), \quad \textbf{[2.2]}$$

where F is the forces on the tool to cause movement (draft), T_S is the tool shape, T_m is the manner of tool movement, S_i is the initial soil condition, S_f is the soil final condition. If F or S_f, along with T_S, T_m and S_i are known, then an empirical relationship can be derived from their values (Gill and Vanden Berg 1968).

2.3.2 Tool shape and tool movement

The shape of a tillage tool has received much attention from manufacturers as it is one of the few variables over which the designer has complete control. For example, optimizing tool geometry and the manner of tool movement with the intention of reducing the soil loading on the tool, while maintaining the desired final soil condition, will result in a more efficient tillage tool. Tillage tools are often used in a range of soil types, tool depths and tilling speeds, but the shape of the tool will remain the same during different operations (Gill and Vanden Berg 1968).

The manner in which a tool moves can be described by the tool's orientation, the path through the soil and its speed along this path (Gill and Vanden Berg 1968). Orientation relates the shape of a tool to its path through the soil. Orientation is important because it influences the performance of the tool (either the forces on the tool or final soil condition) as it relates tool shape with tool direction.

The path through the soil is often described based on a fixed coordinate system. For a rotating tool, the path of travel is relatively complex and difficult to describe mathematically. Three reference systems are needed to describe the path of motion of a rotary tillage tool: the earth reference system, the implement reference system with respect to the axis of the rotating tool and the tool shape reference system of which the motion of the tool shape is described (Gill and Vanden Berg 1968).

The final variable when describing manner of tool movement is speed. Speed of a tool is the velocity of the shape reference system of the tool along its path of motion (Gill and Vanden Berg 1968). Tool speed is a variable that has been a focus of much research as it can be readily changed. A study of narrow tines in a range of soil conditions by Stafford (1979) showed that soil forces on narrow tine tillage tools increased with forward velocity.

Describing tool shape is meaningless without describing tool movement; likewise tool movement is meaningless without a description of tool shape. To make effective use of a tool shape and manner movement, the shape and movement must be quantitatively related to forces and resultant final soil condition (Gill and Vanden Berg 1968).

2.3.3 Initial soil conditions

Soil is a complex medium that varies in strength dramatically as the soil type and working conditions change. Soil type is defined as the percentage of the component aggregates which make up the soil. The particulates are defined as sand, silt and clay. Particles sized between two millimetres and 0.05 mm are classified as sand, between 0.05 mm and 0.002 mm are classified as silt and particles, less then 0.002 mm are classified as clay (ASTM 1988). Sandy soils are often described as frictional soils. The large size of sand particles limits the effect that moisture content has on its strength. Clay soils, because of their fine particle size, vary widely in strength and volume as soil moisture content changes.

Onwualu and Watts (1998), in a study of draft and vertical forces on a tillage tool at various velocities noted that the soil type determined whether an increase in tool forces was linear (cohesive forces) or a squared relation (inertial forces) to tool velocity. Rosa and Wulfsohn (1999) stated that in sandy soils, inertial forces are predominant and thus there is a squared relationship with velocity. Clay soils are not as sensitive to inertial forces, thus the predominant increase in force was due to cohesive forces of the soil as velocity increased.

Soil type has also often been seen to affect the forces on tillage tools in an indirect manner. Stafford (1979) saw the moisture content was a major determinant in the mode of soil failure; however, soil type determined the range at which the mode of soil failure would change.

The moisture content has a dramatic effect on clay soil strength and thus draft force. In a tillage study by Stafford (1979) in clay soils, cohesion was found to increase

with moisture content to a peak between 26% and 30% and then decreased. It was suggested that the soil changed its mode of failure from brittle to plastic as it approached its plastic limit, reaching a maximum strength at a moisture content several percent below the plastic limit of the soil.

Similar results were seen by Sanchez-Giron *et al*. (2005) when studying openers in a range of moisture contents and densities. With incremental increases in moisture content from 60g kg^{-1} to 180 g kg^{-1}, there was a corresponding increase in vertical and draft forces.

Soil density has been shown to affect draft forces in many studies. Stafford (1979) saw small increases in draft force with increase of density. Sanchez-Giron *et al.* (2005) also saw increases in both vertical and draft forces with increases in soil density. These increases were further influenced by changes in moisture content.

When examining soil failure, it is evident that soil fails in different ways depending on the soil type, moisture content and rate of loading. In a study by Elijah and Weber (1971), soil was found to fail in four ways when cut by a flat cutting blade. The modes of failure were coined as shear, flow, bending and tensile. Their study observed shear-type failure in granular-brittle soils at low tool speeds. In similar soils, flow-type failure was seen at higher speeds or lower tool angles. Flow failure was seen in loose granular soils at all speeds. Bending-type failure was seen in high moisture clays. Bending-type failure was attributed to a soil that was tough enough not to fail in shear and plastic enough to deform without forming major tension cracks. Tension failure was seen in dry clay soils. Under tensile conditions, soil failed in large clods.

The transition of soil failure modes and moisture content was also observed by Rajaram and Gee-Clough (1988). In their study of a single soil-type, the moisture content (MC) was set at 5.2, 18.3, 28.6 and 42.0% dry basis (DB). When a vertical tine was forced through the soil at 5.2 % MC, the vertical and horizontal component of the loading had a cyclical loading pattern. Observed soil failure at the surface noticed a number of blocks of soil in front of the tool collapsing. At 18.3% MC, the period of the cyclical pattern of soil failure increased along with the vertical and horizontal forces. Maximum force was seen at 28.6% MC and the soil was seen to fail in a chip-forming manner. At 42.0% MC the soil flowed freely around the tine.

2.3.4 Previous work on rotating tillage tools

There has been much research on rotating tillage tools and especially powered rotary tillers. Powered rotary tillers have been the focus of much attention due to their use in areas where the traction is not reliably available for the uses of draft tillage equipment. Efforts were made to understand the soil tool relationship to reduce the high power requirements of powered rotary tillers (Thankur and Goodwin 1989).

In a series of papers by Hendrick and Gill (1971a, 1971b, 1971c, 1974, 1978) the design parameters were establish (citing many references from Asian researchers) identifying the effects of tilling direction, depth, peripheral and forward velocities, blade clearance angle and kinematics on power requirements and soil tilth. Thakur and Godwin (1989) reviewed the state of force prediction models of rotary powered tools during which they explained many empirical models. They also used it as a precursor to their work in developing a model of forces during soil cutting of blades based on Mohr-Coulomb soil mechanics.

Miszczak (2005) adapted the dimensional relationships developed for powered rotary tillage and passive tillage tools to develop a model of a passive rotary tillage tool, the rotary subsoiler (a tool much like a RTA). Miszczak (2005) stated that narrow working elements (tines) of passive rotary tillage tools, like a rotary subsoiler, act on the soil much like passive narrow static tines. Miszczak (2005) assumed the soil failure at any moment in the tool's rotation to be similar to the failure of narrow non-rotating tines. The model developed in the study for the rotary subsoiler incorporated the changing orientation of the tool, with respect to the direction of travel, with traditional soil cutting models of non-rotating narrow tines. Further consideration was taken to include the effect of overlapping soil failure zones caused by other tines. The model agreed well with the test results.

CHAPTER 3: METHODOLOGIES

In this chapter there will be an explanation of the design and function of the instrumentation used in the experiment and the calibration techniques. The standard procedures used to test the soil will be provided and briefly explained. The chapter will finish with an explanation of the design of the experiment and the statistical background that goes with it. The instrumentation measuring the forces on the tool can be broken down into two sections: instrumentation measuring the frame and bearing mount loading and instrumentation measuring the tine loading. All forces were measured using strain gage based instrumentation.

3.1 Materials

3.1.1 Instrumentation measuring forces on the frame

When considering the forces on the frame, the loading directions of interest were the draft, vertical and side loading of the bearing mounts (Figure 3.1). Draft loading was of interest as it will determine the power requirements needed to pull the implement in the field. The vertical loading on the frame was investigated as it determines the force required, in the case of the RTA, to keep the tool in the ground. The side loading of the bearing mounts was selected opposed to the side loading of the frame, because

the forces on the bearing mounts has a direct relationship with the loading on the tine gang bearings. As the tine gang rotates through 10º, the side forces on the frame might not be a true representation of the side loading on the tine gang bearings. The side loading of the bearings were of interest in this study as bearing failure is a possible mode of failure for the RTA. It is important to be aware that the side loading of the tine gang will vary from 0º to 10º, depending on the settings during the run, from the side load on the frame.

The RTA module, that was used to carry out the experiments, was mounted to the tool carriage that was part of the Terramechanics Rig (TMR) at the Agricultural and Bioresource Engineering Department at the University of Saskatchewan (Figure 3.1). The Terramechanics Rig is a large soil bin, which has a hydraulically driven tool carriage mounted to it. This tool carriage is designed to allow for the mounting of a range of soil engaging tools. The tool carriage also allows for the variation in the depth of soil engagement and velocity of tool being studied.

Figure 3.1: Terramechanics rig without RTA mounted.

Two of the three principal forces on the RTA tool frame, draft and vertical, (Figure 3.2) were measured using elongated octagonal ring (EOR) dynamometers that were built into the tool carriage (Figure 3.3). The EOR dynamometers are specially machined support devices which are instrumented in a way that the forces in two directions are independently measured with minimal crosstalk. The side forces on the bearing mounts were measured via strain gages mounted directly to the RTA module's frame (Figure 3.4).

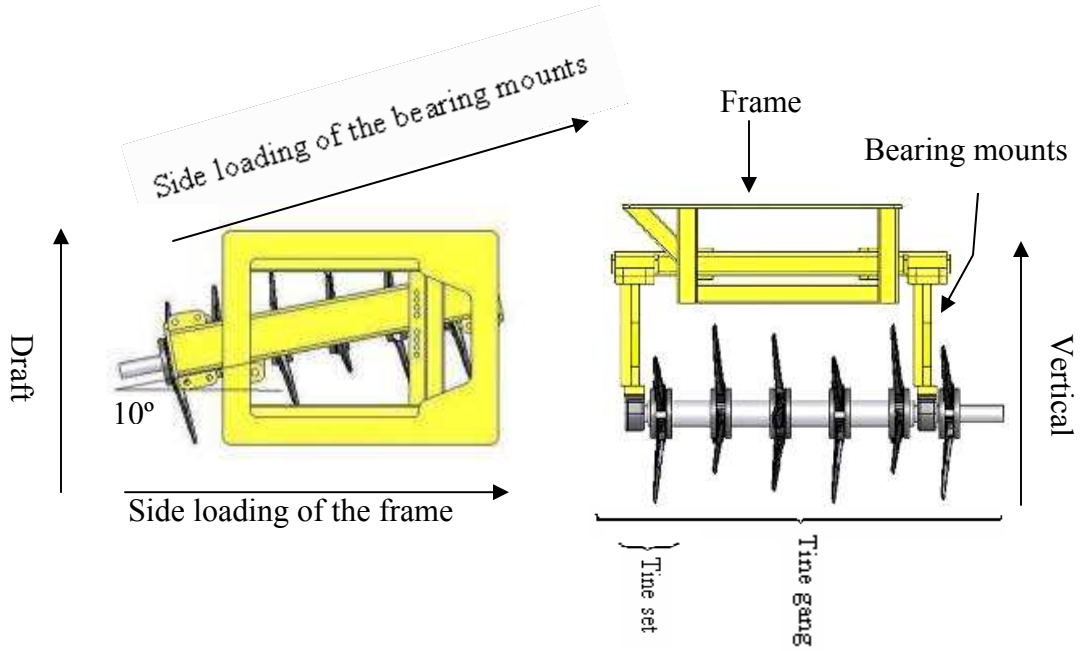

Figure 3.2: The RTA module used in the experiment, component naming convention and the vector loads considered for analysis.

The tool carriage on the TMR has four EOR dynamometers used to measure forces in the vertical and draft directions. The EOR dynamometers were mounted between the mounting plate and tool carriage frame (Figure 3.3). The RTA tool was mounted to the mounting plate, thus any draft or vertical reaction forces from the soil-tool interaction would be measured via the EOR dynamometers.

Figure 3.3: Octagonal ring dynamometers mounted on the tool carriage.

The side loading on the bearing mounts was measured using a strain gage mounted on the bearing mounts of the RTA module frame. The bearing mounts were weakened to increase the frame's sensitivity to loading. The gages were mounted on one side of the bearing mount in a quarter bridge configuration. The gages were arranged in such a way that there were one sensing gage and three dummy gages (Figure 3.4). Three dummy gages were mounted on an unloaded component near the gage location to offset any temperature sensitivity (Appendix A).

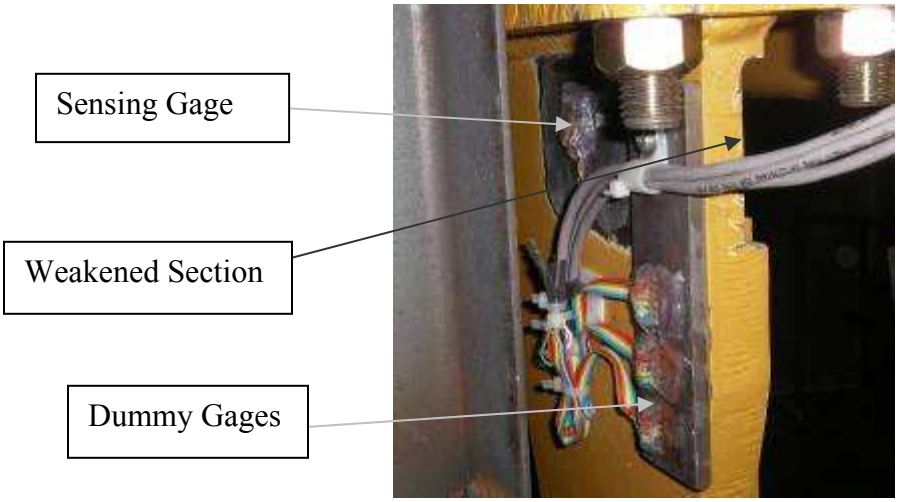

Figure 3.4: Gage mounting for measuring the side loading on the bearing mounts.

3.1.2 Instrumentation measuring forces on the tine

The tine forces were measured via an instrumented tine specially machined to isolate the forces in the X, Y, and Z directions. The tine was machined to create a plane normal to the axis of rotation (Figure 3.5).

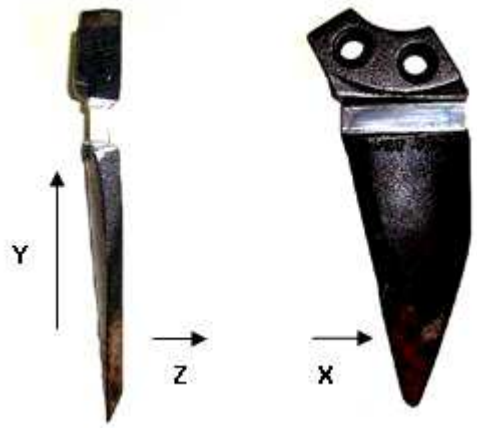

Figure 3.5: Machined tines before gaging.

The intent was to measure the force on the tine in relation to the tine gang's axis of rotation, while measuring the tine's position around its axis. The gages were

mounted in a full bridge configuration with a full bridge measuring the force in X, Y and Z directions (Appendix A).

3.1.3 Calibration of strain gages on the tine

The methodology used for calibrating the tine's gages was a dead load calibration technique. A preliminary test run was carried out under the perceived highest loading case (20 cm depth, 10º gang angle and 4 km/h) to determine the working voltage range for the instrumentation. This was carried out to guarantee that the calibration was carried out beyond the output range of the experiment, so there would be no need for extrapolation of calibration results.

The calibration was carried out by applying a series of weights at 45º to each plane, to a point on the tip of the tine using a pulley system. Calibration forces were applied in this way to load the tine in the X, Y and Z direction at the same time to reduce the effect cross-talk would have on the voltage output of the gages. The tool was loaded through the voltage range determined during the preliminary test run by incrementally increasing the load on the tine to the maximum required and then decreasing the load. Voltage recordings from the gages were taken at each change in weight. Results from calibration can be seen in Appendix B.

3.1.4 Instrumentation measuring position and velocity

One of the objectives of this thesis was to determine the relationship of forces with respect to forward velocity. Because the RTA was mounted to the tool carriage, the velocity of the tool carriage was used to obtain the velocity of the RTA. The tool carriage is driven via a chain mechanism. A proximity switch was used to identify the

rotational speed of the drive sprocket, which in turn was used to calculate the forward velocity of the tool carriage.

The position of the tine was measured via a rotary potentiometer. The potentiometer was driven via a chain and sprocket drive off of the tine gang shaft (Figure 3.6).

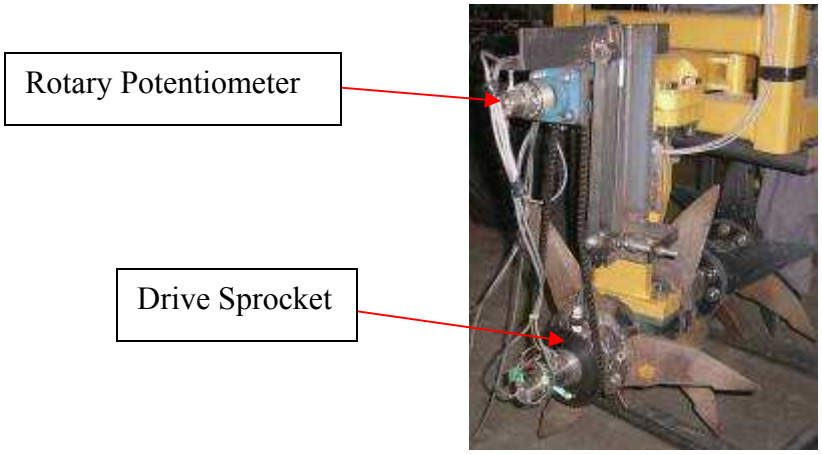

Figure 3.6: The reference position of the potentiometer.

3.2 Methods

3.2.1 Soil measurements experiment methodology

Core samples were taken to the depth of 10 cm to measure the dry bulk density and moisture content. Two samples were taken at random points in the soil bin. An oven drying method was used to assess the bulk density of the core samples (ASTM 1988). The core samplers were cylindrical with a diameter of 7.5 cm and length of 10 cm.

A cone penetrometer (Figure 3.7) was used to take soil strength readings at three locations along the soil bin, at the beginning, middle and end of the run. Effort was made to maintain a consistent penetration velocity while taking a reading every five

centimetres to a depth of 30 cm. Both techniques, core sampling and cone penetrometer, were used to assess the soil density prior to each run. Cone penetrometer tests were of particular interest while the tillage tests were being carried out to assess the build up of deep compaction from the use of the rotary tiller when reconditioning the soil for each run.

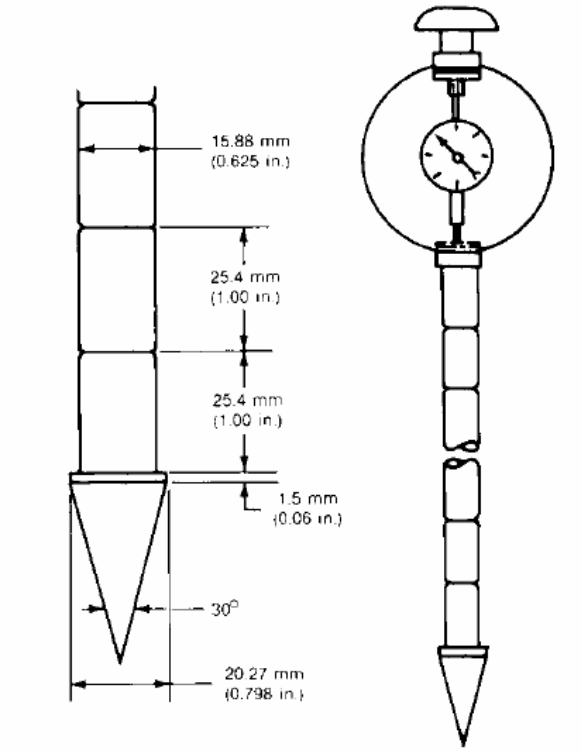

Figure 3.7: Cone penetrometer (ASAE Standards 2009)

As the tests were carried out over multiple days, the moisture content was measured before each run to assess if there was any change from one run to another. The moisture content of the soil was determined from the core samples.

From the core samples taken, further testing was done to determine particle size and soil shear strength. The particle size was determined using a sieve and hydrometer method as prescribed by ASTM standards (ASTM 1988). Soil shear strength was determined based on empirical correlations between soil shear strength and plasticity index. The angle of internal friction is a reflection of the shape of the clay particles

which in-turn can be related to many physical properties of the soil. This relationship was proposed by Bjerrum and Simons (1960) and has been seen to agree well with a range of clay soils (Leroueil *et al*. 1990) (Figure 3.8).

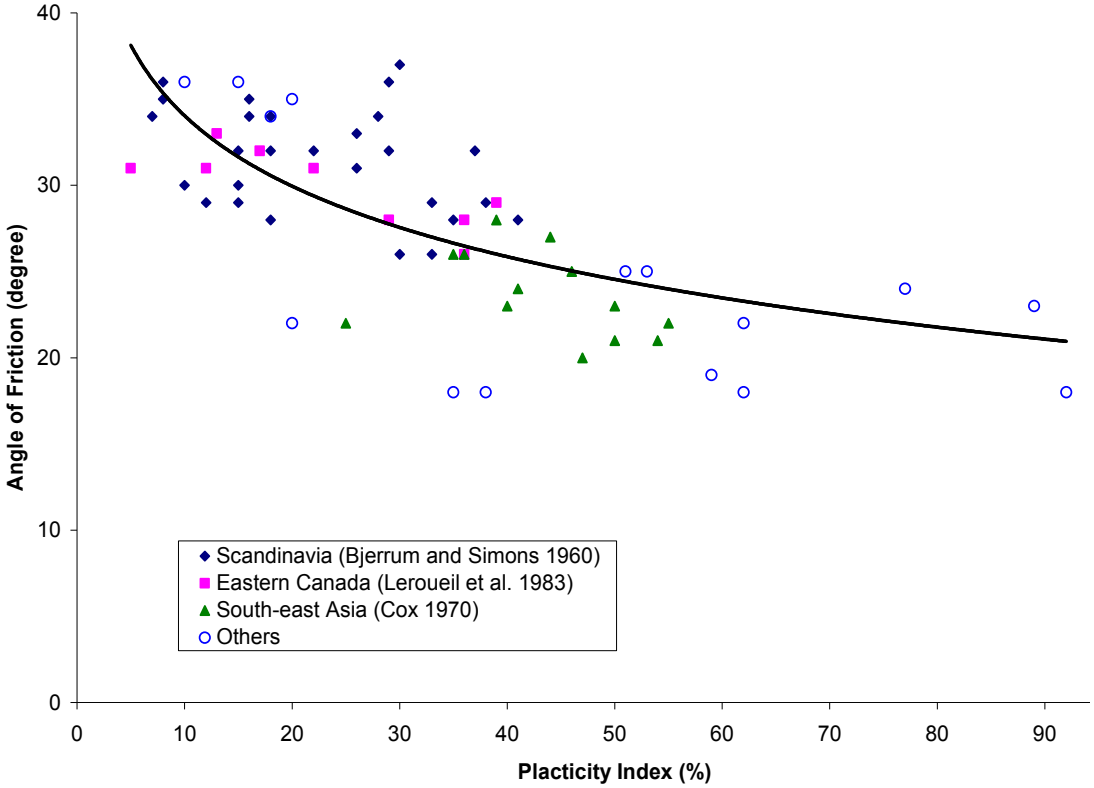

Figure 3.8: Relationship between plasticity index and angle of internal friction (Reproduced from Leroueil *et al.* 1990)

The plasticity index is derived using the following equation:

$$Ip = w_L - w_P \qquad [3.1]$$

where w_L is the water content at the liquid limit and w_p is the water content at the plastic limit determined by the Atterberg test. A soil's liquid and plastic limit represent the water content at which the soil's behaviour shows that it is at the lower limits of viscous flow and the plastic state, respectively (ASTM 1988). Particle size and shear strength were used only for documentation purposes.

3.2.2 Soil preparation

Soil preparation was broken into three phases: moisture conditioning, soil loosening and soil compaction. Each phase was performed as required to produce the required soil properties needed to maintain a consistent medium in which to perform the tests.

To conserve soil moisture, the soil bin was covered with a plastic sheet when tillage exercises were not being carried out. Core samples were taken from soil in the soil bin to track the change in moisture content due to evaporation.

Soil loosening was done, as required, with either a chisel plough or a powered rotary tiller. A chisel plough was used to carry out the deep tillage element of the soil preparation, tilling to a depth of 25 cm. Deep tillage was carried out only when a noticeable compaction layer developed from the rotary tiller. The deep compaction layer was identified using a cone penetrometer. The cone penetrometer would begin reading a high penetration force (at a depth zone of 15-20 cm) when a compaction layer was developing from the rotary tiller. The rotary tiller was used to till the soil to a fine tilth removing any clods formed during the tillage exercise. The soil was rototilled at the end of each repetition to loosen the soil in preparation for soil compaction.

Similar to the soil loosening, deep and shallow soil compaction was carried out before each run. Deep compaction was carried out with a lamb foot compactor. Shallow compaction was carried out with a smooth roller. Before compaction, the soil was levelled using a levelling blade. Two runs, to and fro, were carried out with both rollers to create the necessary density of 1.2 g/cm^3.

3.2.3 Experiment design

The five variables of concern within the experiment were: (1) the setting of the tine gang angle, (2) the depth of the tine, (3) the velocity of the tool frame and the tines, (4) soil moisture content and (5) soil density. Soil moisture content and density are difficult variables to adjust, thus they were fixed at one level. The experiment was randomized to minimize any effect the variation in soil moisture content and density could have on the experiment results.

The design of the experiment was based on a factorial design with three factors and two levels. For each combination of variables, three repetitions were carried out. Two of the factors, depth and gang angle, could be controlled to a reasonable accuracy (± 1 cm and ±1°, respectively). The third factor, velocity, was difficult to set, especially at high velocities. The tool carriage was hydraulically driven and the forward velocity of the carriage was set by changing the flow supplied by the pump. Maintaining a repeatable forward velocity proved difficult as the temperature of the hydraulic oil increased. As hydraulic oil temperature increased, the pump did not have sufficient power to achieve the higher speeds when carrying out the high-draft runs. A series of trial runs was carried out to determine what flow rates were required to achieve a specific velocity. However, even with this information gathered, large inconsistencies in velocity were seen.

The forward velocities selected for the tests were two and four km/h. The forward velocities were chosen based on average tillage velocity of two to eight km/h (Swick and Perumpral 1988). The limitations of the TMR hydraulic system held the velocity, for the majority of the runs, to a maximum of four km/h. The tine depths selected were

10 and 20 cm. The tine gang angles of zero and 10 degrees were selected for the experiment.

3.3 Statistical analysis

The objective of this study was to measure the forces on the RTA unit while undergoing normal working conditions and to develop a statistical model of the tool loading. The statistical model that was to be developed to predict the forces on the tine and frame was based on depth, velocity (forward velocity of the tool carriage for the frame models and rotational velocity of the tine for the tine models) and angle of the tine gang. The soil moisture content and density was kept constant throughout the experiment. The experiment design was chosen to simplify the model and experiment.

A statistical model was selected oppose to other model types because of the rotating nature of the tine, its geometry and the variation of the tine gang angle. For example, semi-empirical tillage models such as the ones base on Mohr-Coulomb soil mechanics required the tool orientation relative to the direction of travel to be understood to determine the soil failure planes. Due to the complex geometry of the tine, its rotation through the soil and the variation of the tine gang angle, identifying the soil failure planes would be difficult and the development of semi-empirical model did not seem practical.

The data was analyzed using a statistical software package, SPSS ™. All possible regressions approach, including interaction variables, was used when assessing the equations. The equations were built one regressor at a time, starting with the main effects and then adding interaction regressors. As the regressors were added, the equation's fit was assessed using the coefficient of determination (R^2) and sum of

squared error (SSE). If there was a discrepancy whether an added regressor's contribution to the fit of the equation was significant, a hypothesis test using the F-statistic was used to justify its addition or removal.

Interaction regressors were used to take into consideration the possibility of an interaction between two of the variables. When adding an interaction regressor, all main effect regressors were also included. Maintaining all the lower level regressors when assessing interactions was suggested as a best practice (ANON 1999). The preferred models were selected based on the number of variables in the equation and the ability to satisfy the test statistics.

CHAPTER 4: RESULTS AND DISCUSSION

4.1 Soil tests

During the testing period an attempt was made to isolate the effect moisture content and soil density had on the variables being analysed. These soil properties were maintained as consistently as possible by sampling the soil at the end of each run and adjusting the soil accordingly. The moisture content was maintained at an average moisture content of 12.3% dry basis (DB) (10.9% wet basis (WB)) with a standard deviation of 0.5% (0.4% WB). The soil density was maintained at an average of 1.23g/cm^3 with a standard deviation of 0.03 g/cm^3.

The particle distribution was obtained for documentation purposes. The particle distribution of the soil showed the soil to be 40% sand, 22% silt and 38% clay. This soil, having a high percentage of clay, was classified as a clay loam soil. The soil particle distribution can be seen in figure 4.1.

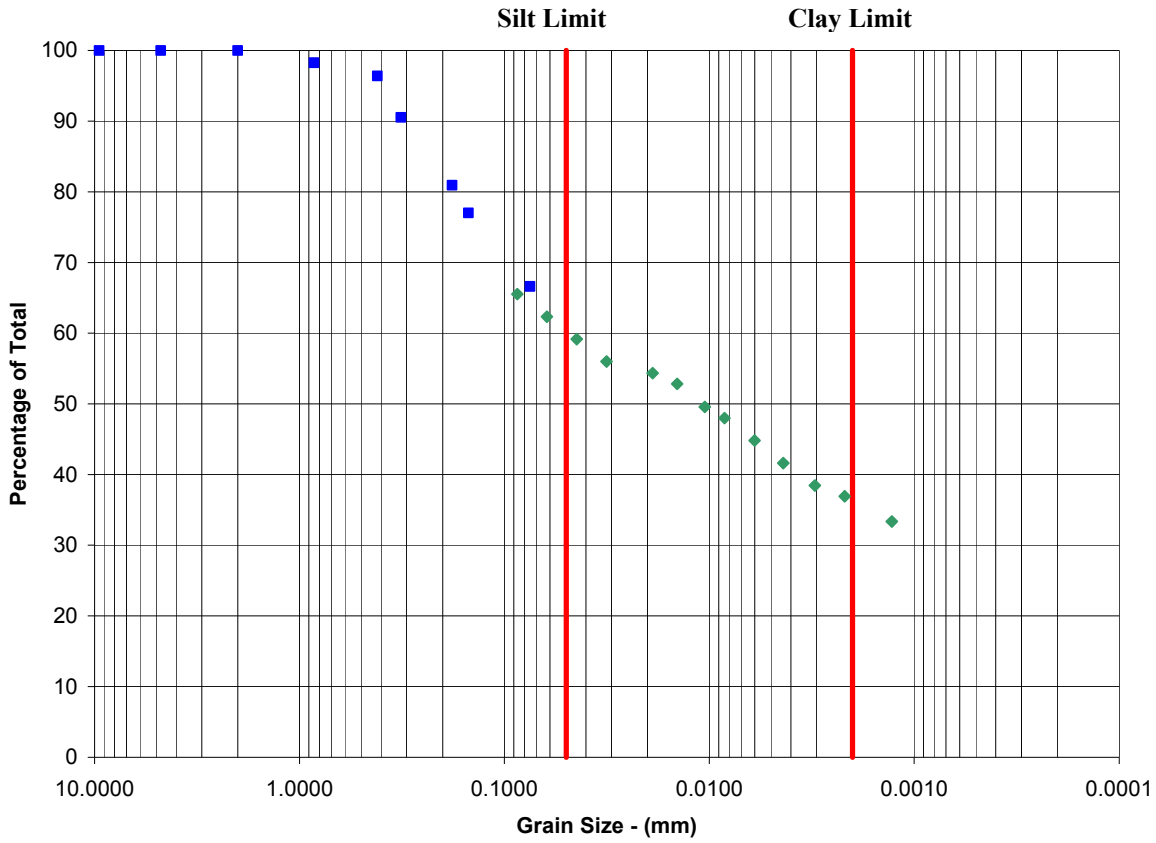

Figure 4.1: Percentage of total particles less then the indicated grain size determined using both the hydrometer and sieve methods (The particles isolated by the hydrometer method are the green diamond and the particles isolated by the sieve are the blue squares)

Also for documentation purposes, an estimate of the angle of internal friction was obtained from the Atterberg liquid and plastic limit. These values were measured from a sub-sample of the soil samples used to determine the density and moisture content of the soil. From these values the plasticity index, I_p, was determined as 26.7. Using the relationship between plasticity index and shear strength that Bjerrum and Simons (1960) derived stated in Leroueil *et al*. (1990), the angle of friction was valued as 29º (Appendix C).

4.2 Maximum loading at the tool and frame level

4.2.1 Loading values, patterns and considerations

A typical plot of the forces on the frame from one run is shown in Figure 4.2. To obtain an average force on the frame, a section of the results was isolated once a steady state was reached. These values were then averaged to give the force on the frame at those specific settings.

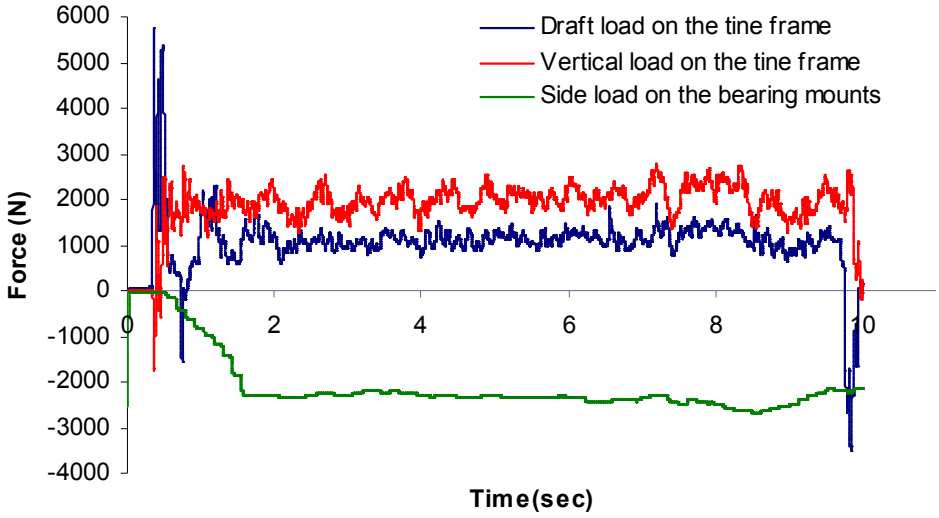

Figure 4.2: Typical forces on the frame at 10 cm of depth, 10 degrees pitch on the tine gang with the frame traveling at a forward velocity of 2 km/h.

The peak forces on the tine repeated in a cyclical manner and the position of the tine at that peak through this rotation was not affected significantly ($\alpha = 0.05$) by depth, tine gang angle or velocity. The forces on the tine were seen to increase to maximum between 90º and 130º rotation, from a horizontal starting point, depending on the direction of the force in question (Figure 4.3 (a) and (b)). Peak forces in the Z and Y directions tended to lag behind forces in the X direction by an average of 14 º and 27º, respectively (Figure 4.4). The peak force in the X direction typically occurred around 90º when the loading changed from the back side of the tine to the flat front edge. After

this the force in the X direction peaked a second time, approximately at the same time as the Z and X direction. It is assumed that the peak loads occur at a point beyond 90º because of a lag between rotational velocity and forward velocity caused by all the tines on the tine gang.

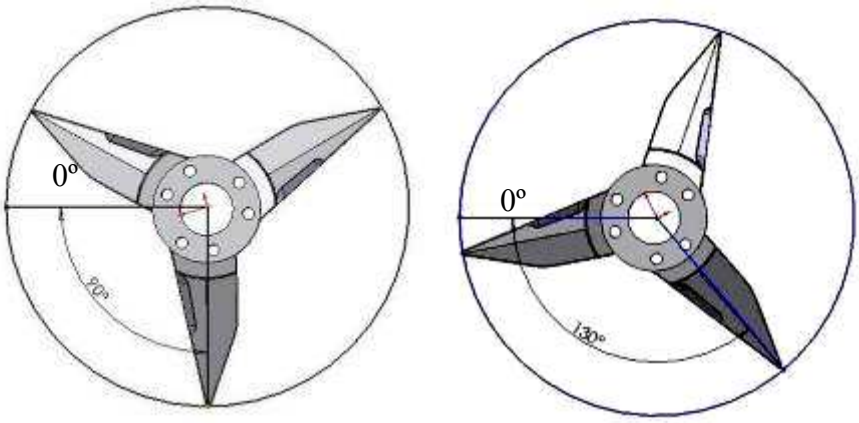

(a) (b)

Figure 4.3: The range where the peak forces were located during the tines rotation is shown in (a) and (b).

Unlike the forces on the frame, the forces on the tine were cyclical, reaching a maximum and then returning to zero (Figure 4.4). The value used in the statistical analysis of the tine loading was an average of the values the tine reached at each peak within a single run (typically a mean of 3 values).

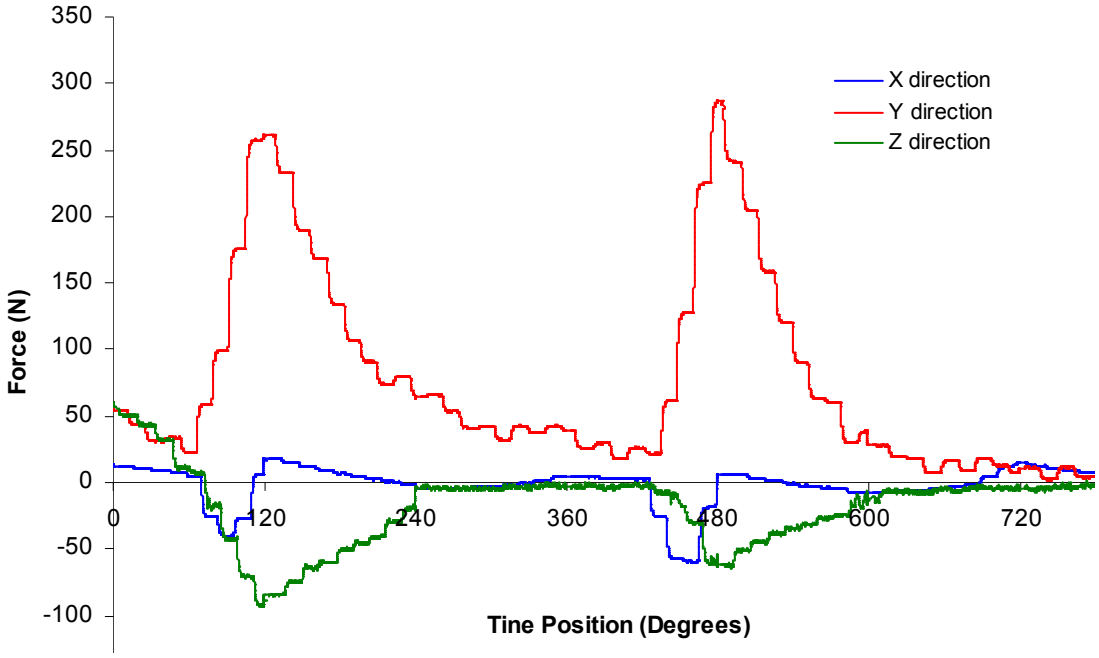

Figure 4.4: Results obtained at 10 cm depth, 10 degrees gang angle, and 2 km/h.

When analyzing the forces on the tine and frame, some similar trends in loading were found. For example, increasing the depth resulted in increasing loading on the tine and the frame. However, it is important to consider the tine gang's orientation when comparing these results of the tine to that of the frame. For example, when the tine gang's angle is increased to 10º, the instrumentation measuring the loading on the bearing mounts is no longer perpendicular to the draft loading plane (Figure 4.5). However, the tine loading in the Z direction is always normal to the tine gang axis of rotation and thus perpendicular with the gages in the X and Y direction on the tine (a summary table of the forces output data can be seen in Appendix D).

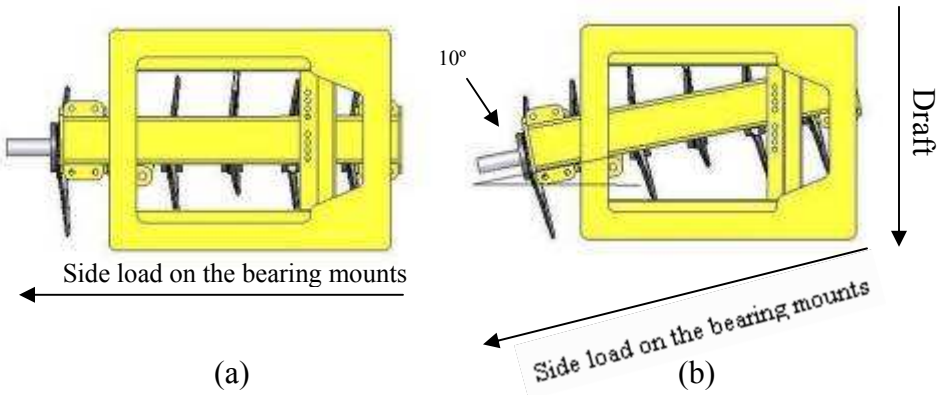

Figure 4.5: Top view of modular RTA at 0º (a) and 10º (b) showing the change in orientation of the plan representing the side loading on the bearing mounts relative to the draft loading.

4.2.2 Side loading on the bearing mounts and forces on the tine in the Z direction

From a design standpoint, tillage tool geometry and orientation with respect to the direction of travel will affect tool load and the principal direction of that load. The tine used in the Rotary Tine Aerator (RTA) has a relatively complex shape. This shape was seen to influence the tine and frame loads. This relationship is evident when analyzing the side loading on the bearing mounts.

The maximum side loading on the bearing mounts was 4704 N, found when the tool ran with the tine gang angle set at 10º, 20 cm depth and traveling at a forward velocity of 2 km/h. The side loading on the bearing mounts was largely affected by the angle at which the gang was positioned. When the tine gang was position at 10º, the highest side loads were measured on the bearing mounts irrespective of depth. By increasing the tine gang angle from 0º to 10º, the broad flat side of the tine was exposed to more soil relative to the direction of travel (Figure 4.6 b). With the tine gang angle set a 10º, the tine displaced more soil, thus higher forces were measured in the Z direction of the tine and there was more side loading on the bearing mount (Figure 4.7).

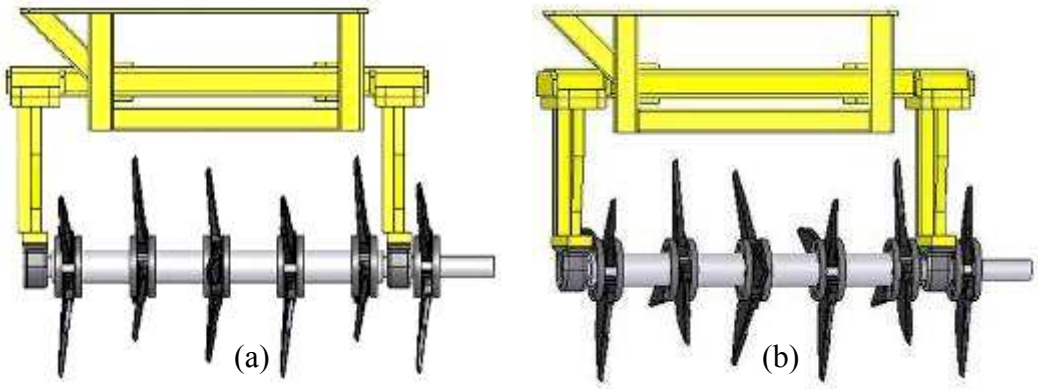

Figure 4.6: Comparison of tine geometry at 0º (a) and 10º (b). Figure (a) shows exposed pitch and cut out which could effect the principal direction of loading. Figure (b) shows the exposed side surface of the tine redirecting loading.

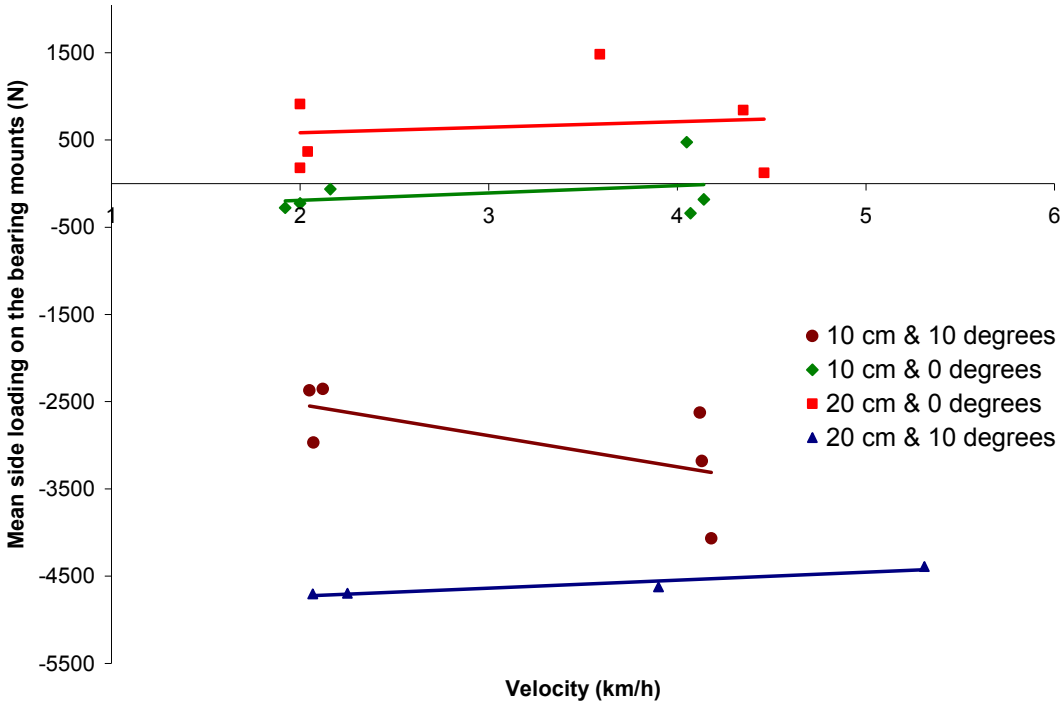

Figure 4.7:Mean side loading on the bearing mounts vs. forward velocity.

At a gang angle of 0º, the side loading on the bearing mount was small; however, at a depth of 20 cm, the accumulative force of all the tines was applied in the opposite direction than was seen when the RTA was set to the other variable combinations (Figure 4.7). As all the tines on the tine gang were identical (there being left and right

handed tines on production frames to keep the frame loading symmetrical) each tine is assumed to load the bearing mounts in a similar manner. It can be assumed that the change in direction of the side loads on the bearing mounts is due to the 6º pitch and the chamfered cut out in the upper portion of the tine. At 20 cm depth the broadest portion of the tine would be interacting with the soil causing the greatest effect from the 6º pitch (Figure 4.8). Furthermore, at this depth the chamfered edge on the upper portion of the front face of the tine becomes exposed to the soil as the tine rotates through the soil adding to the load. Forward velocity of the tool carriage frame was not seen to have significant (α=0.05) effect on the side loading of the bearing mounts.

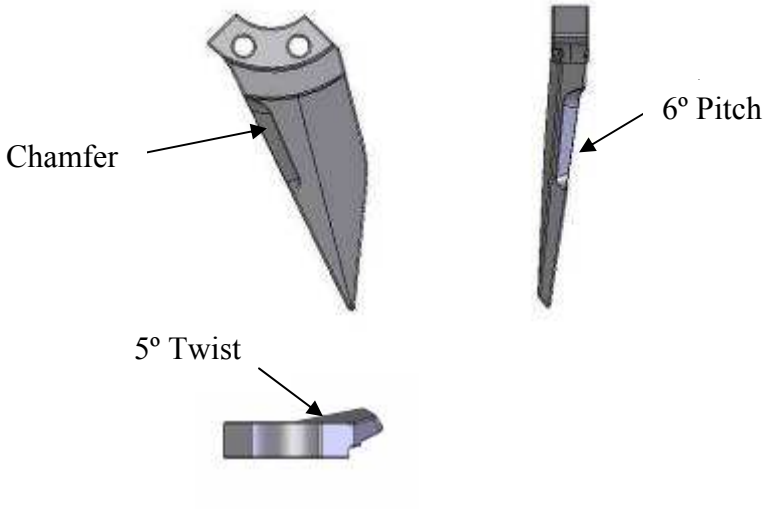

Figure 4.8: Model of tine used in experiment.

When analyzing the loading on the tine in the Z direction, with the tine gang angle set at 0º and a depth of 20 cm, the loading values obtained from the tine peaked in both directions (positive and negative forces denoting opposite directions) (Figure 4.9). As discussed earlier, at a tine gang angle of 0º and a depth of 20cm, the side loading on the bearing mounts was also applied in the opposite direction to all other setting configurations. From this, it can be assumed that the sum of the forces on the bearing

mount changes direction based on this tine gang angle and depth, but there is some variability on the direction of the forces on individual tines based on variable soil conditions.

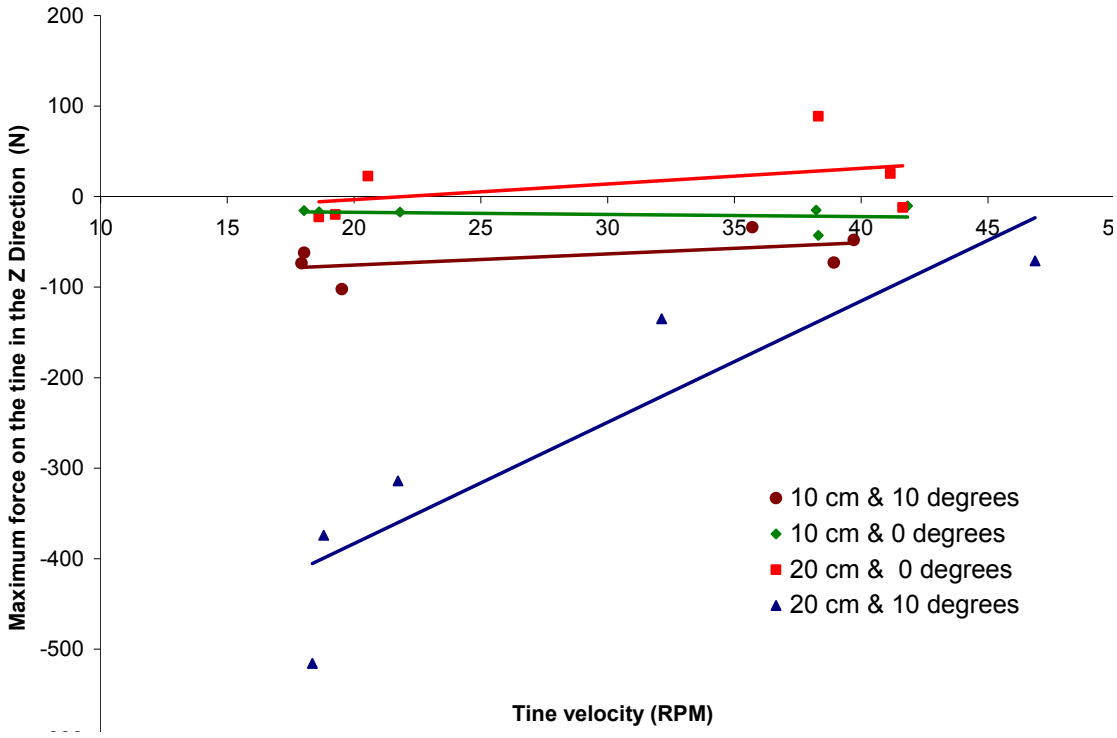

Figure 4.9: Maximum forces in Z direction vs rotational velocity.

The maximum force on the tine in the Z direction was 516 N. This force was measured at a tine rotational velocity of 18.4 rpm (forward velocity of 2 km/h), a gang angle of 10º and a depth of 20 cm. This is the same forward velocity, depth and gang angle that the peak side load on the bearing mounts was found.

The main influence on tine loading in the Z direction was seen to be the gang angle. When the tine gang was set at 0º, the forces were seen to be low regardless of depth. When the tine gang was set at 10º, the force in the Z direction was seen to increase. The forces applied on the tine in the Z direction decreased with velocity.

Depth was seen as having a major effect on the force in the Z direction and there was an interaction between rotational velocity and depth affecting the force in the Z direction (Figure 4.9). Depth was seen to increase the loading on the tine at both 0º and 10º. However, at 10º the loading on the tine was a multiple of four higher at 18.4 rpm (2 km/h) and decreased with increases in rotational velocity. This relationship contradicts what has been seen in narrow tines on rigid tillage tools (Stafford 1979). This could possibly be due to some soil loosening caused by the previous tine that entered the soil. Miszczak (2005) noticed a reduction in torque on a rotary subsoiler caused by an overlap of soil failure zones caused by the tines. This would be accentuated at higher velocities as the soil failure zone would be larger (Sharifat and Kushwaha 2000). Furthermore, when the tine gang is set at 10º, it would increase the possibility of soil failure zones overlapping, thus accentuating the effect of velocity on tool force.

4.2.3 Vertical forces on the frame and forces on the tine in the Y direction

The vertical force on the frame was consistent with previous research showing higher vertical forces at greater depths (Onwualu and Watts 1998). The greatest vertical force was experienced when the working depth was set at 20 cm and the gang angle at 0º, and was near double the vertical forces at other settings. The maximum value measured at this setting was 8211 N at a velocity of 4.5 km/h. The vertical force, when the tine gang was set at 0º was seen to be larger than when at 10º under both depth conditions. Forward velocity was seen to be statistically significant ($\alpha = 0.05$). When analyzing the graphical data, an increasing trend in vertical forces on the frame with respect to velocity was seen under most variable combinations of depth and tine gang

angle; however, at 20 cm depth and 10º tine-gang angle there was a decreasing trend with velocity (Figure 4.10). This change in trend at 20 cm depth and 10º tine-gang angle could be due to the lack of data or possibly the influence of an outlier.

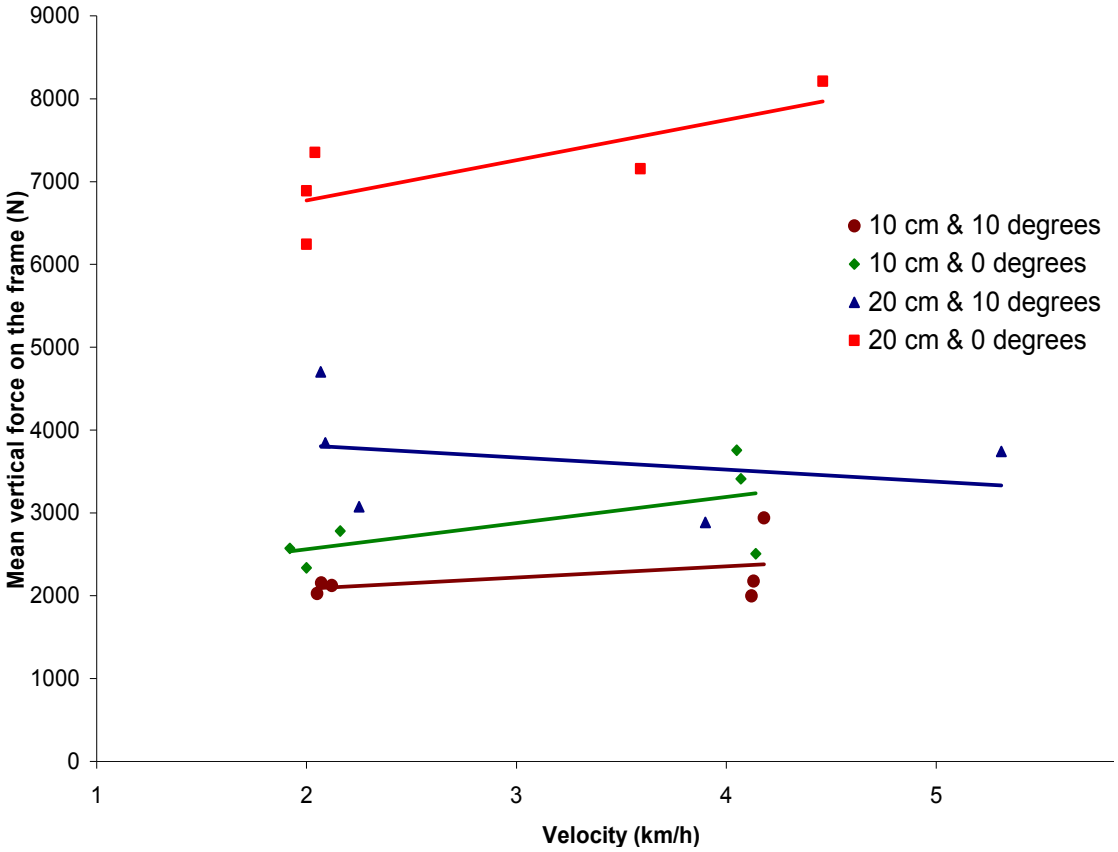

Figure 4.10: Mean vertical force on the frame vs forward velocity.

Like the loading of the tine in the Z direction, the forces in the Y direction on the tine seem to show more consistent trends than the vertical forces on the frame. The consistency of trends was noticed when observing the effect rotational velocity had on tine loading (Figure 4.11).

The maximum force on the tine in the Y direction was 572 N. The force was measured at a rotational velocity of 19.3 rpm (forward velocity of 2.1 km/h), a gang angle of 0º and a depth of 20 cm. The forces in the Y direction on the tine were seen to

increase with the depth at which the tool worked and decreased in loading as rotational velocity increased. The decreasing effect rotational velocity had on the force applied to the tine could be due to overlapping soil failure zones as was suggested for the forces applied in Z direction. Changes of the gang angle did not have a significant ($\alpha = 0.05$) effect on the loading of the tine in the Y direction.

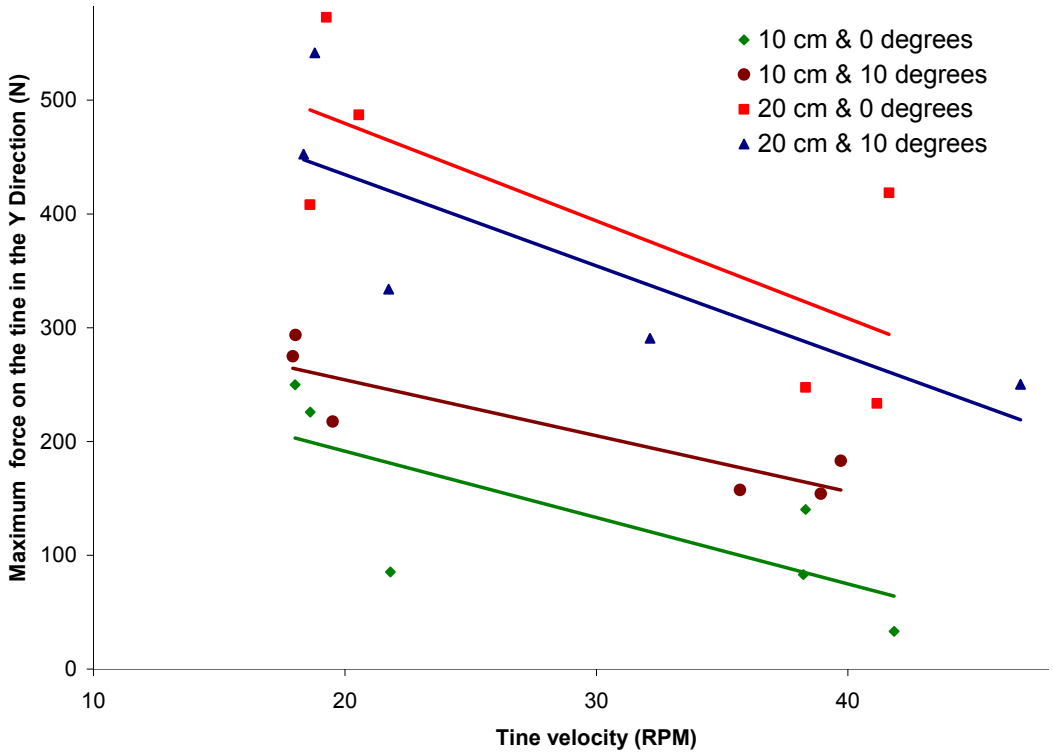

Figure 4.11: Maximum forces in Y direction vs. rotational velocity.

4.2.4 Draft forces on the frame and forces on the tine in the X direction

Like the vertical forces, draft showed a strong increasing relationship with depth, which is typical when compared to other tillage experiments (Wismer and Luth 1972, Perumpral *et al*. 1983). The maximum draft force measure was 7429 N at 20 cm depth, a gang angle of 0º, and a velocity of 3.6 km/h (Figure 4.12).

The relationship between draft force on the frame and forward velocity showed similar trends as did the vertical force on the frame and velocity (Figure 4.12). At a depth of 10 cm the draft force shows an increasing trend as velocity increased. However, at a depth of 20 cm the results showed draft increasing at a gang angle of 0º and decreasing at 10º. This corresponds with the trends found in the vertical loading of the frame (Figure 4.10) suggesting a relationship between vertical and draft forces on the frame, possibly due to the rotating nature of the tine. As discussed before this change in trend at 20 cm depth and 10º tine-gang angle could be due to the lack of data or possibly the influence of an outlier.

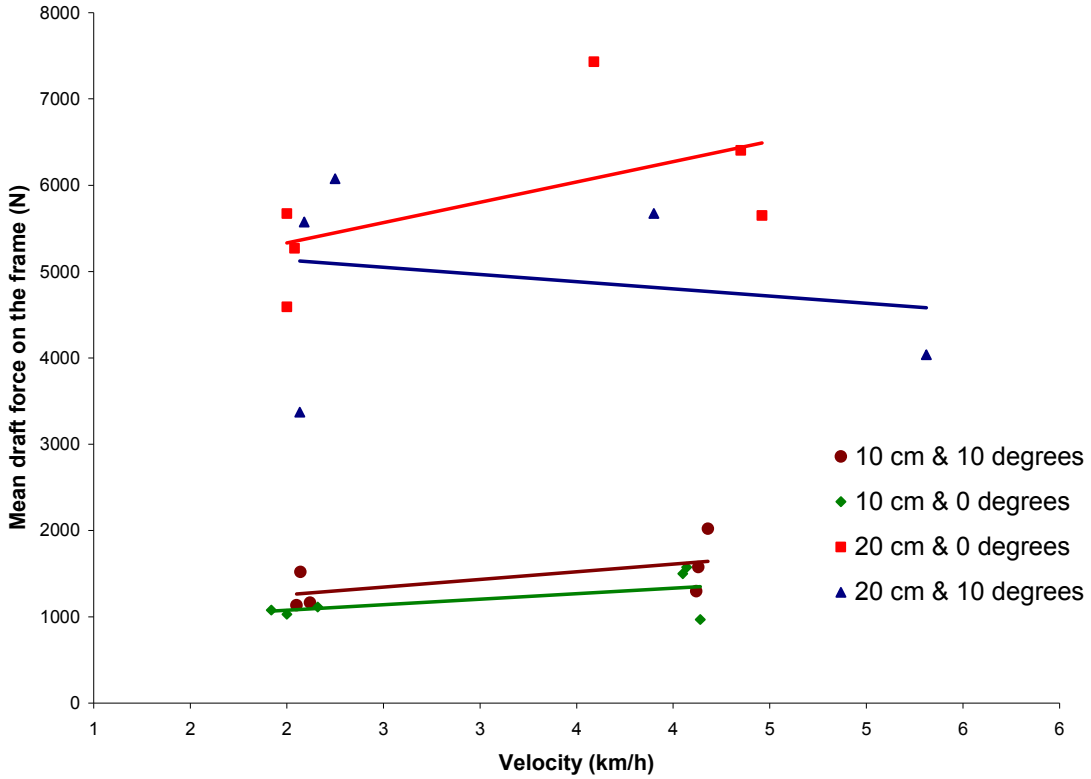

Figure 4.12: Mean draft forces vs. forward velocity.

As seen in the draft loading on the frame (Figure 4.12), loading on the tine in the X direction was seen to predominantly be affected by the depth and rotational velocity

(Figure 4.13). The maximum force on the tine in the X direction was 253 N when the tine was set at a gang angle of 0º, a depth of 20 cm and measured rotational velocity of 19.3 rpm (forward velocity of 2.1 km/h). The force on the tine in the X direction was seen to decrease with increasing rotational velocity. The degree which rotational velocity affected the force on the tine was influenced by the depth at which the tool was working (Figure 4.13). This interaction between depth and velocity affecting the force on the tine was also seen in the force analysis of the forces in the Z direction.

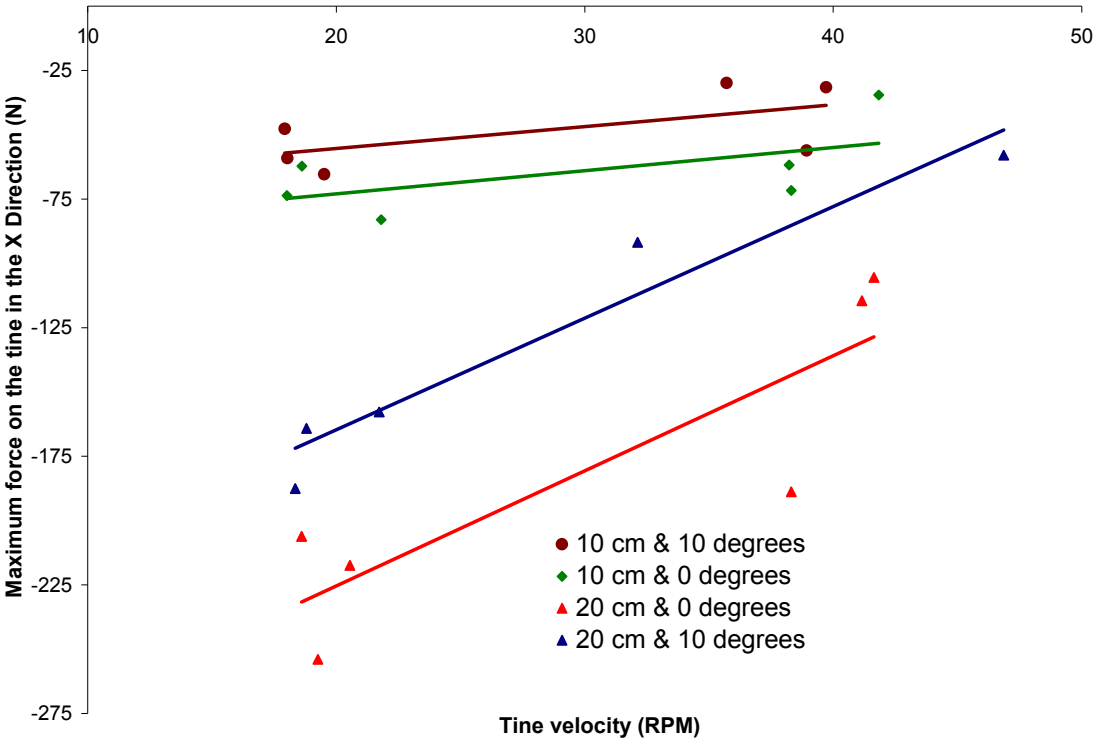

Figure 4.13: Maximum forces in the X direction vs. rotational velocity.

4.2.5 Position along the tine gang and the forces on tine and frame

The trends in the data with regards to the forces on the tine and frame were relatively consistent when considering angle of the tine gang and the depth of the tool engagement. However, the effect velocity, both rotational and forward, had on the tine

and frame, respectively, showed differing trends. The forces measured on the tine were quite sensitive to changes in rotational velocity, decreasing as the velocity increased. The forces on the frame in the vertical and draft directions tended to show a slight increase in force with increasing velocity (with the exception of loading of the frame at a depth of 20 cm and 10º gang angle). The forces on the frame can be assumed to be a sum of the forces applied to all of the tines on the tine gang, which varied in magnitude depending on the individual tine's rotational position in the soil. The sensitivity of the forces on the tine to rotational velocity is assumed to be due to overlapping soil failure zones. The reason similar sensitivities were not seen on the frame is unknown. As the analysis on the tine was carried out only on a single tine at the end of the tine gang, it may not be a true representation of the complete set of tines on the tine gang. Due to the possibility of overlapping soil failure zones, having measurements of the loading on a tine at the beginning, middle and end of the tine gang would allow for a better insight into the effect neighbouring tines have on the tine load and whether this is influenced by the rotational velocity of the tine.

4.2.6 Theoretical rolling radius vs. rotational velocity

For all runs, both the forward velocity of the frame and the rotational velocity of the tine were measured independently. The forces on the frame were compared to the velocities of the tool frame and the forces on the tine were compared to the velocity of the tine shaft (rpm). This was done because the tine rotational velocity was found to decrease when the tine gang angle was changed from 0º to 10º. It is assumed that this is due to the increase in surface area exposed to the direction of travel. As the gang angle increases, the broad face of the tine is more exposed to the soil increasing the surface

area that is under load. Under these conditions the soil tool friction is assumed to be increasing the theoretical rolling radius of the tines and thus causing a decrease in tine velocity. The effect gang angle had on the theoretical rolling radius can be seen in Figure 4.14.

The theoretical rolling radius is a value representing the radius of a theoretical cylinder rolling through the soil based on the measured rotational velocity of the tine and the forward velocity of the frame. It was used because it allowed for a good comparison of forward and rotational velocities irrespective of the rotational velocity. This calculated value assumes zero relative motion between the soil surface and the theoretical surface of a cylinder with equal radius as the rolling radius. Equation 4.1 was used to calculate the theoretical rolling radius.

$$R = \frac{V}{0.0012\pi\theta} \qquad \textbf{[4.1]}$$

where R is the theoretical rolling radius(cm), V is forward velocity (km/h) and $\emptyset$ is the rotational velocity (rpm).

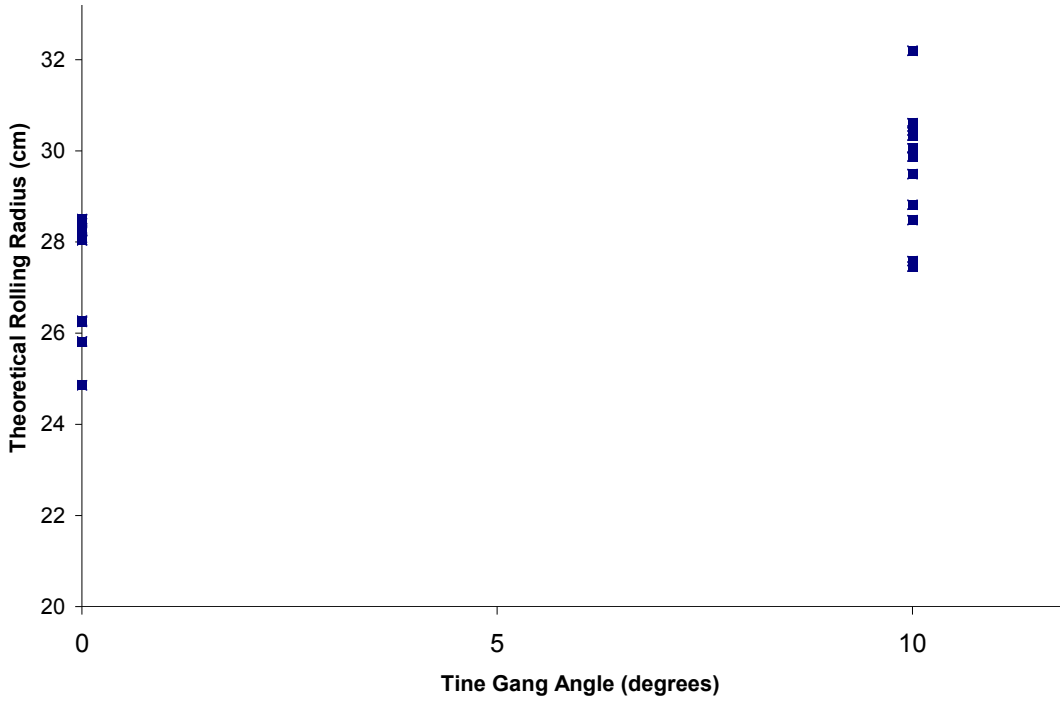

Figure 4.14: Plotting of the theoretical rolling radius compared to the tine gang angle.

4.2.7 Statistical modeling of the tine and frame loading

A series of statistical models were created to aid in the analysis. As discussed in chapter 3, the analysis was carried out using the statistical software package SPSS. The "all possible regressions" method was used to select the variables within the model. The equations developed for the analysis can be seen in appendix E. The objective of the statistical exercise was to explain as much of the variability in the data with the fewest variables. Variables were added to the equation if they added significantly to the equations fit to the data. This was determined using a hypothesis testing based on the F-test. A summary of the equations developed and their values for the coefficient of determination (R^2), Sum Squared Error (SSE) and Residual Mean Squared (RMS) obtained from the statistical package SPSS for the tine can be seen in Table 4.1

Table 4.1: Equations selected for the tine loading based on all possible regressions method.

	R Square	SSE	RMS
X=-25.1D+3.7A+2.7V-50.7	0.84	16081.3	846.4
Y=52.5D-6.9V+163.5	0.78	103537.8	5176.9
Z = -6.3D+43.8A-2.2V+0.5DV-13.1DA-0.9VA+0.3DVA+12.8	0.92	34075.16	2271.7

- X, Y and Z are the forces (N) in the X, Y and Z direction, respectively, on the tine.
- D is the depth that the tool was working within the soil (cm), A is the angle of the tine gang in degrees, and V is the rotational velocity (rpm).
- R Squared is the coefficient of determination, SSE is the sum of squared error and RMS is the residual mean squared.

The model of the forces on the tine in the X direction contained all the main effect variables. From the graphical analysis, it was assumed that there would be an interaction between depth and velocity. However, the addition of an interaction variable between depth and velocity was not seen to be significant ($\alpha = 0.05$). The X direction model had an R^2 value of 0.84. When plotting the predicted force values relative to the measured force values, there was an even distribution of points above and below the 45º line at the lower end of the forces but the model tended to under predict the higher loads (Figure 4.15).

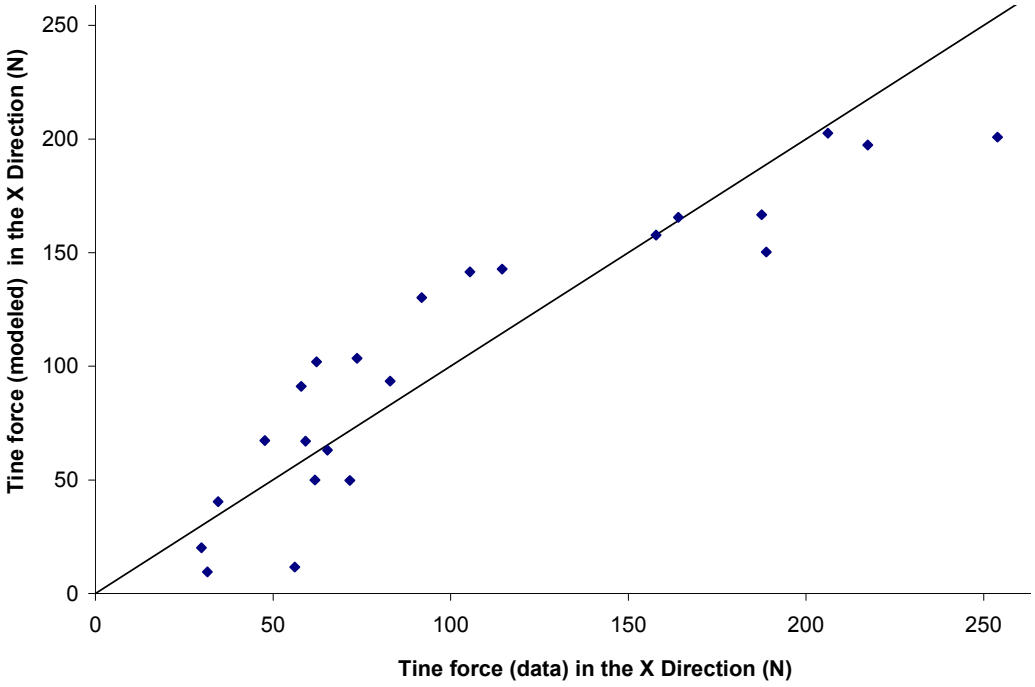

Figure 4.15: Comparison of force model vs. data for the X-direction on the tine.

The model of the forces in the Y direction was comprised of the main effects of depth and velocity. The variables seemed logical based on the graphical analysis. The Y direction model had an R^2 value of 0.78. When plotting the predicted force values relative to the measured force values, there was an even distribution of points above and below the 45º line (Figure 4.16).

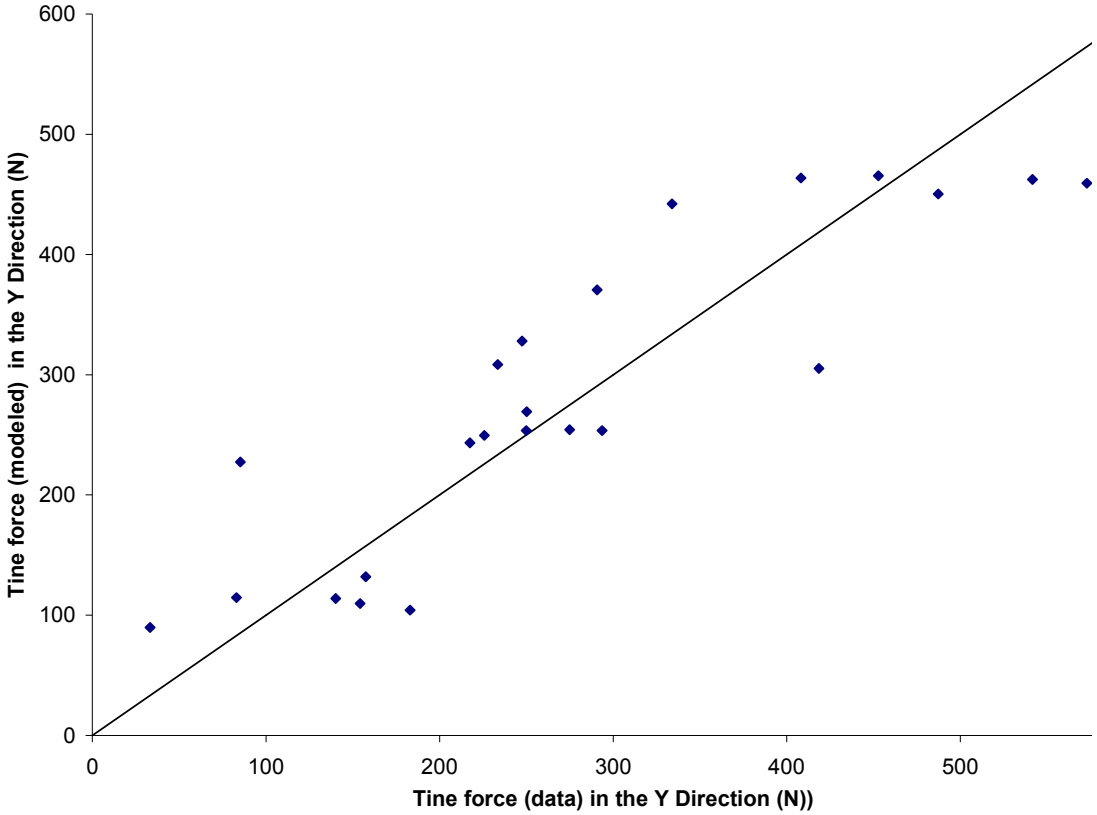

Figure 4.16: Comparison of force model vs. data for the Y-direction on the tine.

The model of the forces in the Z direction required the inclusion of many regressors. The Z direction model had an R^2 value of 0.92. When building the model, the addition of each regressor was evident as indicated by significant ($\alpha = 0.05$) improvement in the R^2 value. The force on the tine in the Z direction had a complex relationship, thus the inclusion of many variables. When plotting the predicted force

values relative to the measured force values, the points tended to be below the 45º line, suggesting the model under-predicted the force output. A large portion of the results was clustered at the low end of the graph (Figure 4.17).

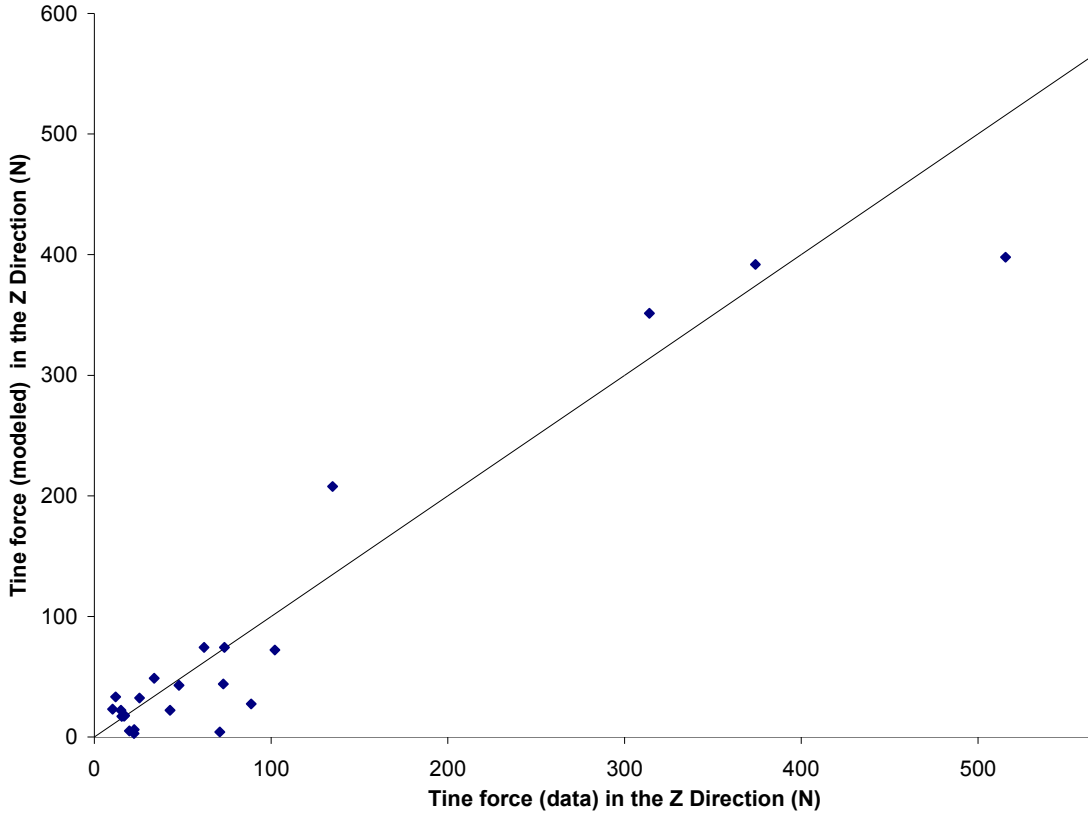

Figure 4.17: Comparison of force model vs. datafor the Z-direction on the tine.

Equations for the frame were developed using the same methodology as the tine. The equations for the frame can be seen in Table 4.2.

Table 4.2: Equations selected for the frame loading based on all possible regression method.

	R Square	SSE	RMS
Draft =1025.1D-2769.1	0.88	13530058.0	644288.5
Vertical =1092.4D+356.5A+391.8V-41.5AV-73.9DA-2672.1	0.95	4533553.0	283347.1
Side =-338.3A+274.9	0.63	38697703.0	1842747.8

- Draft, Vertical and Side are the forces (N) represents the draft and vertical on the frame and the side loading on the bearing mounts.
- D is the depth that the tool was working (cm), A is the angle of the tine gang in degrees, and V is the forward velocity (km/h).
- R Squared is the coefficient of determination, SSE is the sum of squared error and RMS is the residual mean squared.

The equation developed for the model of the draft force on the tool frame had a R^2 of 0.88. There was only one regressor included because there was no significant reduction in SSE, based on the F-test, when additional regressors were added. When plotting the predicted force values relative to the measured force values, the data points are spread across in groups parallel to the X axis, not parallel to the 45º line. This may not have been an issue if all the points were clustered together like the lower value points; however, at the higher values, the points spread parallel to the x-axis showing greater error (Figure 4.18).

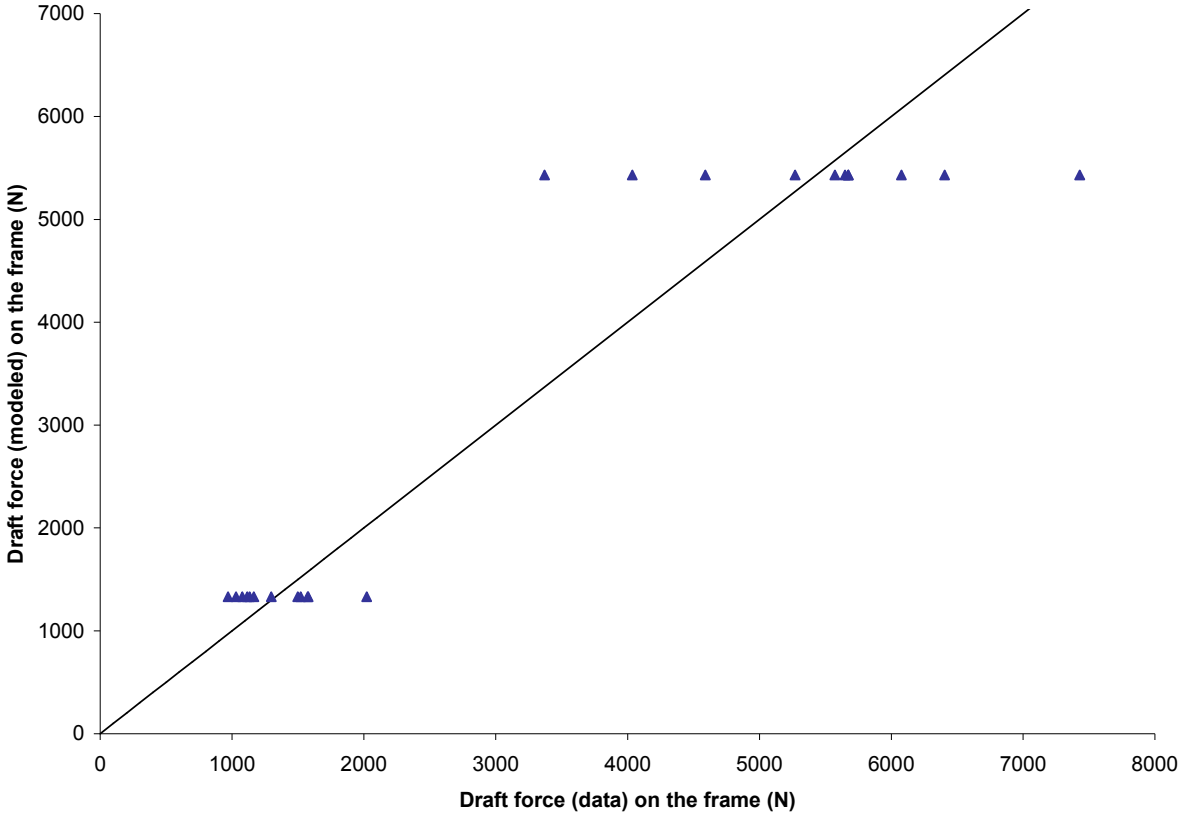

Figure 4.18: Comparison of force model vs. data for the draft loading of the frame.

The model of the forces on the frame in the vertical direction had a R^2 value of 0.95. The model contained all main effects pulse interactions between depth and angle and angle and velocity. The inclusion of depth and angle was expected based on the graphical analysis. When comparing the predicted force values relative the measured force values, the data points tended to follow evenly above and below the 45º line suggesting good fit (Figure 4.19).

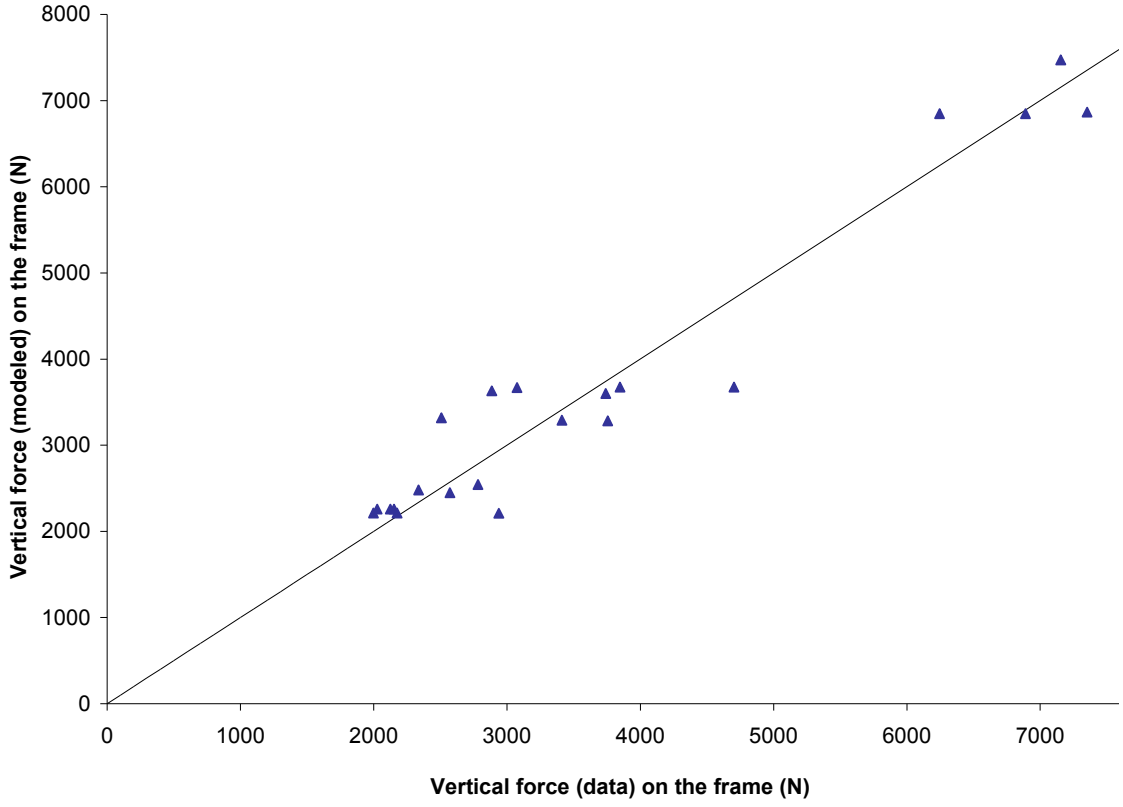

Figure 4.19: Comparison of predicted force vs. data for the vertical loading of the frame.

The model of the side loading of the tine gang had the lowest R^2 value of all the models at 0.63. The side loading scenario is a complex system. Considering the number of regressors used to model the force on the tine was high, it was expected that the side loading of the tine gang would be difficult to model. When selecting the

regressors for the modeling of the frame, it was seen that adding additional regressors was not improving the model significantly. The model was limited to one regressor for this reason. As seen with the model of the draft loading, when plotting the modeled values against the measured values, the points were spread across parallel to the x-axis. Much like the draft loading model, the spread between the points increased across the x-axis for the higher values showing greater error. When plotting predicted force values relative measured values it was seen that the predicted values were under predicting the forces at the lower values (Figure 4.20).

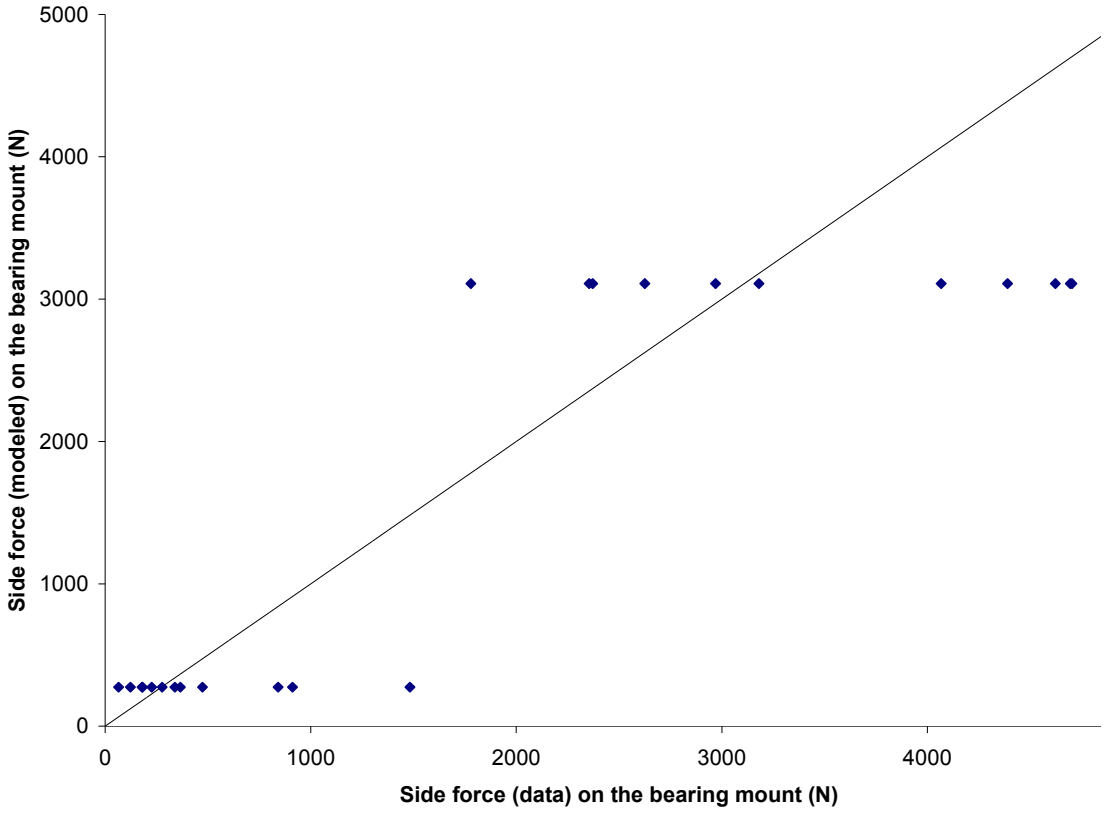

Figure 4.20: Comparison of predicted force vs. data for the side loading of the tine gang frame.

4.2.8 A comparison of the forces on the tine and on the frame

A comparison was made between the vertical forces on the frame and the forces on the tine to see if a relationship could be made between the two sets of data. By summing the component forces in the X and Y direction on the tine as they rotate through the soil (Figure 4.21) and multiplying that sum by the total number of tines, it was assumed that the resultant would be similar to the vertical forces on the frame. Due to the complexity of the tine shape and orientation, the analysis was carried out when the tine gang was place at an angle of 0º. In this position there should be low (assumed zero) loading in the Z direction, simplifying the calculations needed to sum the forces.

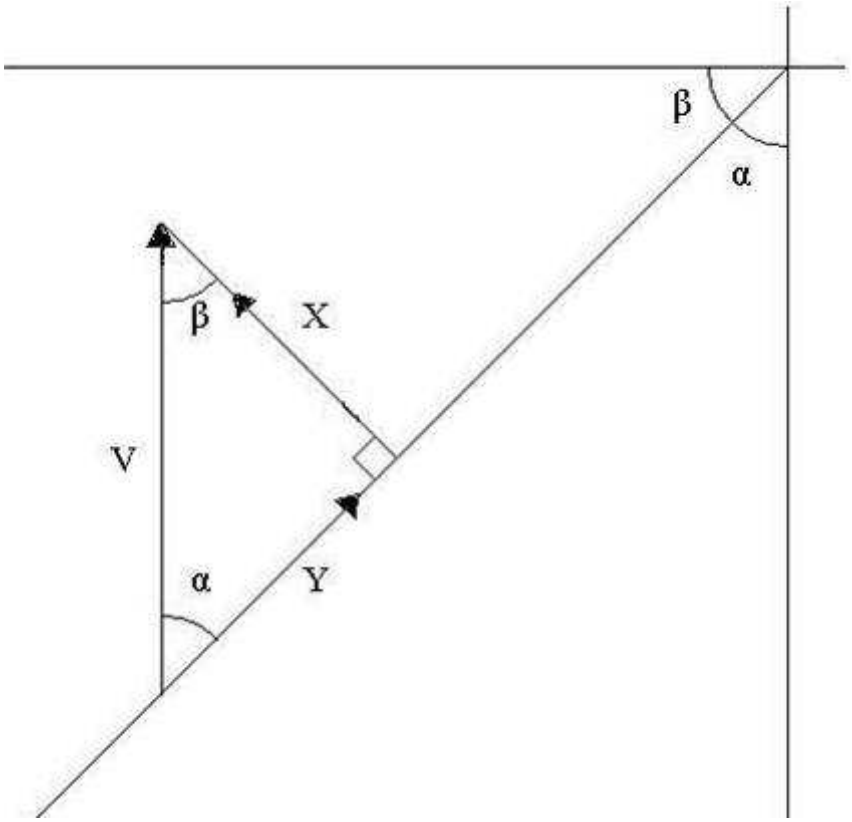

Figure 4.21: Vector diagram used to calculate the total forces (V is the total vertical force, X and Y is the forces in X and Y direction on the tine).

To calculate the total vertical forces created by the tines, 360º of the tine data in the X and Y direction was selected and their vertical components, based on rotary position, isolated using the following equation:

$$V = X\cos(\alpha) + Y\sin(\alpha) \qquad \textbf{[4.2]}$$

where V is the sum total of the absolute vertical force calculated from two component forces X and Y relative to the rotational angle (α), X is the forces in the X direction on the tine and Y is the force in the Y direction on the tine. As the data was only collected on one tine, and there being three tines in each set of tines, to recreate the total load created by a set of tines, the data segment was offset by 0º, 120º and 240º and summed (Figure 4.22).

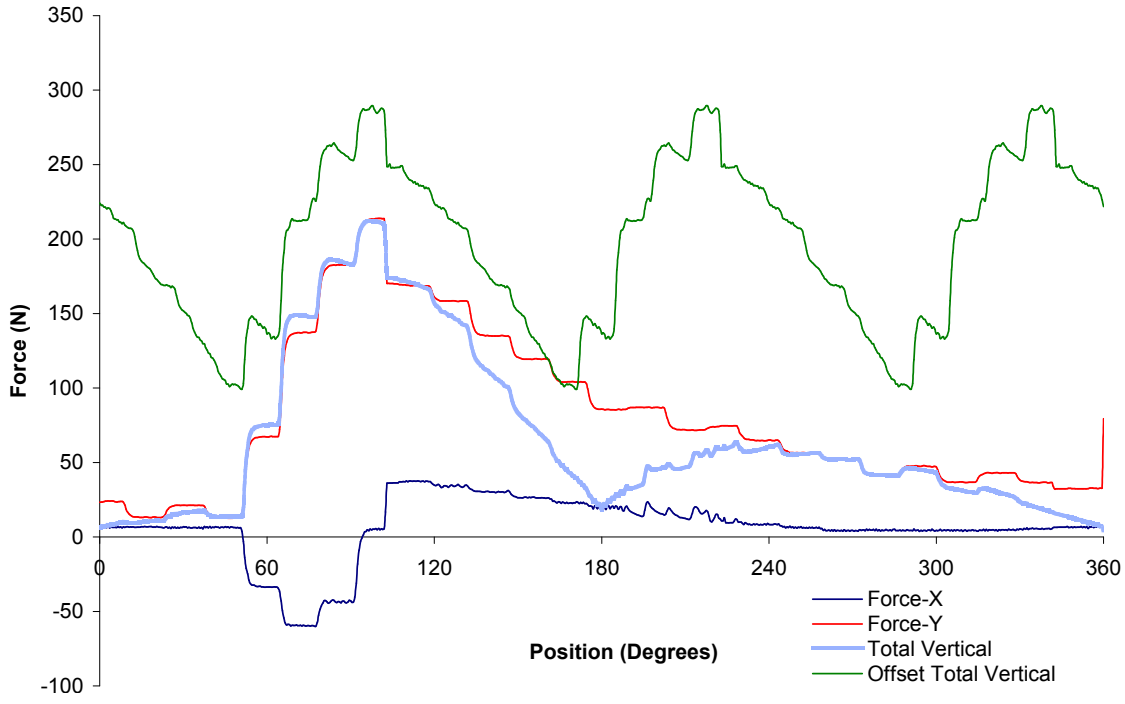

Figure 4.22: Modified tine data at 10cm depth, 0º tine gang angle and 2 km/h.

There are 6 sets of tines (three tines in each set) on the modular RTA that was used in the experiment, each set having a rotational offset of 20º. The total vertical

forces transferred by the tines would be a sum total of the forces from each set of tines on the modular RTA with each set having a rotational offset of 20º (Figure 4.23).

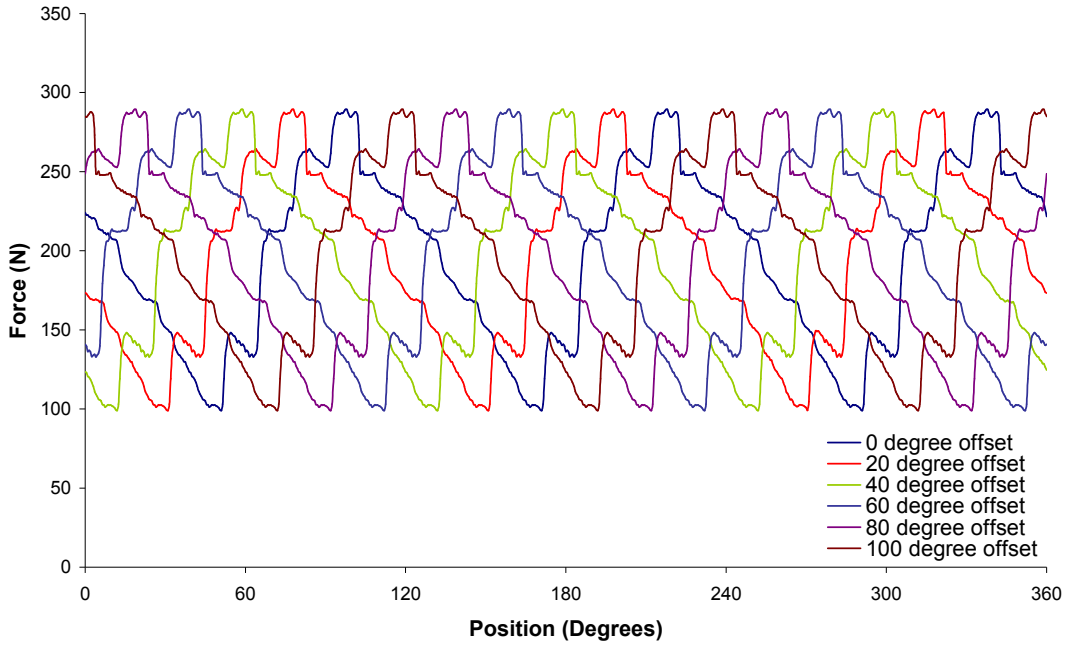

Figure 4.23: Tine force data set with 20º offset with six sets of data.

This total was compared to the total vertical forces measure by the EOR dynamometers (Figure 4.24). The average total calculated force from the tine data was 1.2 kN and average from the measured data was 2.3 kN. The average difference between the measured data and the calculated total from the tine data is a multiple of 1.96. Other sets of data with similar loading scenarios were summed with similar results.

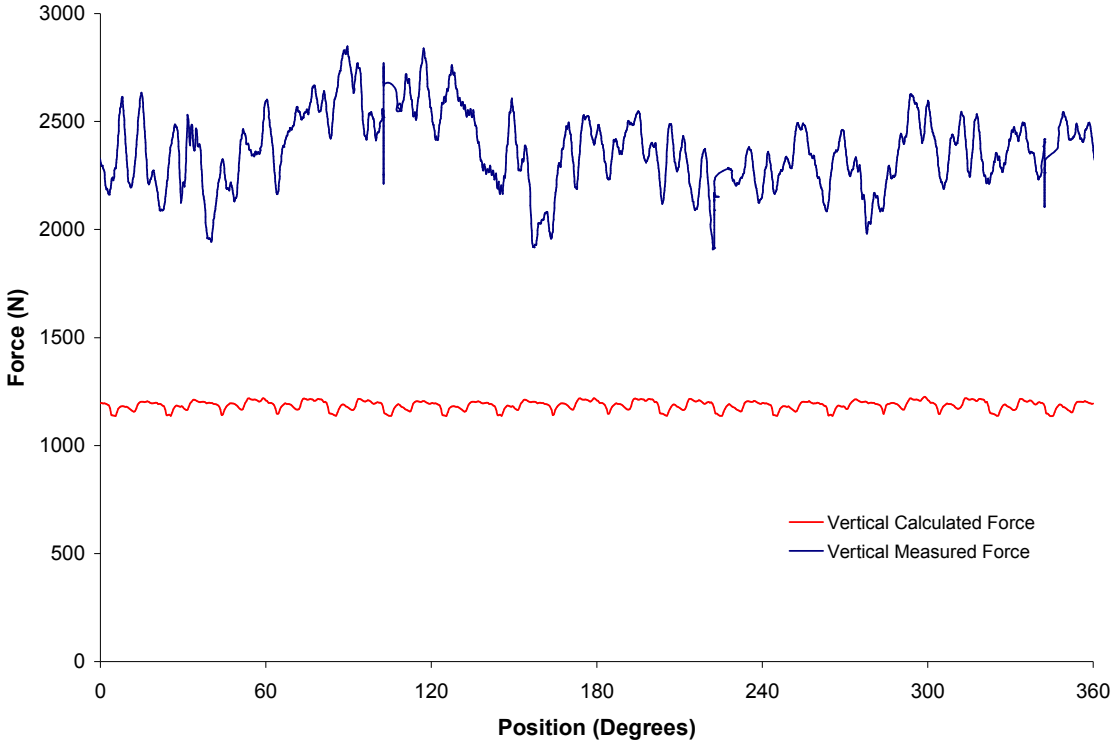

Figure 4.24: Plot showing the calculated vertical force based on the tine forces and measured vertical forces.

The cause of this discrepancy is assumed to be due to the calibration method used to calibrate the tine. The calibration equations for the tine were based on a point load at the tip of the tine. This was used because the tine, as a rotating body, would be engaged with the soil at varying depths through its rotation. The soil load on the tine would increase with the depth at which the tine engaged with the soil. This would result in the equivalent point load of the distributed soil load changing as the tine rotated through the soil. Furthermore, the tine being wedge shaped would result in having more surface loading at the wider portion of the tine closer to the axis of rotation. This change in shape would result in the loading being unevenly distributed. For these reasons, it was difficult to select a point for calibration that would represent the equivalent point load of

the soil load. Thus, the calibration equations were based on a point load on the tip of the tine.

If the equivalent point load of the soil loading was at some point midway between the tip of the tine and the axis of rotation, the forces measured in the X and Z direction would have the potential to be under valued (Figure 4.25). Depending on the distribution of the force, a range of forces could result in the same bending moment as the point load used in the calibration. The following equations show the possible force relationship between the calibration load and the soil load.

$$BM = F_S D_S = F_C D_C \quad \textbf{[4.3]}$$

$$F_S = F_C \times \frac{D_C}{D_S} \quad \textbf{[4.4]}$$

where BM is the bending moment, *Fs* is the force on the soil, *Fc* is the force used during the calibration, *Dc* is the distance from the gage location to the calibration load point and *Ds* is the distance from the gage location to the equivalent point load of the distributed load of the soil.

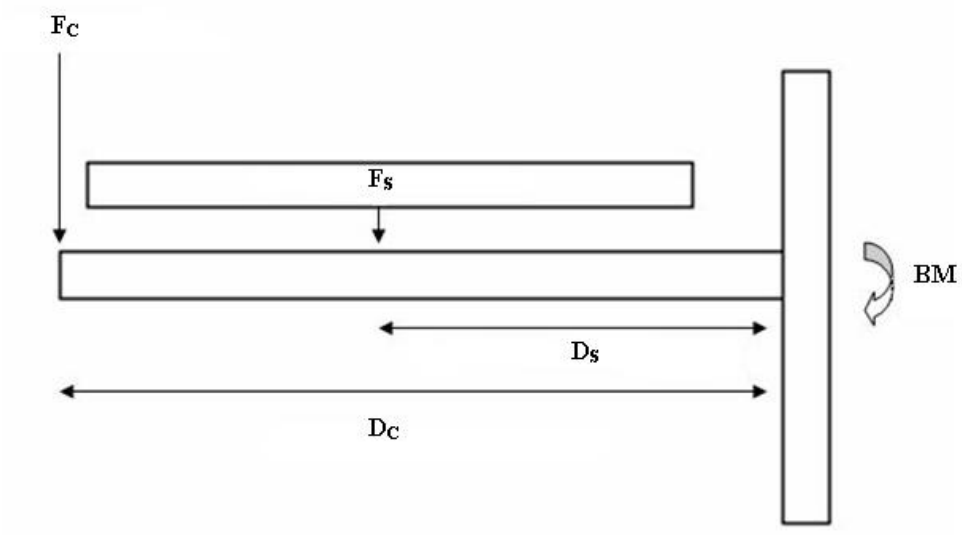

Figure 4.25: Diagram depicting the possible two different loading scenarios that could result in similar bending moments but vary different actual force values.

The values obtained from the gages placed to isolate the force on the tine in the Y direction should be accurate as their placement and orientation was such that they isolated only radial strain on the tine, not bending (Appendix A).

4.2.9 Residual strain and its possible effect on data analysis

The tine is made from austempered ductile iron (ADI). Ductile iron is similar to grey cast iron in the respect that the graphite precipitates out of the solution, but is different because graphite precipitates in the form of spherical particles as oppose to flakes. These nodules are formed using inoculants such as magnesium or cerium. Austempering uses a high-temperature salt quench-tank that causes the austenite to transform into acicular ferrite and high-carbon austenite. This heat treatment allows strengths comparable to carbon steels (Fisher 2005).

The tine that was instrumented for the experiment had to be machined to create a surface normal to the axis of rotation. Due to the difficulty of machining ADI, residual stress was more than likely induced into the material. The failure mechanism of the ADI when undergoing machining compares with that of ferrite ductile iron, yet the compression force is more than twice as high (Klocke *et al.* 2007). Machining under these conditions has the potential to induce high levels of residual stress. This stress from the machining processes could vary in magnitude and direction and has the potential to yield beneath the strain-gage grid (Prevey 1988). This yielding could be the cause of errors like that seen in figure 4.26.

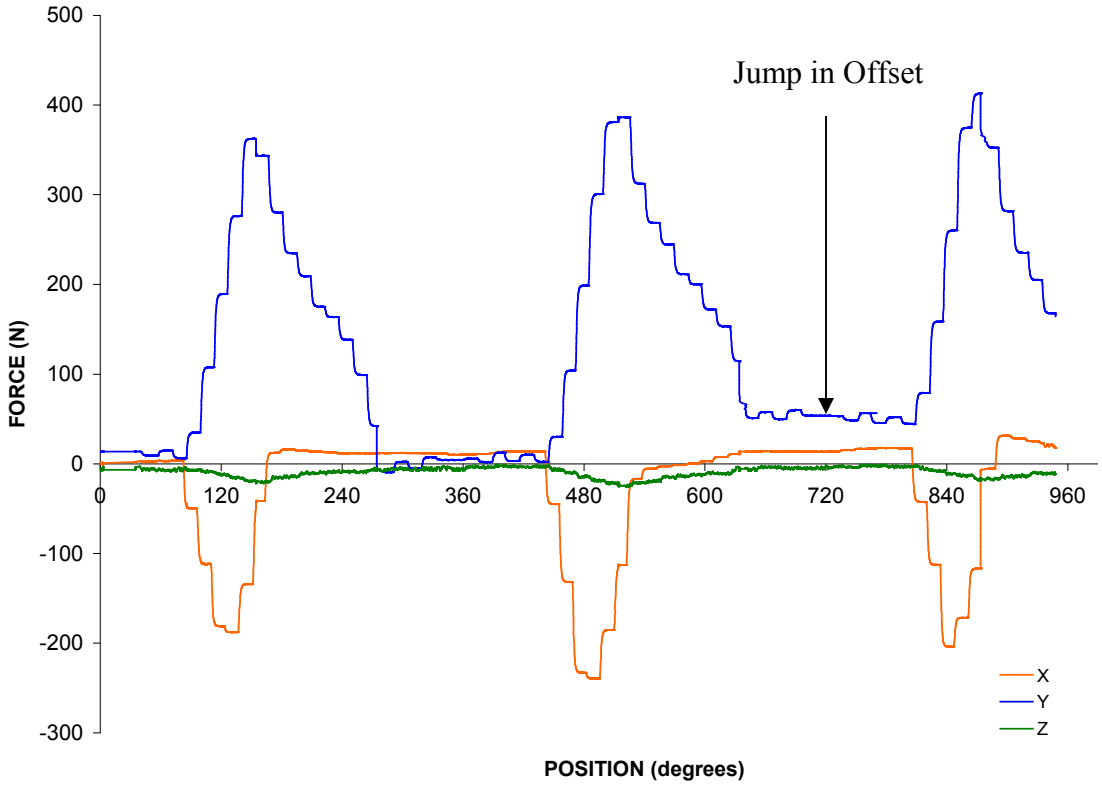

Figure 4.26: Tine loading results at 20 cm depth, 0 degrees tine gang angle and 2 km/h showing occasional change in offset in unloading.

In future experiments, it would be preferred to fabricate an instrumented adaptor to fix the tool being tested. Having an instrumented adaptor would allow for use of a more ductile material that would be easier to machine and would provide a better strain response under low loads. It would also allow the testing of a range of tine shapes in the same orientation and path of movement as previous tests, while maintaining the instrumentation in a consistent position.

CHAPTER 5: CONCLUSION

A new tillage philosophy, coined conservation tillage, has opened up a new realm of tillage equipment design. The aim of conservation tillage tools is to modify the soil structure while minimising disturbance to surface residue. The Rotary Tine Aerator (RTA) is a tool that fits this category but it is in the early stages of development in both design and application.

The objectives of this study were to; (1) measure the forces on the rotary tine aerator (RTA) while undergoing normal working conditions, and (2) to develop a statistical model of the tool loading. An experiment was carried out which varied the depth (10cm and 20cm), angle of the tine gang (0º and 10º) and forward velocity (2km/h and 4km/h). A statistical model was developed using the all possible regressions method.

This study showed that as depth increased, so did the loading on the tine in the X, Y and Z directions. When considering forces in the Z direction, it was seen that depth would interact with the rotational velocity and the angle of the tine gang. This interaction would result in a decreasing force on the tine, varying with depth, when increasing the rotational velocity of the tine.

The rotational velocity of the tine was seen to reduce forces on the tine in X, Y and Z directions. An increase in tine speed may have reduced the forces required to cause the soil to fail by inducing a brittle-like failure of the soil and resulting in more overlap of the soil failure zones.

The angle of the tine gang was seen to affect the loading of the tine in the Z direction and X direction. Increasing the gang angle from 0º to 10º opened up the broad flat side of the tine and exposes it to loading in the Z direction by the soil. In the X direction there was a reduction of loading when the gang was increased from 0º to 10º.

When considering the frame forces, depth was seen to increase vertical and draft loading on the tool frame. The side loading of the bearing mounts was primarily influenced by the angle of the tine gang. The forces increased when the gang angle increased. When the tine gang angle was set at 0º and 20cm depth, the side loading of the bearing mounts was seen to be applied in the opposite direction than all other loading scenarios. This result shows the importance of defining tool shape and orientation when modeling tillage tools.

Forward velocity of the frame was seen to have less of an effect on the frame forces than rotational velocity of the tine had on the tine forces. Forward velocity was only seen to be statistically significant when considering the vertical forces on the frame.

As only one tine was instrumented at the end of the tine gang, the relationships developed may not be consistent with the rest of the tines across the tine gang. It was suggested that in further experiments, a series of tines be instrumented at the beginning, middle and end of the tine gang, allowing for better insight into the affect neighbouring

tines would have on the tine load and whether this would be influenced by the rotational velocity of the tine.

When attempting to compare the sum of the component tine forces in the X and Y direction to the vertical forces on the frame there was a consistent under prediction. The under prediction of the vertical loading of the frame is assumed to be due to the calibration method used to calibrate the tine loading. Further investigation is required into loading of the tine with respect to its rotational position to determine the best calibration method for the tine.

The statistical models developed were seen to be a beneficial aid in the understanding the force relationships of the RTA. The all possible regressions method allowed for the assessment of many possible trends showing the degree of improvement of the test statistics as each regressor was added. This method could be seen to be cumbersome when analyzing data with many variables. The models developed fit well with the data.

CHAPTER 6: RECOMMENDATIONS

6.1 Areas of further study

The decreasing effect which rotational velocity had on the forces on the tine was noticed in all directions. This relationship contradicts force/velocity relationships of many studies of rigid tines. This relationship was more predominant at the deeper depths. It has been suggest by Miszczak (2005) in his study of a rotary subsoiler that overlap of soil failure zones could cause a reduction in the cohesion forces of the soil. This would result in lower forces on the tine. At higher velocities more soil movement occurs resulting in a larger area for overlap. A better understanding of the soil failure zone caused by the tine under various settings would be required to determine whether this would be a possible cause of the force / velocity relationship on the tine. Achieving a better understanding of the soil failure would also aid in optimizing the final soil condition suitable for slurry application while maintaining good soil surface finish.

Another aspect of interest would be the angle and offset at which the tine is placed relative to the center pivot. The current design uses a forward inclined tine relative to the direction at which the tine revolves (Figure 6.1). This orientation of the tool, relative to its path of travel around the tine shaft will affect the way forces are

transferred from the tine into the frame. An investigation into the effects of tine orientation on the draft and vertical forces on the frame and the forces in the X, Y and Z direction on the tine would be of interest for optimization of the tine mount.

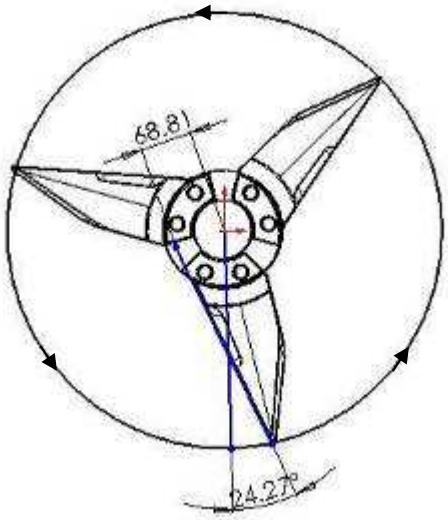

Figure 6.1: Figure showing the forward incline of tines relative to direction of travel.

The prominent application of this tool is its use in conjunction with manure application equipment. As depth is a major factor in the draft requirements for the implement, further study should be carried out to optimise the tine length specifically for the proper placement of liquid manure slurries. The objective of the tool should be to create a void suitable for the absorption of slurries at a depth optimal for root uptake.

6.2 Improvements to tine design

Depth is a key factor in the draft and vertical loading of the tool and frame. If the length of the tool could be reduced and still create a suitable void for manure absorption, the benefits will be seen in the reduction in the draft requirements.

The rotational velocity of the tine gang was a factor that showed to be affected by the tine gang angle. By increasing the rotational velocity of the tine gang, more soil

disturbance will occur allowing for more pockets per unit of area for slurry absorption. It was suggested in earlier chapters that one way of increasing the tine velocity was to adjust the rolling diameter of the tine by creating more soil tool friction. One possible method of achieving this is to create a broad section on the tine that would act against the soil at a set distance away from the axis of rotation. By moving this broad section closer to the tines rotational axis it would be possible to increase the rotational velocity of the tine's using the passive force of the soil (Figure 6.2).

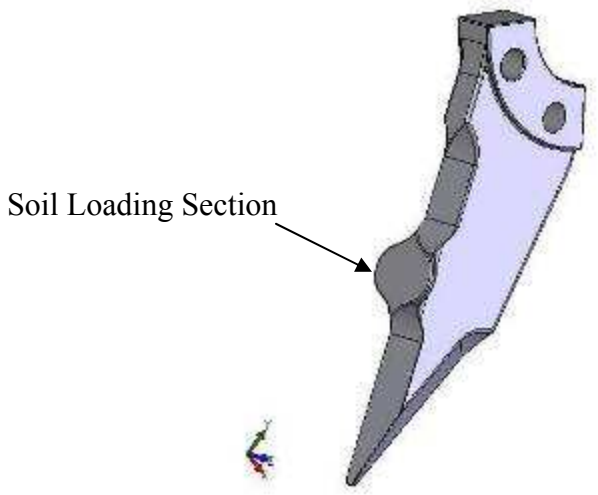

Figure 6.2: Tine concept aimed to increase rotational velocity of tine gang.

Another method of increasing the frequency of soil penetration would be to increase the number of tines on the tine gang. Going from three to four tines per revolution has been seen to be an effective way of increasing the frequency of soil penetration by other manufactures. The effect this would have on draft and vertical forces would have to identified and assessed against the benefits (or negative effects) of the extra soil failure.

With all design changes it is important to maintain the benign nature of the tillage tool, as it is the main reason why it has seen so much attention in the slurry application

industry. Without this benign effect to crop potential, the RTA system would lose its advantage over other slurry application tillage tools.

REFERENCES

ANON. 2002. Conservation Technology Information Center Avaliable at: http://www.ctic.purdue.edu/Core4/CT/Definitions.html [Accessed on December 1 2005]

ANON. 1999. Fundamentals of Statistical Interactions. [Accessed on November 17 2006]. Available at: http://www.ruf.rice.edu/~branton/interaction/faqfund.htm

ASAE Standards. 2005. EP291.3: Terminology and definitions for soil tillage and soil tool relationships – Agricultural Equipment. St. Joseph, Mich.: ASAE.

ASAE Standards. 2009. S313.3: Soil Cone Penetrometer. ASAE St. Joseph, Mich.: ASAE.

ASTM. 1988. "1988 Annual Book of ASTM Standards", Vol.4.08. *Soil and Rocks, Building Stones; Geotextiles*.

Bengough, A.G., M. F. Bransby, J. Hans, S.J. McKenna, T.J. Roberts. T.A. Valentine, 2006. Root responses to soil physical conditions; growth dynamics from field to cell, *Journal of Experimental Botany*. 5 (2): 437-447.

Bittman, S., L.J.P van Vliet, C. G. Kowalenko, S. McGinn, D.E. Hunt, F. Bounaix, 2005. Surface-Banding Liquid Manure over Aeration Slots: A New Low-Disturbance Method for Reducing Ammonia Emissions and Improving Yields of Perennial Grasses. *American Society of Agronomy*. 97: 1304-1313.

Chen, Y., Q, Zhang, and D Petkau, 2000, *Evaluation of different techniques for liquid manure application on grassland*, CSAE/SCGR Paper No. FL099

Davies, A., W.A. Adams and D. Wilman, 1989. Soil compaction in permanent pasturs and its amelioration by slitting. *Journal of Agricultural Sicence*, Cambridge 113: 189-197.

Dabney, S.M., J.A. Delgado, and D.W. Reeves, 2001. Using winter cover crops to improve soil and water quality. *Commun. Soil. Sci. Plant Anal*. 32 (7&8):1221-1250.

Douglas, J.T., Crawford, D.J., Campbell, D.J. 1995. Traffic Systems and Soil Aeration Effects on Grassland for Silage Production. *Journal of Agricultural Engineering Research* 60: 261-270.

Elijah, D.L., J. A. Weber. Soil failure and pressure patterns for flat cutting blades. *Transaction of the ASAE* 14(4): 597-617.

Fisher, L.W. 2005.*Selection of Engineering Materials and Adhesives*. Taylor and Francis: Boca Ranton.: 233-266.

Fortune, R.A., P.D. Forristal and F.Kelly. 1999. Effects of soil aeration in minimising/alleviating soil compaction and sward damage in grasslands. Available at: http://www.teagasc.ie/research/reports/crops/4352/eopr-4352.htm . [Accessed on December 10, 2006].

Gill, W.R., and G.E. Vanden Berg. 1968. Design of tillage tools. In *Soil Dynamics in Tillage and Traction.* U.S. Government Printing Office. 211-297.

Guerif, J., G. Richard, C. Durr, J.M. Machet, S. Recous, and J. Roger-Estrade, 2001. A review of tillage effects on crop residue management, seedbed conditions and seedling establishment, *Soil and tillage Research* 61: 13-32.

Harrigan, T.M., D.R. Mutch,. S.S. Snapp, 2006. *Stabilizing Nutrient-Rich Farm Land with Manure Slurry-Enriched Seeding of Cover Crops in Diverse Cropping Systems*. ASABE Paper No. 061031. Portland, Oregon: ASABE.

Harrigan, T., S. Snapp, R. Leep, D. Mutch, and N. Rector. 2007. *Manure Slurry-Enriched Seeding of Cover Crops*. Resource 14 (2):6-7.

Hayes, W.A. 1985. Conservation tillage systems and equipment requirements. In *A Systems Approach to Conservation Tillage*. 21-40. Chelsea Michigan. Lewis Publishers, Inc.

Hendrick, J.G., W. R. Gill, 1971. Rotary tiller design parameters part I – direction of rotation. *Transactions of the ASAE*: 669-674.

Hendrick, J.G., W. R. Gill, 1971. Rotary tiller design parameters part II – depth of tillage. *Transactions of the ASAE*: 675-678.

Hendrick, J.G., W. R. Gill, 1971. Rotary tiller design parameters part III – ratio of peripheral and forward velocities. *Transactions of the ASAE*: 679-683.

Hendrick, J.G., W. R. Gill, 1974. Rotary tiller design parameters part IV – blade clearance angle. *Transactions of the ASAE*: 4-7.

Hendrick, J.G., W. R. Gill, 1978. Rotary tiller design parameters part V – kinematics. *Transactions of the ASAE*: 658-660.

Johnson, C.E., A.C. Bailey. 2002. Soil compaction. In *Advances in Soil Dynamics Volume 2*. 155-178. St. Joseph, Mich.: ASAE.

King, K.W., D.C. Flanagan, L.D. Norton, and J.M. Laflen. 1995. Rill erodibility parameters influenced by long-term management practices. *American Society of Agricultural Engineers* 38(1): 159-164.

Klocke, F., C. Klopper, D.Lung and C. Essig. 2007. Fundamental wear mechanisms when machining austempered ductile iron (ADI). *Annals of the CIRP* 56(1): 73-76.

Lafond, G.P and A. Derksen. 1996. Long-term potential of conservation tillage on the Canadian prairies. *Canadian Journal of Plant Pathology* 18:151-158.

Leroueil, S., J. Magnan, F. Tavenas, 1990. *Embankments on Soft Clays*. Ellis Horwood. New York.

Malhi, S.S., Heier, K., Nielsen, K., Davies, W.E. and Gill, K.S. 2000. Efficacy of pasture rejuvenation hrough mechanical aeration or N fertilization. *Can.J. Plant Sci*. 80: 813-815.

McKyes, E. 1985. *Soil Cutting and Tillage*, *Developments in agricultural engineering 7*. Elsevier. New York.

Misselbrook, T.H., F.A. Nicholson, B.J. Chambers, 2005. Predicting ammonia losses following the application of livestock manure to land. *Bioresource Technology* 96: 159-168.

Miszczak, M. 2005. A torque evaluation for a rotary subsoiler. *Soil and Tillage Research* 84: 175-183.

Mrabet, R., K. Ibno-namr, F. Bessam and N. Saber. 2001. Soil chemical quality changes and implications for fertilizer management after 11 years of no-tillage wheat production system in semiarid Morocco. *Land Degradation and Development* 12: 505-517.

Onwualu, A.P. and K.C. Watts. 1998. Draught and vertical forces obtained from dynamic soil cutting by plane tillage tools. *Soil & Tillage Research* 48: 239-253.

Perumpral, J.V., R.D. Grisso, C.S. Desai. 1983. A Soil-Tool Model Based on Limit Equilibrium Analysis. *Transactions of the ASAE.* 26(4): 991-993.

Prevey, P.S. 1988. Residual-stress distributions produced by strain-gage surface preparation. *Experimental Mechanics* 28(1): 92-97.

Rajaram, G., and D. Gee-Clough. 1988. Force-Distance Behaviour of Tine Implements. *Journal of Agricultural Research* 41: 81-98.

Rosa, U.A. and D. Wulfsohn. 1999. Constitutive model for high speed tillage using narrow tools. *Journal of Terramechanics* 36: 221-234.

Sanchez-Giron, V., J.J Ramirez, J.J. Litage, and J.L. Hernanz. 2005. Effect of soil compaction and water content on the resulting forces acting on three seed drill furrow openers. *Soil & Tillage Research* 81: 25-37.

Shah, S.B., J.L Miller, T.J. Basden, 2004. Mechanical Aeration and Liquid Dairy Manure Application Impacts on Grassland Runoff Water Quality and Yield. *Transactions of the ASAE* 47(3):777-778.

Sharifat, K., R.L. Kushwaha 2000. Modeling soil movement by tillage tools. Canadian Agricultural Engineering 43(4):165-172.

SPSS. 2004. *SigmaPlot for Windows*. Ver. 13. Chicago, Ill.: SPSS, Inc.

Stafford, J.V. 1979. The performance of a rigid tine in relation to soil properties and speed. *Journal of Agriculture Engineering Research* 25: 41-56.

Swick, W.C. and Perumpral, J.V. 1988. A model for predicting soil tool interaction. *Journal of Terramechanics* 25 (1): 43-56.

Thankur, T.C and R.J. Godwin. 1989. The present state of force prediction models for rotary powered tillage tools. Journal of Terramechanics 26 (2): 121-138.

Wismer, R.D. and Luth, H.J. 1972. Performance of plan soil cutting blades in clay. *Transactions of the ASAE* 15(2): 211- 216.

CHAPTER 7: Appendices

APPENDIX A

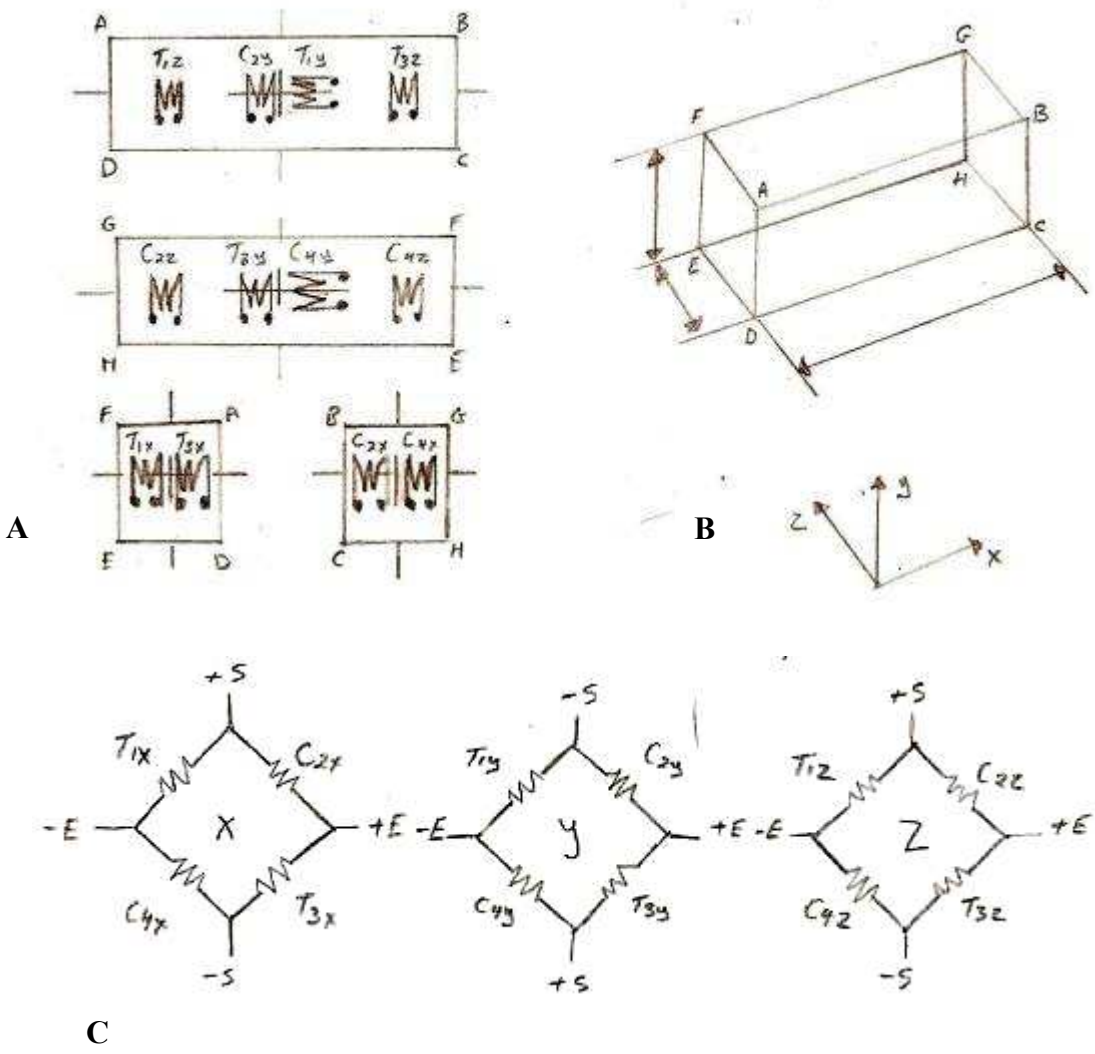

Figure 7.1: Diagram showing the orientation of strain gages on machined portion of the tine (A), a simplified representation of the machined portion of the tine (B) and wiring diagram of the strain gages (C).

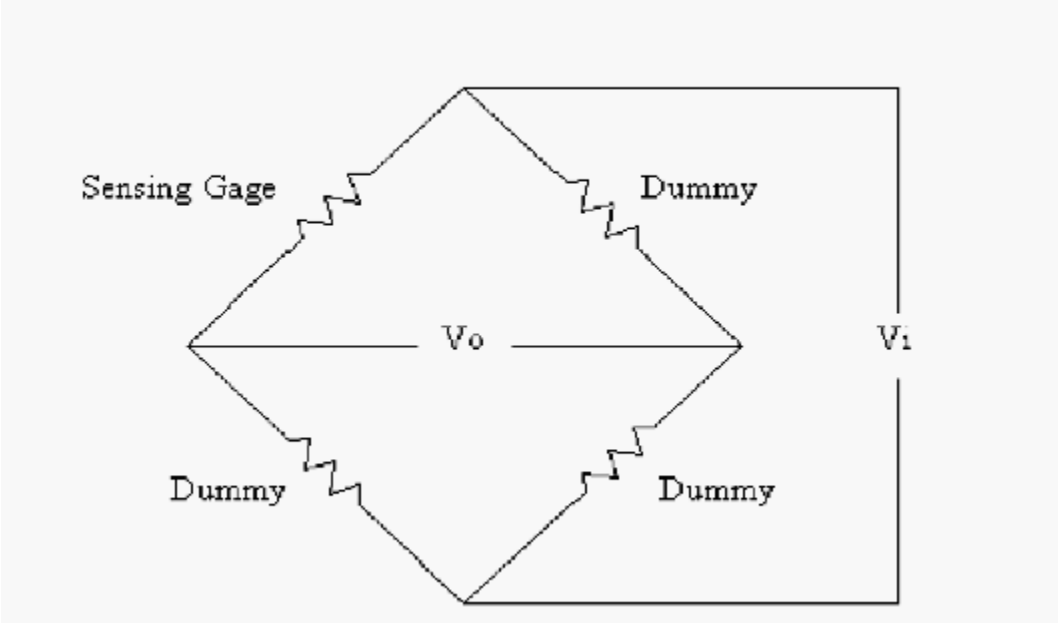

Figure 7.2: Diagram showing the arrangement of the gages used to measure the side forces on the bearing mounts of the tine gang.

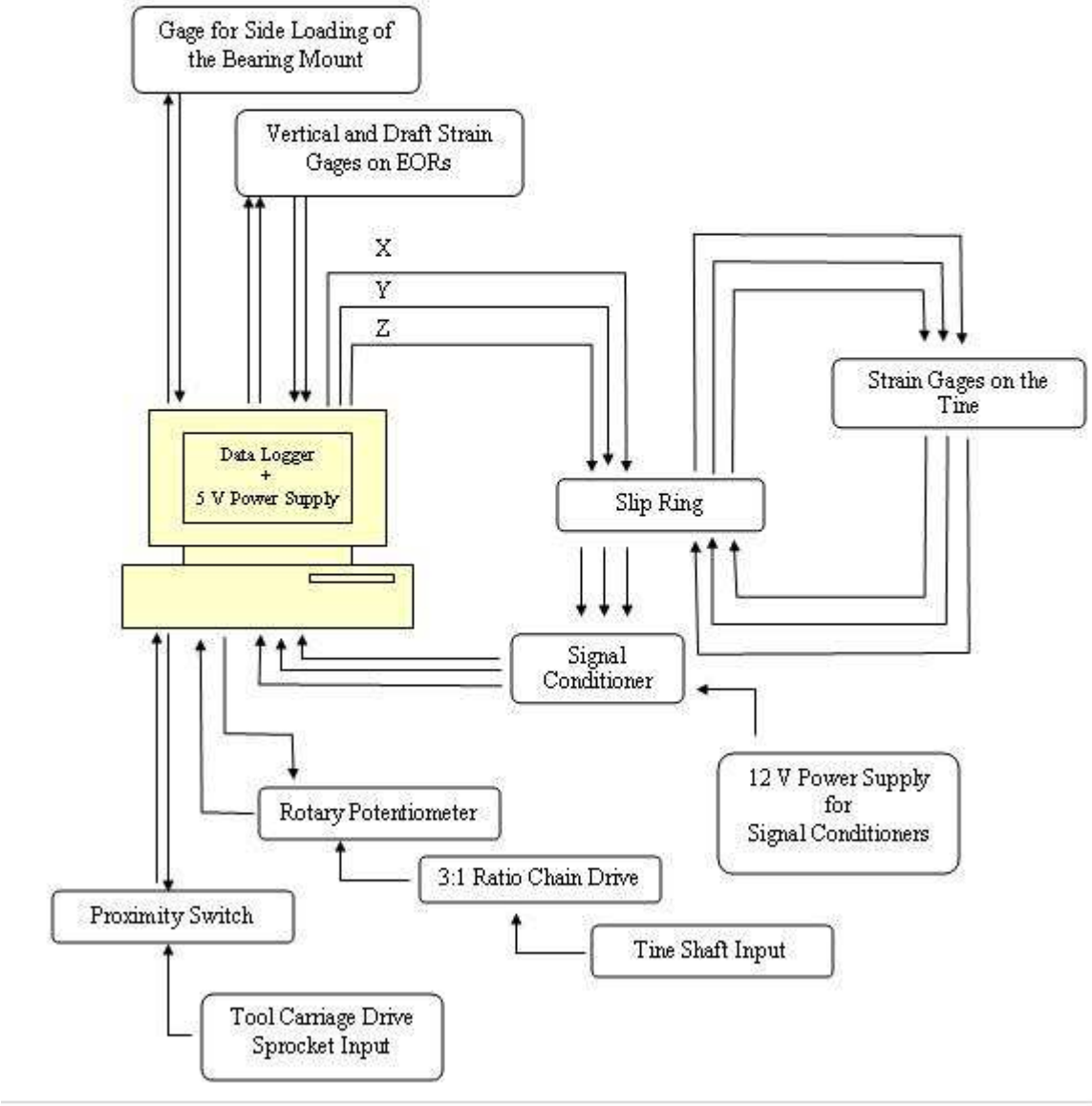

Figure 7.3: Flow chart for instrumentation.

APPENDIX B

Calibration Data for the Tine

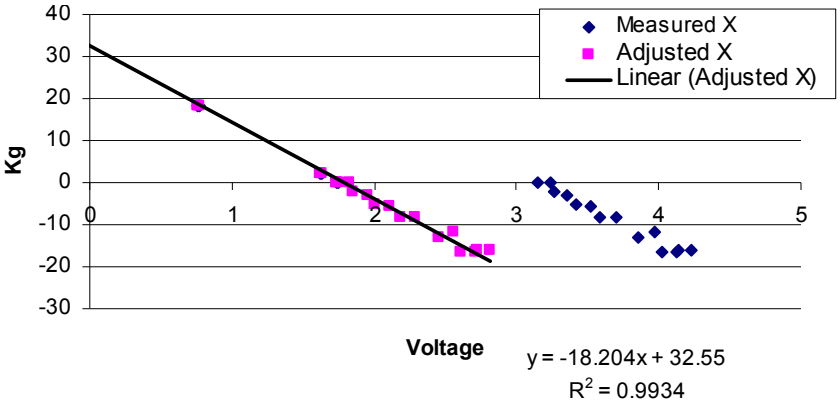

Figure 7.4: Calibration data for strain gages in the X direction.

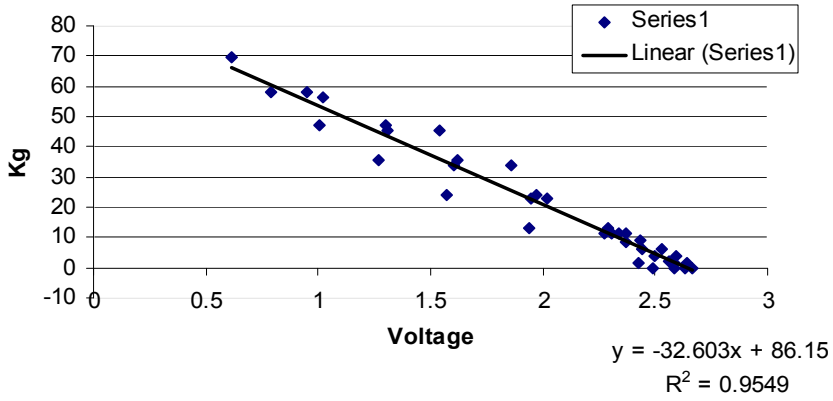

Figure 7.5: Calibration data for the forces in the Y direction.

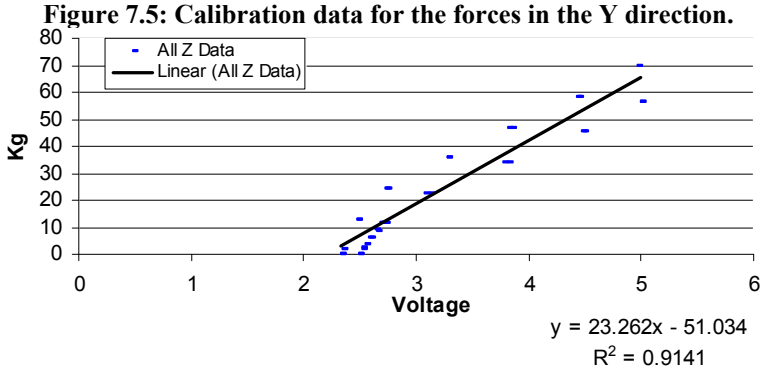

Figure 7.6: Calibration data for the forces in the Z direction

Tine Calibration Raw Data

Table 7.1: Calibration data for the tine in the X direction

		qi	qo					
	Y	ADJ Y	Mass	qi*qo	qi^2	qo^2	yixi	
	1.73295	1.73295	0	0	3.003116	0	yi	
	1.61855	1.61855	2.3331	3.776239	2.619704	5.443356	xi	
	0.753741	0.753741	18.3113	13.80198	0.568125	335.3037	xi	
	-0.012351	-0.012351	34.2895	-0.423496	0.000153	1175.77	yi	
	-0.0299	-0.0299	34.2895	-1.025242	0.000894	1175.77		
	0.773166	0.773166	18.3113	14.15767	0.597786	335.3037		
	1.62663	1.62663	2.3331	3.79509	2.645925	5.443356		
	1.75284	1.75284	0	0	3.072448	0		
	3.14848	1.73948	0	0	3.025791	0		
	3.25884	1.84984	-2.3331	-4.315862	3.421908	5.443356		
	3.41619	2.00719	-5.22473	-10.48703	4.028812	27.2978		
	3.59133	2.18233	-8.43451	-18.40688	4.762564	71.14096		
	3.85905	2.45005	-13.13606	-32.184	6.002745	172.5561		
	4.02301	2.61401	-16.35291	-42.74667	6.833048	267.4177		
	4.13484	2.72584	-16.0489	-43.74673	7.430204	257.5672		
	4.22969	2.82069	-16.0489	-45.26897	7.956292	257.5672		
	4.12398	2.71498	-16.35291	-44.39782	7.371116	267.4177		
	3.96723	2.55823	-11.65136	-29.80686	6.544541	135.7542		
	3.69747	2.28847	-8.44158	-19.3183	5.237095	71.26027		
	3.51566	2.10666	-5.54995	-11.69186	4.438016	30.80195		
	3.35833	1.94933	-3.21685	-6.270702	3.799887	10.34812		
	3.23308	1.82408	0	0	3.327268	0		
Total:	59.77281	40.04681	-12.92396	-274.5595	86.68744	4607.606		

Sum(qiqo)	-274.5595
Sum(qo)	-12.92396
Sum(qi)	40.04681
Sum(qi)^2	86.68744
Sum(qo)^2	4607.606
N	22
Avg qo	-0.587453
Avg qi	1.820309
M	-18.20424
b	32.54989
R^2	0.993449

Table 7.2:Calibration data for the tine in the Y direction

		qi	qo					
	Y	ADJ Y	Mass	qi*qo	qi^2	qo^2	yixi	
	2.48638	2.48638	0	0	6.182086	0	yi	
	2.42157	2.42157	1.65	3.995591	5.864001	2.7225	xi	
	1.94203	1.94203	12.95	25.14929	3.771481	167.7025	xi	
	1.56919	1.56919	24.25	38.05286	2.462357	588.0625	yi	
	1.2649	1.2649	35.55	44.9672	1.599972	1263.803		
	1.00447	1.00447	46.85	47.05942	1.00896	2194.923		
	0.79051	0.79051	58.15	45.96816	0.624906	3381.423		
	0.616405	0.616405	69.45	42.80933	0.379955	4823.303		
	0.947788	0.947788	58.15	55.11387	0.898302	3381.423		
	1.30149	1.30149	46.85	60.97481	1.693876	2194.923		
	1.61929	1.61929	35.55	57.56576	2.6221	1263.803		
	1.9726	1.9726	24.25	47.83555	3.891151	588.0625		
	2.28769	2.28769	12.95	29.62559	5.233526	167.7025		
	2.58841	2.58841	1.65	4.270876	6.699866	2.7225		
	2.63203	2.63203	0	0	6.927582	0		
	3.11564	2.66624	0	0	7.108836	0		
	3.0942	2.6448	1.65	4.36392	6.994967	2.7225		
	3.0459	2.5965	3.695	9.594068	6.741812	13.65303		
	2.98092	2.53152	5.965	15.10052	6.408594	35.58123		
	2.88523	2.43583	9.29	22.62886	5.933268	86.3041		
	2.82273	2.37333	11.565	27.44756	5.632695	133.7492		
	2.7873	2.3379	11.35	26.53517	5.465776	128.8225		
	2.46504	2.01564	22.675	45.70464	4.062805	514.1556		
	2.31239	1.86299	33.975	63.29509	3.470732	1154.301		
	1.98801	1.53861	45.255	69.6298	2.367321	2048.015		
	1.46776	1.01836	56.58	57.61881	1.037057	3201.296		
	1.7596	1.3102	45.255	59.2931	1.716624	2048.015		
	2.05039	1.60099	33.975	54.39364	2.563169	1154.301		
	2.39643	1.94703	22.675	44.14891	3.790926	514.1556		
	2.72442	2.27502	11.35	25.82148	5.175716	128.8225		
	2.75294	2.30354	11.565	26.64044	5.306297	133.7492		
	2.8156	2.3662	8.24	19.49749	5.598902	67.8976		
	2.89168	2.44228	5.97	14.58041	5.964732	35.6409		
	2.94527	2.49587	3.925	9.79629	6.229367	15.40563		
	3.00803	2.55863	2.275	5.820883	6.546587	5.175625		
	3.03175	2.58235	0	0	6.668532	0		
Totals:	80.78598	71.34858	775.48	1105.299	154.6448	31442.34		

Sum(qiqo)	1105.299
Sum(qo)	775.48
Sum(qi)	71.34858
Sum(qi)^2	154.6448
Sum(qo)^2	31442.34
N	36
Avg qo	21.54111
Avg qi	1.981905
M	-32.6035
b	86.15815
R^2	0.954875

Table 7.3: Calibration data for the tine in the Z direction

qi	qo	y					
Volt	Kg	Pre KG	SSE	qi*qo	qi^2	qo^2	yixi
2.49258	0	6.948396	48.28021	0	6.212955	0	yi
2.51358	1.65	7.436898	33.48819	4.147407	6.318084	2.7225	xi
2.54218	3.695	8.102191	19.42333	9.393355	6.462679	13.65303	xi
2.57608	5.965	8.890773	8.560147	15.36632	6.636188	35.58123	yi
2.63587	9.29	10.28161	0.983286	24.48723	6.947811	86.3041	
2.68267	11.565	11.37027	0.03792	31.02508	7.196718	133.7492	
2.71231	11.35	12.05976	0.503752	30.78472	7.356626	128.8225	
3.069	22.675	20.35708	5.372762	69.58958	9.418761	514.1556	
3.7709	33.975	36.68468	7.342343	128.1163	14.21969	1154.301	
4.46787	45.255	52.89759	58.40921	202.1935	19.96186	2048.015	
4.99756	56.58	65.21924	74.63648	282.7619	24.97561	3201.296	
4.99756	56.58	65.21924	74.63648	282.7619	24.97561	3201.296	
4.48438	45.255	53.28165	64.42707	202.9406	20.10966	2048.015	
3.81047	33.975	37.60515	13.17801	129.4607	14.51968	1154.301	
3.12169	22.675	21.58275	1.193004	70.78432	9.744948	514.1556	
2.72482	11.35	12.35076	1.001526	30.92671	7.424644	128.8225	
2.69496	11.565	11.65616	0.00831	31.16721	7.262809	133.7492	
2.65301	8.24	10.68032	5.955155	21.8608	7.038462	67.8976	
2.59011	5.97	9.217139	10.54391	15.46296	6.70867	35.6409	
2.55176	3.925	8.325041	19.36036	10.01566	6.511479	15.40563	
2.51363	2.275	7.438061	26.6572	5.718508	6.318336	5.175625	
2.49285	0	6.954677	48.36753	0	6.214301	0	
2.33666	0	3.321385	11.0316	0	5.45998	0	
2.34893	1.65	3.60681	3.829104	3.875735	5.517472	2.7225	
2.47988	12.95	6.652969	39.6526	32.11445	6.149805	167.7025	
2.74199	24.25	12.75017	132.2461	66.49326	7.518509	588.0625	
3.27548	35.55	25.16022	107.9476	116.4433	10.72877	1263.803	
3.81402	46.85	37.68773	83.94713	178.6868	14.54675	2194.923	
4.42051	58.15	51.7959	40.37454	257.0527	19.54091	3381.423	
4.95959	69.45	64.33598	26.15317	344.4435	24.59753	4823.303	
4.44887	58.15	52.45561	32.42603	258.7018	19.79244	3381.423	
3.85085	46.85	38.54447	68.98178	180.4123	14.82905	2194.923	
3.2774	35.55	25.20488	107.0215	116.5116	10.74135	1263.803	
2.72979	24.25	12.46637	138.8538	66.19741	7.451753	588.0625	
2.47985	12.95	6.652271	39.66139	32.11406	6.149656	167.7025	
2.34846	1.65	3.595877	3.786435	3.874959	5.515264	2.7225	
2.33549	0	3.294168	10.85155	0	5.454514	0	
Totals: 116.9436	832.06	832.0843	1369.131	3255.887	396.5293	34643.63	

Sum(qiqo)	3255.887
Sum(qo)	832.06
Sum(qi)	116.9436
Sum(qi)^2	396.5293
Sum(qo)^2	34643.63
N	37
Avg qo	22.48811
Avg qi	3.160638
M	23.26194
b	-51.03445
R^2	0.914065

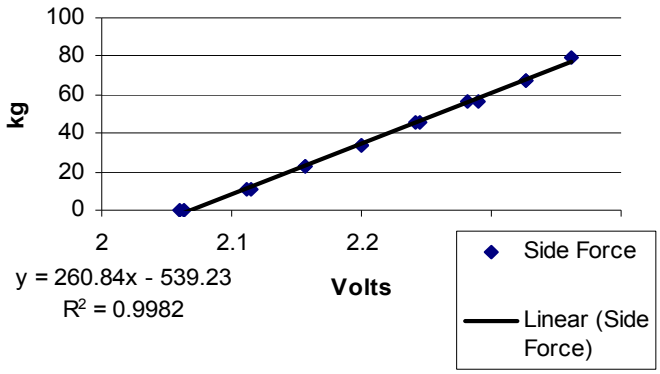

Figure 7.7: Calibration data for the side loading on the frame.

Table 7.4: Calibration data for the loading on the bearing mounts.

	qi		qo				
	V	Mass	Adjusted Mass	qi*qo	qi^2	qo^2	yixi
	2.06	0.00	0.00	0.00	4.24	0.00	yi
	2.11	22.70	11.35	23.96	4.46	128.82	xi
	2.16	45.30	22.65	48.86	4.65	513.02	xi
	2.20	67.90	33.95	74.69	4.84	1152.60	yi
	2.24	90.50	45.25	101.55	5.04	2047.56	
	2.29	113.10	56.55	129.46	5.24	3197.90	
	2.33	135.70	67.85	157.91	5.42	4603.62	
	2.36	158.30	79.15	186.94	5.58	6264.72	
	2.33	135.70	67.85	157.92	5.42	4603.62	
	2.28	113.10	56.55	129.02	5.21	3197.90	
	2.24	90.50	45.25	101.40	5.02	2047.56	
	2.20	67.90	33.95	74.69	4.84	1152.60	
	2.16	45.30	22.65	48.85	4.65	513.02	
	2.11	22.60	11.30	23.89	4.47	127.69	
	2.06	0.00	0.00	0.00	4.26	0.00	
Totals:	33.13	1108.60	554.30	1259.13	73.33	29550.66	

Sum(qiqo)	1259.13
Sum(qo)	554.30
Sum(qi)	33.13
Sum(qi)^2	73.33
Sum(qo)^2	29550.66
N	15.00
Avg qo	36.95
Avg qi	2.21
M	260.84
b	-539.23
R^2	0.9982

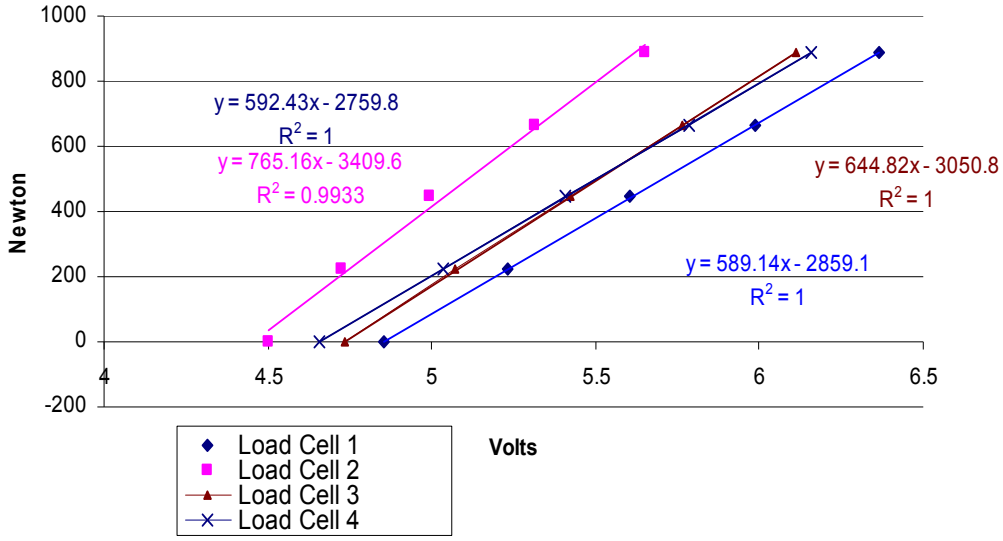

Figure 7.8: Calibration curves for the EOR.

Table 7.5: Raw data for the calibration of the EORs.

Force (N)	Load Cell 1 (V)	Load Cell 2 (V)	Load Cell 3 (V)	Load Cell 4 (V)
0	4.854	4.503	4.733	4.658
222.4	5.23	4.723	5.074	5.034
444.8	5.606	4.995	5.421	5.41
667.2	5.987	5.316	5.765	5.784
889.6	6.363	5.65	6.112	6.16

APENDIX C

Atterberg Limit Tests

Table 7.6: Data collected for the determination of the plasticity index.

Liquid Limit				**Plastic Limit**		
Trial No	1	2	3	Trail No	1	2
No. Blows	39	16	28	Container No	T5-6	T5-11
Moisture Content	0.38	0.42	0.41	Moisture Content	15.01	13.55
Derived Value				Average Value		
W_L=	40.983			W_P=	14.28	
				Ip=	26.70	

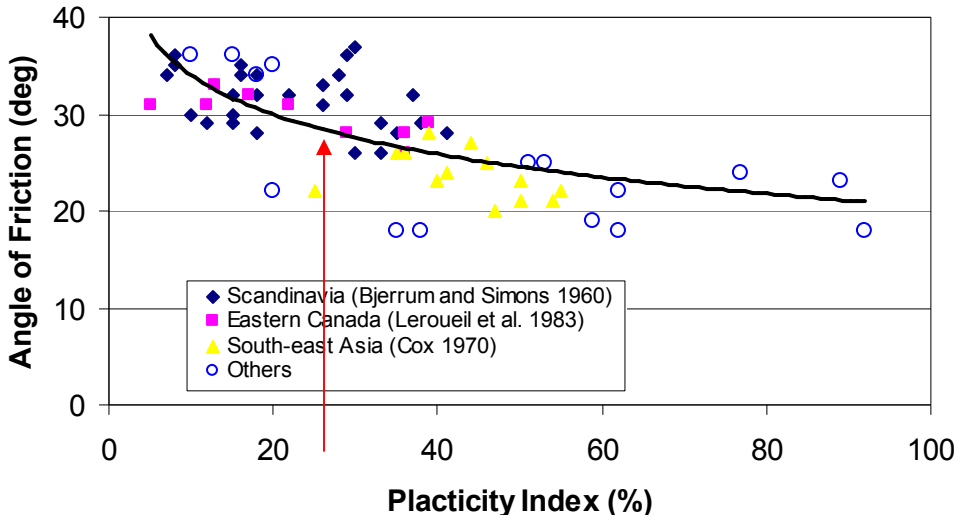

Figure 7.9: Relationship between plasticity index and angle of internal friction (Reproduced from Leroueil *et al.* 1990)

APPENDIX D

Table 7.7: Summary table of results.

Settings				Soil Data		Cone Penetrometer N/cm2					Average Forces (N)					
Depth	Angle	Tine RPM	Speed	DBD	DB MC	5	10	15	20	25	Max X	Max Y	Max Z	Side	Draft	Vertical
4	10	39.7	4.13	1.17	0.123	189.4	296.0	249.4	182.1	155.8	-31.5	183.0	-47.9	-3180.6	1576.7	2175.5
4	10	19.5	2.12	1.23	0.128	162.0	229.8	253.3	283.5	229.3	-65.3	217.5	-102.1	-2354.2	1164.2	2124.0
4	10	38.9	4.18	1.25	0.122	170.4	287.4	382.3	320.3	267.6	-56.1	154.2	-72.9	-4067.4	2020.4	2939.0
4	10	18.0	2.07	1.24	0.121	150.0	299.4	482.7	429.3	394.3	-59.1	293.6	-62.1	-2969.9	1520.3	2153.2
4	10	35.7	4.12	1.22	0.124	219.9	293.7	443.3	428.5	384.7	-29.9	157.5	-33.9	-2625.5	1297.0	1997.3
4	10	17.9	2.05	1.25	0.120	199.8	341.1	547.4	471.5	349.0	-47.7	274.9	-73.6	-2371.5	1133.3	2026.3
4	0	21.8	2.16	1.25	0.128	201.4	298.9	383.4	398.8	252.8	-83.0	85.3	-17.1	-64.6	1114.5	2782.2
4	0	41.8	4.14	1.23	0.130	152.9	266.6	382.1	369.6	277.3	-34.5	33.2	-10.3	-181.6	969.7	2507.6
4	0	18.6	2.00	1.24	0.121	158.4	293.4	481.7	415.5	354.7	-62.2	225.8	-16.9	-226.3	1029.6	2337.0
4	0	38.2	4.07	1.23	0.121	155.5	291.1	529.1	528.1	370.3	-61.8	83.0	-15.1	-339.4	1573.4	3411.6
4	0	18.0	1.92	1.23	0.120	189.7	331.8	439.7	374.0	305.7	-73.7	249.9	-15.5	-277.6	1077.4	2572.0
4	0	38.3	4.05	1.25	0.118	169.9	398.2	364.6	306.5	199.8	-71.6	140.2	-42.9	473.4	1498.8	3756.2
8	0	38.3	3.59	1.22	0.125	208.4	275.7	276.2	239.5	213.9	-188.9	247.6	88.8	1482.9	7429.4	7154.0
8	0	20.5	2.00	1.22	0.121	177.4	263.4	388.9	404.0	313.8	-217.4	487.2	22.5	911.6	5672.6	6245.2
8	0	41.2	4.35	1.19	0.131	128.9	242.9	356.0	344.0	241.0	-114.5	233.5	25.6	841.1	6404.3	
8	0	19.3	2.04	1.24	0.121	164.6	259.8	386.2	337.2	296.3	-253.9	572.8	-19.9	365.6	5270.9	7352.4
8	0	41.6	4.46	1.27	0.119	196.7	335.7	484.8	430.6	362.5	-105.4	418.6	-12.1	122.3	5649.2	8211.1
8	0	18.6	2.00	1.25	0.117	195.4	398.2	552.3	455.3	308.3	-206.1	408.1	-22.6	179.1	4589.8	6889.5
8	10	21.7	2.25	1.24	0.129	192.8	306.5	253.8	296.0	213.9	-157.8	334.0	-314.1	-4694.6	6076.5	3075.6
8	10	46.9	5.31	1.26	0.120	162.5	282.7	550.2	431.6	334.6	-57.9	250.2	-71.0	-4390.1	4036.4	3741.4
8	10	32.1	3.90	1.15	0.127	205.3	248.1	248.1	230.1	231.6	-91.8	290.7	-134.8	-4623.0	5675.0	2886.7
8	10	18.4	2.07	1.26	0.117	226.4	433.7	592.0	517.7	475.2	-187.5	452.7	-515.6	-4703.8	3369.6	4703.8
8	10	18.8	2.09	1.26	0.115	162.3	259.8	292.4	333.8	305.9	-164.1	541.5	-374.0	1779.1	5573.7	3848.3

APENDIX E

Table 7.8: Equations for the forces in the X direction

				Coefficients							
X Equations	**R Square**	**SSE**	**RMS**	**C**	**α_1**	**α_2**	**α_3**	**α_4**	**α_5**	**α_6**	**α_7**
$X=\alpha_1 D+C$	0.60	39225.9	1867.9	45.93	-25.58	-	-	-	-	-	-
$X=\alpha_1 A+C$	0.08	91648.3	4364.2	-122.76	3.65	-	-	-	-	-	-
$X=\alpha_1 V+C$	0.16	83627.8	2982.3	-177.93	2.52	-	-	-	-	-	-
$X=\alpha_1 D+\alpha_2 A+C$	0.66	33394.3	1669.7	28.52	-26.21	3.19	-	-	-	-	-
$X=\alpha_1 D+\alpha_2 V+C$	0.76	23656.2	1182.8	-26.61	-25.56	2.51	-	-	-	-	-
$X=\alpha_1 V+\alpha_2 A+C$	0.25	73995.4	3699.8	-202.34	2.68	4.11	-	-	-	-	-
$X=\alpha_1 D+\alpha_2 A+\alpha_3 V+C$	0.84	16081.3	846.4	-50.73	-25.14	3.65	2.65	-	-	-	-
$X=\alpha_1 D+\alpha_2 A+\alpha_3 V+\alpha_4 DV+C$	0.91	9067.2	503.7	95.83	-49.45	3.73	-2.44	0.84	-	-	-
$X=\alpha_1 D+\alpha_2 A+\alpha_3 V+\alpha_4 DA+C$	0.86	14213.6	789.6	-25.63	-29.45	-1.69	2.68	0.90	-	-	-
$X=\alpha_1 D+\alpha_2 A+\alpha_3 V+\alpha_4 AV+C$	0.84	16063.0	892.4	-53.12	-25.15	4.15	2.74	-0.02	-	-	-
$X=\alpha_1 D+\alpha_2 A+\alpha_3 V+\alpha_4 DV+\alpha_5 DA+C$	0.93	6525.7	383.9	132.63	-55.18	-2.51	-2.67	0.89	1.06	-	-
$X=\alpha_1 D+\alpha_2 A+\alpha_3 V+\alpha_4 DV+\alpha_5 AV+C$	0.91	9025.7	532.9	94.19	-49.44	4.05	-2.38	0.84	-0.11	-	-
$X=\alpha_1 D+\alpha_2 A+\alpha_3 V+\alpha_4 AV+\alpha_5 DA+C$	0.86	14198.0	839.2	-27.85	-29.45	-1.22	2.76	-0.02	0.90	-	-
$X=\alpha_1 D+\alpha_2 A+\alpha_3 V+\alpha_4 DV+\alpha_5 DA+\alpha_6 VA+C$	0.93	6525.7	401.5	131.25	-553.71	-2.24	-2.62	1.06	0.88	-0.01	-
$X=\alpha_1 D+\alpha_2 A+\alpha_3 V+\alpha_4 DV+\alpha_5 DA+\alpha_6 VA+\alpha_7 DVA+C$	0.93	6519.2	434.6	133.14	-56.02	-2.62	-2.68	0.90	1.12	0.004	-0.002

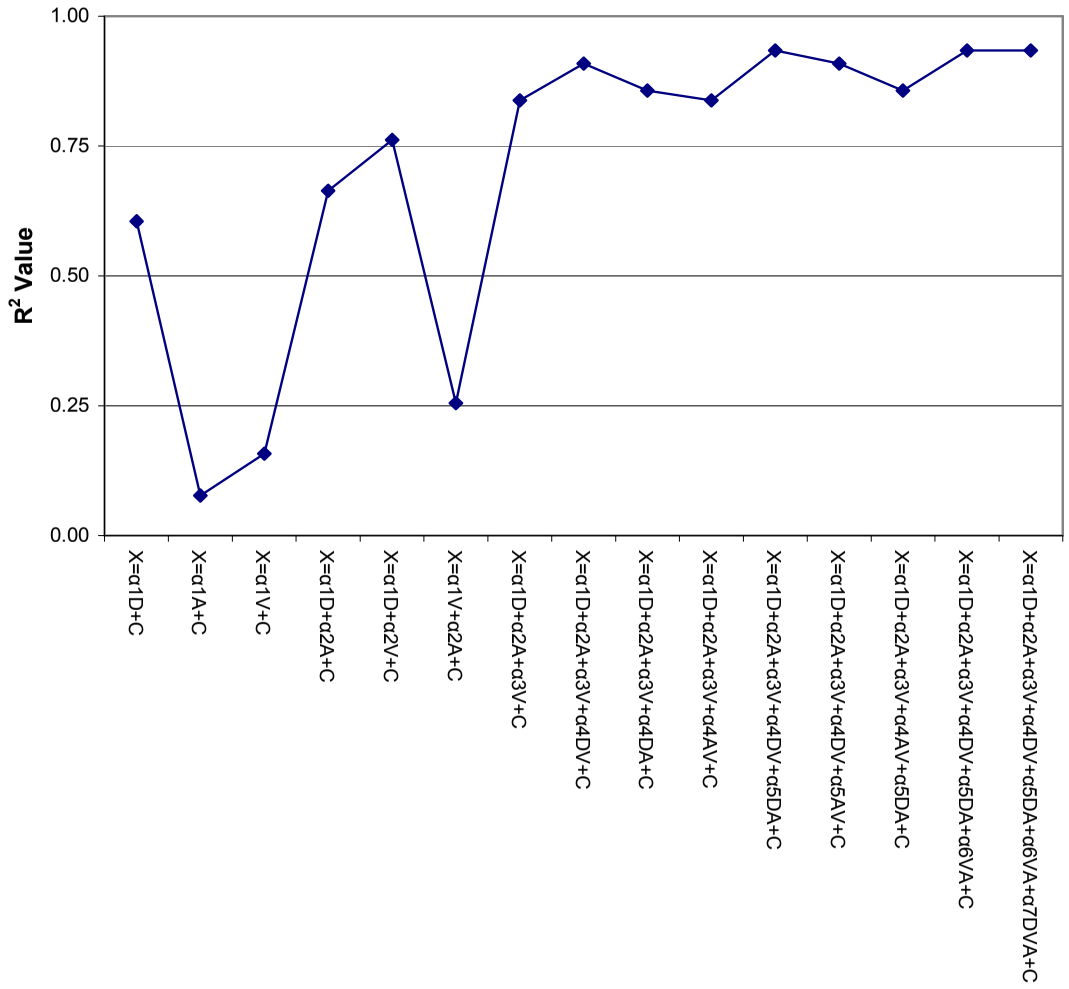

Figure 7.10: Graph of the coefficient of determination for the equation of the forces in the X direction.

Table 7.9: ANOVA tables for the equation for the forces in the X direction

ANOVA

Model		Sum of Squares	df	Mean Square	F	Sig.
1	Regression	83210.25764	3	27736.75255	32.77082206	1.03003E-07
	Residual	16081.32678	19	846.3856199		
	Total	99291.58442	22			

a Predictors: (Constant), Tine RPM, Depth , Angle

b Dependent Variable: Max x

ANOVA

Model		Sum of Squares	df	Mean Square	F	Sig.
1	Regression	92765.85401	5	18553.1708	48.33235269	1.8648E-09
	Residual	6525.730408	17	383.8664946		
	Total	99291.58442	22			

a Predictors: (Constant), DxA, Tine RPM, Depth , Angle , DxRPM

b Dependent Variable: Max x

Comparison Table

ANOVA

Model		Sum of Squares	df	Mean Square	F	Sig.
1	Regression	83210.25764	3	27736.75255	32.77082206	1.03003E-07
	Departure	9555.59637	2	4777.798185	12.44651006	Not Significant to 0.05
	Residual	6525.730408	17	383.8664946		
	Total	99291.58442	22			

Table 7.10: Equations for the forces in the Y direction.

				Coefficients							
Y Equations	**R Square**	**SSE**	**RMS**	**C**	**α_1**	**α_2**	**α_3**	**α_4**	**α_5**	**α_6**	**α_7**
$X=\alpha_1 D+C$	0.54	220656.5	10507.45	-35.48	52.58	-	-	-	-	-	-
$X=\alpha_1 A+C$	0.01	472024.9	22477.37	265.43	2.09	-	-	-	-	-	-
$X=\alpha_1 V+C$	0.25	356889.6	16994.75	474.99	-6.89	-	-	-	-	-	-
$X=\alpha_1 D+\alpha_2 A+C$	0.55	215311.0	10765.55	-52.14	52.93	3.06	-	-	-	-	-
$X=\alpha_1 D+\alpha_2 V+C$	0.78	103537.8	5176.89	163.45	-6.88	52.53	-	-	-	-	-
$X=\alpha_1 V+\alpha_2 A+C$	0.25	356416.0	17820.80	469.08	-6.86	0.91	-	-	-	-	-
$X=\alpha_1 D+\alpha_2 A+\alpha_3 V+C$	0.79	101527.8	5343.57	151.03	52.74	1.88	-6.80	-	-	-	-
$X=\alpha_1 D+\alpha_2 A+\alpha_3 V+\alpha_4 DV+C$	0.79	97711.0	5428.00	42.91	70.67	1.82	-3.05	-0.62	-	-	-
$X=\alpha_1 D+\alpha_2 A+\alpha_3 V+\alpha_4 DA+C$	0.82	85447.6	4747.09	77.40	65.37	17.54	-6.88	-2.65	-	-	-
$X=\alpha_1 D+\alpha_2 A+\alpha_3 V+\alpha_4 AV+C$	0.79	101114.3	5617.46	162.36	52.80	-0.48	-7.20	0.08	-	-	-
$X=\alpha_1 D+\alpha_2 A+\alpha_3 V+\alpha_4 DV+\alpha_5 DA+C$	0.83	85073.7	4715.76	-53.77	18.22	18.22	-2.45	-0.73	-2.78	-	-
$X=\alpha_1 D+\alpha_2 A+\alpha_3 V+\alpha_4 DV+\alpha_5 AV+C$	0.80	97340.9	5725.93	54.23	70.63	-0.42	-3.44	-0.62	0.08	-	-
$X=\alpha_1 D+\alpha_2 A+\alpha_3 V+\alpha_4 AV+\alpha_5 DA+C$	0.82	80167.9	5004.33	88.25	65.42	15.27	-7.25	0.08	-2.65	-	-
$X=\alpha_1 D+\alpha_2 A+\alpha_3 V+\alpha_4 DV+\alpha_5 DA+\alpha_6 VA+\alpha_7 DVA+C$	0.83	79821.6	5321.44	-34.80	85.72	14.45	-3.10	-0.68	-2.50	0.13	0.01

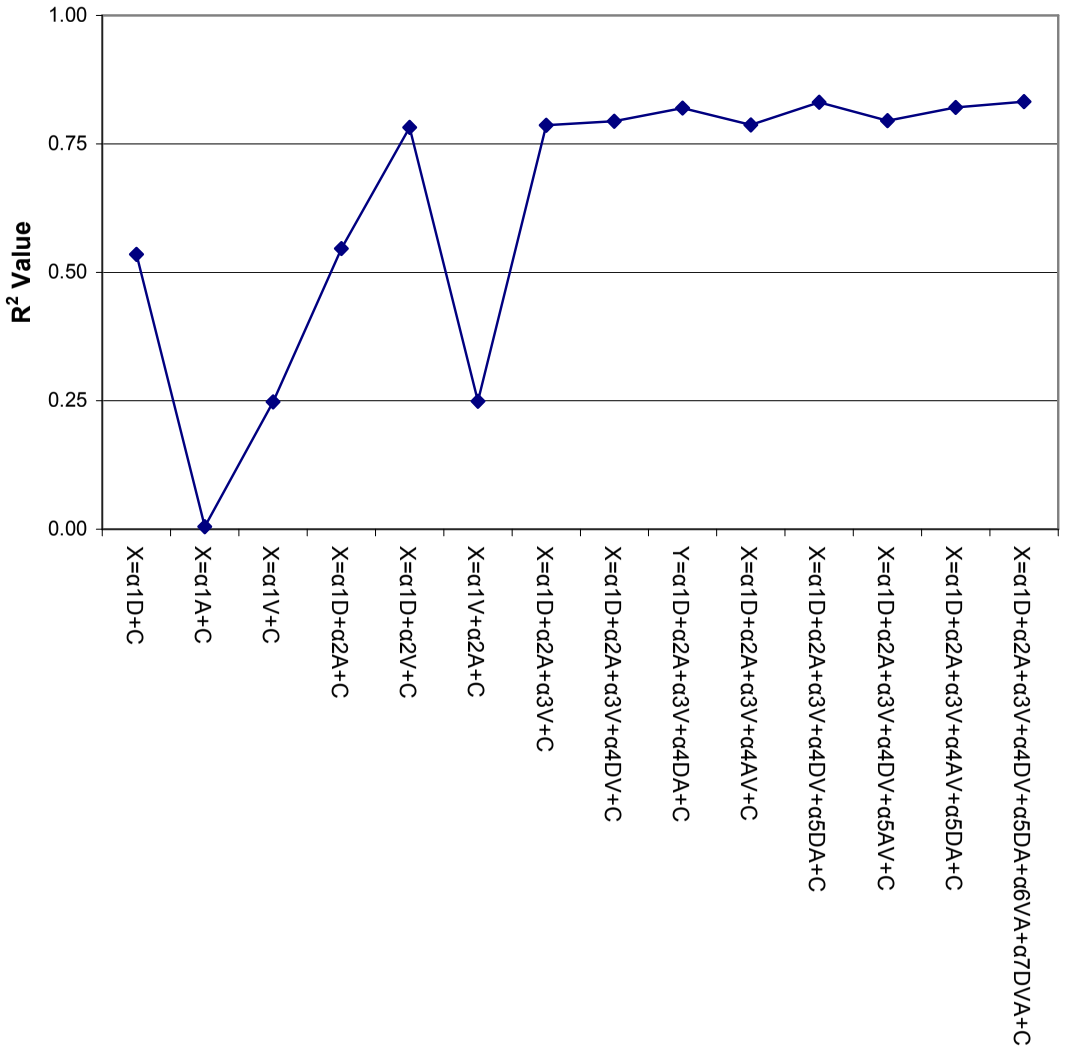

Figure 7.11: Graph of the coefficient of determination for the equations of the forces in the X direction.

Table 7.11: ANOVA tables for the equations in the Y direction.

ANOVA

Model		Sum of Squares	df	Mean Square	F	Sig.
1	Regression	371000.57	2	185500.28	35.83	2.44E-07
	Residual	103537.78	20	5176.89		
	Total	474538.35	22			

a Predictors: (Constant), Depth , Tine RPM

b Dependent Variable: Max Y

ANOVA

Model		Sum of Squares	df	Mean Square	F	Sig.
2	Regression	373010.55	3	124336.85	23.27	1.41E-06
	Residual	101527.80	19	5343.57		
	Total	474538.35	22			

a Predictors: (Constant), Tine RPM, Depth , Angle

b Dependent Variable: Max Y

ANOVA

Model		Sum of Squares	df	Mean Square	F	Sig.
3	Regression	389090.73	4	97272.68	20.49	1.67E-06
	Residual	85447.62	18	4747.09		
	Total	474538.35	22			

a Predictors: (Constant), DxA, Tine RPM, Depth , Angle

b Dependent Variable: Max Y

Model 1 vs 2

	Sum of Squares	df	Mean Square	F	
Regression	371000.57	2	185500.28	35.83	
Departure	2009.98	1	2009.979732	0.376149	not significant to 0.95
Residual	101527.80	19	5343.57		
Total	474538.35	22			

Model 1 vs 3

	Sum of Squares	df	Mean Square	F	
Regression	371000.57	2	185500.28	35.83	
Departure	18090.16	2	9045.080703	1.905395	not significant to 0.95
Residual	85447.62	18	4747.09		
Total	474538.35	22			

Table 7.12: Equations for the forces in the Z direction.

Z Equations	R Square	SSE	RMS	Coefficients							
				C	α_1	α_2	α_3	α_4	α_5	α_6	α_7
$X=\alpha_1 D+C$	0.08	387351.7	18445.32	35.07	-19.53	-	-	-	-	-	-
$X=\alpha_1 A+C$	0.35	273854.7	13040.70	-2.95	-16.09	-	-	-	-	-	-
$X=\alpha_1 V+C$	0.13	367233.7	17487.32	-216.18	4.72	-	-	-	-	-	-
$X=\alpha_1 D+\alpha_2 A+C$	0.45	231868.5	11593.43	125.48	-21.41	-16.48	-	-	-	-	-
$X=\alpha_1 D+\alpha_2 V+C$	0.21	332333.9	16616.69	-100.74	4.72	-19.50	-	-	-	-	-
$X=\alpha_1 V+\alpha_2 A+C$	0.45	232407.7	11620.38	-124.89	4.11	-15.38	-	-	-	-	-
$X=\alpha_1 D+\alpha_2 A+\alpha_3 V+C$	0.58	190863.8	10045.46	3.52	-21.29	-15.72	4.084	-	-	-	-
$X=\alpha_1 D+\alpha_2 A+\alpha_3 V+\alpha_4 DV+C$	0.63	154455.7	8580.87	337.43	-76.67	-15.59	-7.51	1.92	-	-	-
$X=\alpha_1 D+\alpha_2 A+\alpha_3 V+\alpha_4 DA+C$	0.75	105039.8	5835.55	-166.61	7.89	20.40	3.92	-6.13	-	-	-
$X=\alpha_1 D+\alpha_2 A+\alpha_3 V+\alpha_4 AV+C$	0.61	163924.1	9106.89	94.99	-20.81	-34.85	0.91	0.66	-	-	-
$X=\alpha_1 D+\alpha_2 A+\alpha_3 V+\alpha_4 DV+\alpha_5 DA+C$	0.82	77201.8	4541.28	134.55	-42.10	18.82	-6.25	1.68	-5.84	-	-
$X=\alpha_1 D+\alpha_2 A+\alpha_3 V+\alpha_4 DV+\alpha_5 AV+C$	0.70	126382.0	7434.23	436.03	-77.04	-35.08	-10.94	1.95	0.68	-	-
$X=\alpha_1 D+\alpha_2 A+\alpha_3 V+\alpha_4 AV+\alpha_5 DA+C$	0.81	78848.9	4638.17	-75.67	8.25	1.42	0.78	0.65	-6.10	-	-
$X=\alpha_1 D+\alpha_2 A+\alpha_3 V+\alpha_4 DV+\alpha_5 DA+\alpha_6 VA+C$	0.88	49992.6	3124.54	232.76	-42.65	-0.55	-9.63	1.71	-5.80	0.67	-
$X=\alpha_1 D+\alpha_2 A+\alpha_3 V+\alpha_4 DV+\alpha_5 DA+\alpha_6 VA+\alpha_7 DVA+C$	0.92	34075.2	2271.68	12.78	-6.35	43.78	-2.21	0.49	-13.14	-0.872	0.255

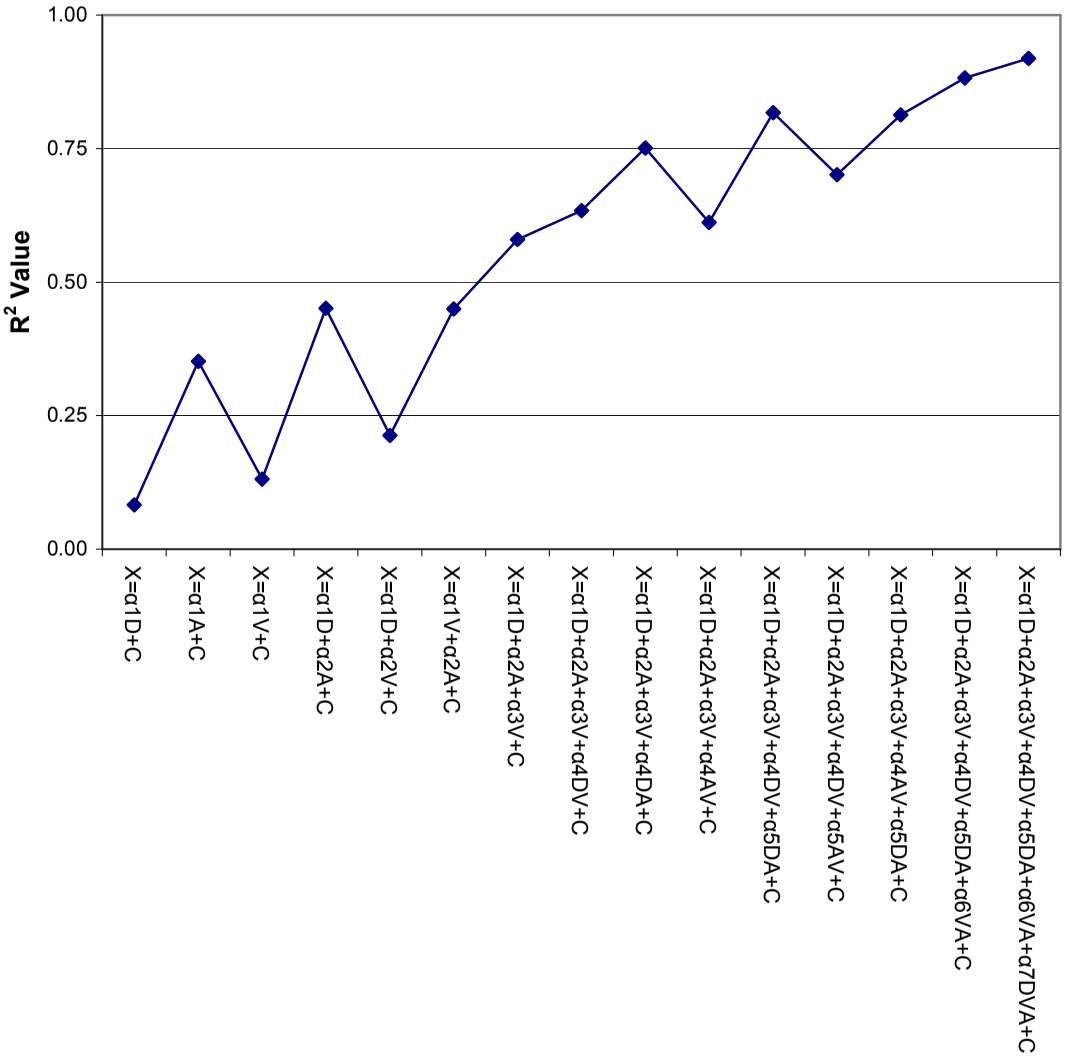

Figure 7.12: Graph of the coefficient of determination for the equations of the forces in the Z direction.

Table 7.13: ANOVA tables for the equations of the forces in the Z direction.

1 ANOVA

Model		Sum of Squares	df	Mean Square	F	Sig.
1	Regression	317346.5261	4	79336.63152	13.59541045	2.82334E-05
	Residual	105039.8127	18	5835.545152		
	Total	422386.3388	22			

a Predictors: (Constant), DxA, Tine RPM, Depth , Angle

b Dependent Variable: Max Z

2 ANOVA(b)

Model		Sum of Squares	df	Mean Square	F	Sig.
1	Regression	345184.588	5	69036.91759	15.20208527	9.32291E-06
	Residual	77201.75085	17	4541.279462		
	Total	422386.3388	22			

a Predictors: (Constant), DxA, Tine RPM, Depth , Angle , DxRPM

b Dependent Variable: Max Z

3 ANOVA

Model		Sum of Squares	df	Mean Square	F	Sig.
1	Regression	372393.6973	6	62065.61621	19.86392055	1.38772E-06
	Residual	49992.64153	16	3124.540096		
	Total	422386.3388	22			

a Predictors: (Constant), AxRPM, Depth , Tine RPM, DxA, Angle , DxRPM

b Dependent Variable: Max Z

4 ANOVA

Model		Sum of Squares	df	Mean Square	F	Sig.
1	Regression	388311.1842	7	55473.02632	24.41941659	4.08645E-07
	Residual	34075.15458	15	2271.676972		
	Total	422386.3388	22			

a Predictors: (Constant), AxRPMxD, Depth , Tine RPM, Angle , DxA, DxRPM, AxRPM

b Dependent Variable: Max Z

Comparision Tables

Model 1 vs 2

ANOVA

Model		Sum of Squares	df	Mean Square	F	Sig.
1	Regression	317346.5261	4	79336.63152	13.59541045	2.82334E-05
	Departure	27838.06189	1	27838.06189	6.130004137	Not Significant to 0.05
	Residual	77201.75085	17	4541.279462		
	Total	422386.3388	22			

Model 1 vs 3

Model		Sum of Squares	df	Mean Square	F	Sig.
1	Regression	317346.5261	4	79336.63152	13.59541045	2.82334E-05
	Departure	55047.17121	2	27523.5856	8.808843786	Not Significant to 0.05
	Residual	49992.64153	16	3124.540096		
	Total	422386.3388	22			

Model 1 vs 4

Model		Sum of Squares	df	Mean Square	F	Sig.
1	Regression	317346.5261	4	79336.63152	13.59541045	2.82334E-05
	Departure	70964.65816	3	23654.88605	10.41296203	Significant to 0.05
	Residual	34075.15458	15	2271.676972		
	Total	422386.3388	22			

Table 7.14: Equations for the draft forces.

Draft Load Equations	R Square	SSE	RMS	Coefficients							
				C	α_1	α_2	α_3	α_4	α_5	α_6	α_7
$X=\alpha_1 D+C$	0.88	13530058.0	644288.47	-2769.05	1025.08	-	-	-	-	-	-
$X=\alpha_1 A+C$	0.01	100000000.0	5175267.64	3523.27	-48.30	-	-	-	-	-	-
$X=\alpha_1 V+C$	0.01	100000000.0	5210151.90	2840.25	146.29	-	-	-	-	-	-
$X=\alpha_1 D+\alpha_2 A+C$	0.88	13024072.0	651203.62	-2606.93	1021.70	-29.72	-	-	-	-	-
$X=\alpha_1 D+\alpha_2 V+C$	0.88	13003082.0	650154.05	-3188.08	1024.67	136.39	-	-	-	-	-
$X=\alpha_1 V+\alpha_2 A+C$	0.02	100000000.0	5401553.86	3059.04	151.46	-49.09	-	-	-	-	-
$X=\alpha_1 D+\alpha_2 A+\alpha_3 V+C$	0.89	12472055.0	656423.93	-3031.90	1021.20	-30.46	139.631	-	-	-	-
$X=\alpha_1 D+\alpha_2 A+\alpha_3 V+\alpha_4 DV+C$	0.89	12465767.0	692375.97	-3205.72	1049.30	-30.48	195.96	-9.10	-	-	-
$X=\alpha_1 D+\alpha_2 A+\alpha_3 V+\alpha_4 DA+C$	0.90	10646146.0	591452.55	-3838.58	1155.79	136.43	139.35	-28.26	-	-	-
$X=\alpha_1 D+\alpha_2 A+\alpha_3 V+\alpha_4 AV+C$	0.89	11698911.0	649939.48	-3558.09	1021.05	71.74	311.61	-33.08	-	-	-
$X=\alpha_1 D+\alpha_2 A+\alpha_3 V+\alpha_4 DV+\alpha_5 DA+C$	0.90	10642023.0	626001.32	3953.52	1174.37	136.23	176.89	-6.06	-28.23	-	-
$X=\alpha_1 D+\alpha_2 A+\alpha_3 V+\alpha_4 DV+\alpha_5 AV+C$	0.89	11694836.0	687931.55	-3671.89	1039.67	71.45	348.48	-6.03	-32.99	-	-
$X=\alpha_1 D+\alpha_2 A+\alpha_3 V+\alpha_4 AV+\alpha_5 DA+C$	0.91	9888171.0	581657.13	-4356.25	1155.08	236.94	309.64	-32.75	-28.15	-	-
$X=\alpha_1 D+\alpha_2 A+\alpha_3 V+\alpha_4 DV+\alpha_5 DA+\alpha_6 VA+C$	0.91	9857141.0	617946.33	-4413.04	1164.37	236.70	328.18	-3.03	-28.13	-32.71	-
$X=\alpha_1 D+\alpha_2 A+\alpha_3 V+\alpha_4 DV+\alpha_5 DA+\alpha_6 VA+\alpha_7 DVA+C$	0.92	9062527.0	604168.45	-2752.71	892.68	-91.30	-214.09	85.63	24.91	73.52	17.17

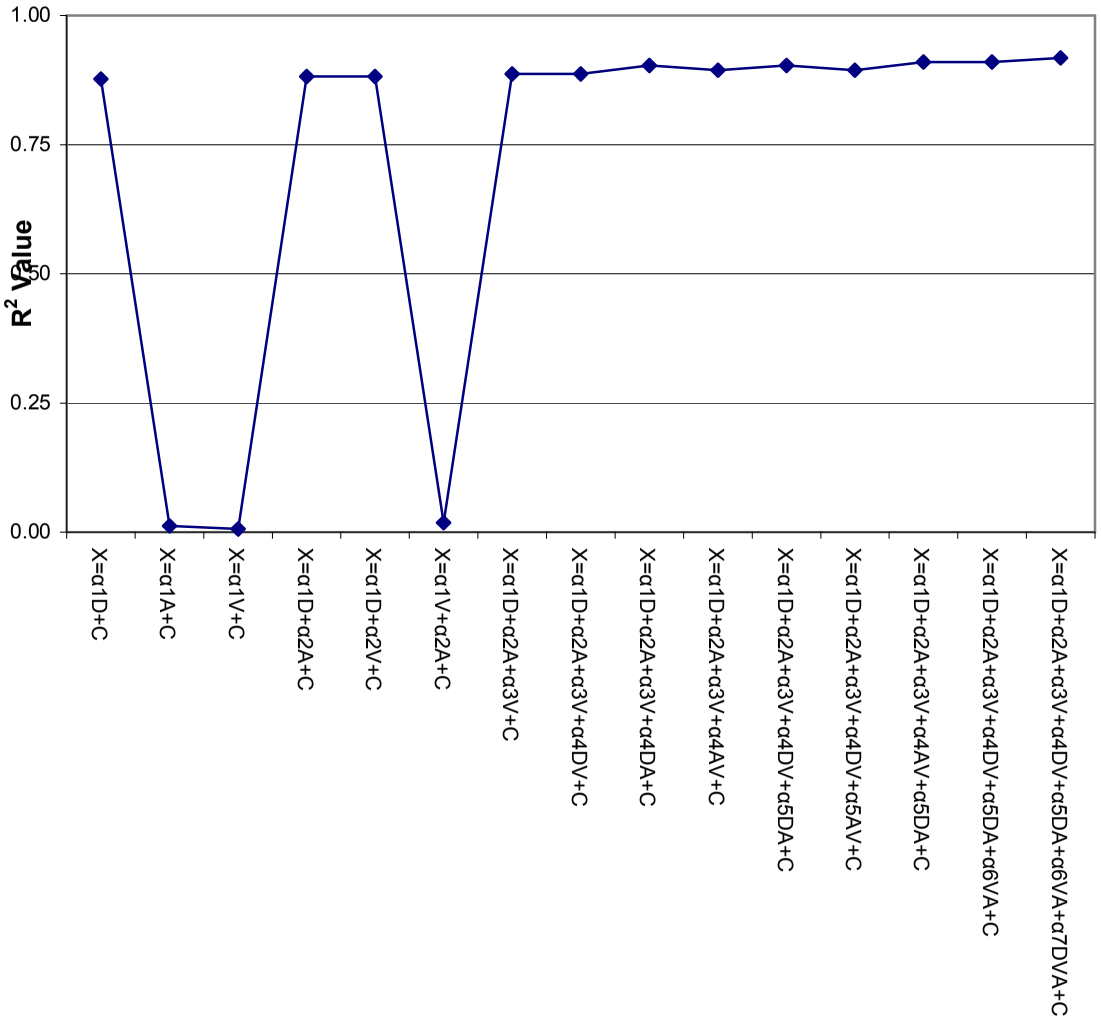

Figure 7.13: Graph of the coefficient of determination for the equations of the draft forces.

Table 7.15: ANOVA tables for the equations for the draft forces.

ANOVA

1 Model		Sum of Squares	df	Mean Square	F	Sig.
1	Regression	96489412.68	1	96489412.68	149.761197	5.06712E-11
	Residual	13530057.9	21	644288.4715		
	Total	110019470.6	22			

a Predictors: (Constant), Depth

b Dependent Variable: Draft

ANOVA

2 Model		Sum of Squares	df	Mean Square	F	Sig.
1	Regression	99373324.75	4	24843331.19	42.00392976	6.791E-09
	Residual	10646145.82	18	591452.5457		
	Total	110019470.6	22			

a Predictors: (Constant), DxA, SPEED, Depth , Angle

b Dependent Variable: Draft

ANOVA

3 Model		Sum of Squares	df	Mean Square	F	Sig.
1	Regression	100131299.3	5	20026259.86	34.42966422	2.57579E-08
	Residual	9888171.297	17	581657.1351		
	Total	110019470.6	22			

a Predictors: (Constant), DxA, SPEED, Depth , AxS, Angle

b Dependent Variable: Draft

ANOVA

4 Model		Sum of Squares	df	Mean Square	F	Sig.
1	Regression	100956943.8	7	14422420.55	23.87152217	4.75865E-07
	Residual	9062526.749	15	604168.45		
	Total	110019470.6	22			

a Predictors: (Constant), AxSxD, Depth , SPEED, Angle , DxA, DxS, AxS

b Dependent Variable: Draft

Model Comparison

Model 1 vs 2

Model		Sum of Squares	df	Mean Square	F	Sig.
1	Regression	96489412.68	1	96489412.68	149.761197	5.06712E-11
	Departure	2883912.078	3	961304.026	1.625327396	Not Significant to 0.05
	Residual	10646145.82	18	591452.5457		
	Total	110019470.6	22			

Model 1 vs 3

Model		Sum of Squares	df	Mean Square	F	Sig.
1	Regression	96489412.68	1	96489412.68	149.761197	5.06712E-11
	Departure	3641886.604	4	910471.651	1.565306425	Not Significant to 0.05
	Residual	9888171.297	17	581657.1351		
	Total	110019470.6	22			

Model 1 vs 4

Model		Sum of Squares	df	Mean Square	F	Sig.
1	Regression	96489412.68	1	96489412.68	149.761197	5.06712E-11
	Departure	4467531.152	6	744588.5253	1.232418749	Not Significant to 0.05
	Residual	9062526.749	15	604168.45		
	Total	110019470.6	22			

Table 7.16: Equations for the vertical forces on the frame.

				Coefficients							
Vertical Load Equation	**R Square**	**SSE**	**RMS**	**C**	**α_1**	**α_2**	**α_3**	**α_4**	**α_5**	**α_6**	**α_7**
$X=\alpha_1 D+C$	0.53	38591705.0	1929585.26	-280.49	711.41	-	-	-	-	-	-
$X=\alpha_1 A+C$	0.23	61656316.0	3082815.80	4838.07	-195.88	-	-	-	-	-	-
$X=\alpha_1 V+C$	0.00	82756660.0	4137833.01	3897.18	-12.71	-	-	-	-	-	-
$X=\alpha_1 D+\alpha_2 A+C$	0.79	17487051.0	920371.13	698.95	711.41	-195.89	-	-	-	-	-
$X=\alpha_1 D+\alpha_2 V+C$	0.54	38515667.0	2027140.34	-451.45	712.93	53.47	-	-	-	-	-
$X=\alpha_1 V+\alpha_2 A+C$	0.26	61573722.0	3240722.20	4673.52	55.81	-196.83	-	-	-	-	-
$X=\alpha_1 D+\alpha_2 A+\alpha_3 V+C$	0.79	17089812.0	949434.03	317.38	714.89	-197.96	122.57	-	-	-	-
$X=\alpha_1 D+\alpha_2 A+\alpha_3 V+\alpha_4 DV+C$	0.79	16734180.0	984363.50	-759.83	890.35	-196.76	474.02	-57.92	-	-	-
$X=\alpha_1 D+\alpha_2 A+\alpha_3 V+\alpha_4 DA+C$	0.93	5652352.0	332491.27	-1908.92	1078.52	223.35	160.03	-75.52	-	-	-
$X=\alpha_1 D+\alpha_2 A+\alpha_3 V+\alpha_4 AV+C$	0.80	16353487.0	961969.83	-268.07	720.69	-96.38	309.70	-33.60	-	-	-
$X=\alpha_1 D+\alpha_2 A+\alpha_3 V+\alpha_4 DV+\alpha_5 DA+C$	0.93	5545407.0	346587.94	-2484.26	1172.26	220.74	353.08	-31.86	-71.96	-	-
$X=\alpha_1 D+\alpha_2 A+\alpha_3 V+\alpha_4 DV+\alpha_5 AV+C$	0.81	16098384.0	1006149.01	-1147.86	869.82	-101.97	596.99	-49.35	-31.42	-	-
$X=\alpha_1 D+\alpha_2 A+\alpha_3 V+\alpha_4 AV+\alpha_5 DA+C$	0.95	4533553.0	283347.08	-2672.60	1092.38	356.49	391.77	-41.49	-73.85	-	-
$X=\alpha_1 D+\alpha_2 A+\alpha_3 V+\alpha_4 DV+\alpha_5 DA+\alpha_6 VA+C$	0.95	4490881.0	299392.06	-3021.18	1151.65	351.82	509.29	-20.26	-73.46	-40.55	-
$X=\alpha_1 D+\alpha_2 A+\alpha_3 V+\alpha_4 DV+\alpha_5 DA+\alpha_6 VA+\alpha_7 DVA+C$	0.95	4164435.0	297459.67	-1940.75	967.93	146.21	145.04	42.54	-39.50	27.20	-11.28

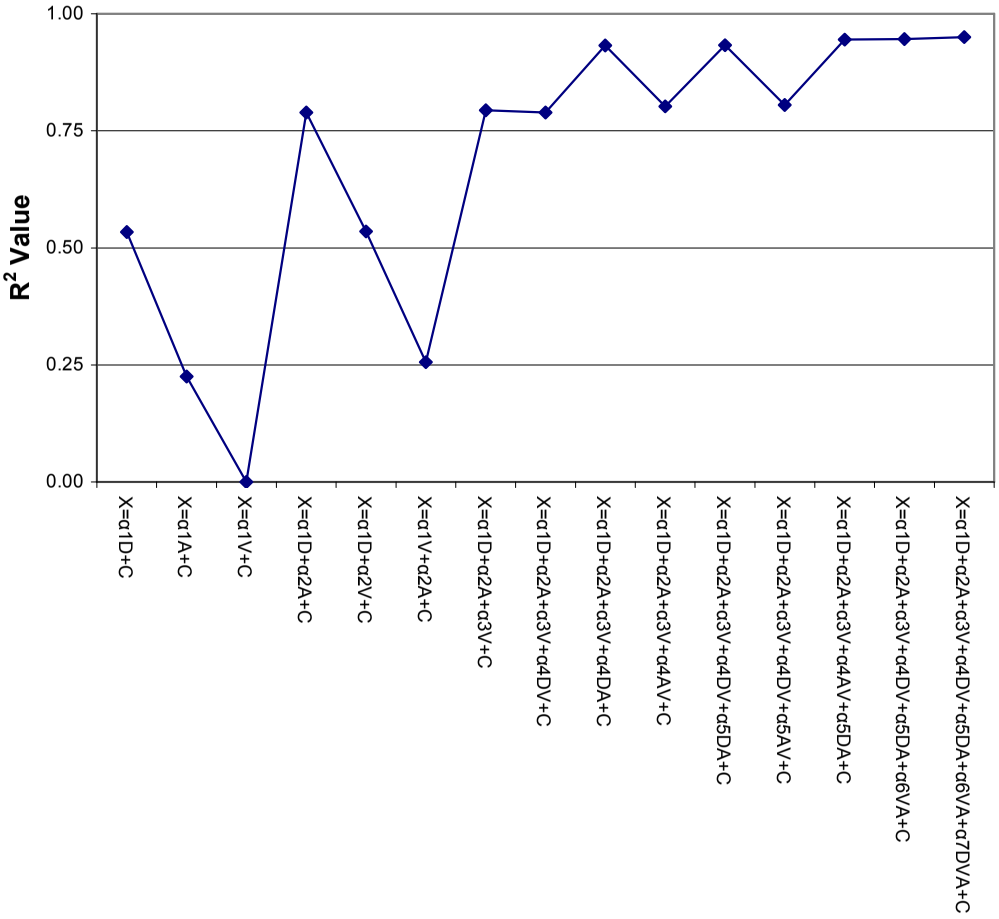

Figure 7.14: Graph of the coefficient of determination for the equations of the vertical forces on the frame.

Table 7.17: ANOVA tables of the equations for the vertical forces.

ANOVA

1 Model		Sum of Squares	df	Mean Square	F	Sig.
1	Regression	65273918.38	2	32636959.19	35.46065	3.86E-07
	Residual	17487051.38	19	920371.1252		
	Total	82760969.75	21			

a Predictors: (Constant), Angle , Depth

b Dependent Variable: Vertical

ANOVA

2 Model		Sum of Squares	df	Mean Square	F	Sig.
1	Regression	77108618.16	4	19277154.54	57.97793	1.1E-09
	Residual	5652351.592	17	332491.2701		
	Total	82760969.75	21			

a Predictors: (Constant), DxA, SPEED, Depth , Angle

b Dependent Variable: Vertical

ANOVA

3 Model		Sum of Squares	df	Mean Square	F	Sig.
1	Regression	78227416.44	5	15645483.29	55.21667	1.59E-09
	Residual	4533553.313	16	283347.0821		
	Total	82760969.75	21			

a Predictors: (Constant), DxA, SPEED, Depth , AxS, Angle

b Dependent Variable: Vertical

Model Comparison

Model 1 vs 2

Model		Sum of Squares	df	Mean Square	F	Sig.
1	Regression	65273918.38	2	32636959.19	35.46065	3.86E-07
	Departure	11834699.79	2	5917349.894	17.79701	Not Significant to 0.05
	Residual	5652351.592	17	332491.2701		
	Total	82760969.75	21			

Model 1 vs 3

Model		Sum of Squares	df	Mean Square	F	Sig.
1	Regression	65273918.38	2	32636959.19	35.46065	3.86E-07
	Departure	12953498.07	3	4317832.689	12.9863	Significant to 0.05
	Residual	5652351.592	17	332491.2701		
	Total	82760969.75	21			

Table 7.18: Equations for the forces on the bearing mounts.

				Coefficients							
Side Load Equation	**R Square**	**SSE**	**RMS**	**C**	**α_1**	**α_2**	**α_3**	**α_4**	**α_5**	**α_6**	**α_7**
$X=\alpha_1 D+C$	0.01	100000000.00	4935629.58	-1873.60	89.55	-	-	-	-	-	-
$X=\alpha_1 A+C$	0.63	38697703.00	1842747.79	273.89	-338.31	-	-	-	-	-	-
$X=\alpha_1 V+C$	0.02	100000000.00	4853961.36	-446.97	-296.35	-	-	-	-	-	-
$X=\alpha_1 D+\alpha_2 A+C$	0.63	38457426.00	1922871.30	-33.35	51.21	-337.38	-	-	-	-	-
$X=\alpha_1 D+\alpha_2 V+C$	0.03	100000000.00	5062278.94	-978.89	90.41	-291.23	-	-	-	-	-
$X=\alpha_1 V+\alpha_2 A+C$	0.65	36858696.00	1842934.78	1055.01	-254.85	-336.99	-	-	-	-	-
$X=\alpha_1 D+\alpha_2 A+\alpha_3 V+C$	0.65	36609772.00	1926830.09	744.14	52.12	-336.04	-255.457	-	-	-	-
$X=\alpha_1 D+\alpha_2 A+\alpha_3 V+\alpha_4 DV+C$	0.65	36238193.00	2013232.94	-355.34	229.86	-336.15	100.84	-57.53	-	-	-
$X=\alpha_1 D+\alpha_2 A+\alpha_3 V+\alpha_4 DA+C$	0.67	34711652.00	1928425.12	-78.33	189.35	-165.88	-255.74	-28.82	-	-	-
$X=\alpha_1 D+\alpha_2 A+\alpha_3 V+\alpha_4 AV+C$	0.68	33740685.00	1874482.51	-269.51	51.83	-139.16	75.84	-63.72	-	-	-
$X=\alpha_1 D+\alpha_2 A+\alpha_3 V+\alpha_4 DV+\alpha_5 DA+C$	0.67	34378804.00	2022282.60	-1111.03	356.24	-167.68	81.57	-54.47	-28.53	-	-
$X=\alpha_1 D+\alpha_2 A+\alpha_3 V+\alpha_4 DV+\alpha_5 AV+C$	0.68	31872374.00	1967134.12	-1244.98	211.48	-141.62	391.92	-51.68	-62.95	-	-
$X=\alpha_1 D+\alpha_2 A+\alpha_3 V+\alpha_4 AV+\alpha_5 DA+C$	0.70	33441280.00	1874845.53	-1080.26	187.97	28.64	73.84	-63.39	-28.59	-	-
$X=\alpha_1 D+\alpha_2 A+\alpha_3 V+\alpha_4 DV+\alpha_5 DA+\alpha_6 VA+C$	0.70	31607069.00	1975441.80	-1991.55	337.09	24.83	371.47	-48.66	-28.34	-62.67	-
$X=\alpha_1 D+\alpha_2 A+\alpha_3 V+\alpha_4 DV+\alpha_5 DA+\alpha_6 VA+\alpha_7 DVA+C$	0.67	31408518.00	2093901.22	-1176.84	203.77	-136.12	105.38	-5.16	-2.31	-10.546	-8.424

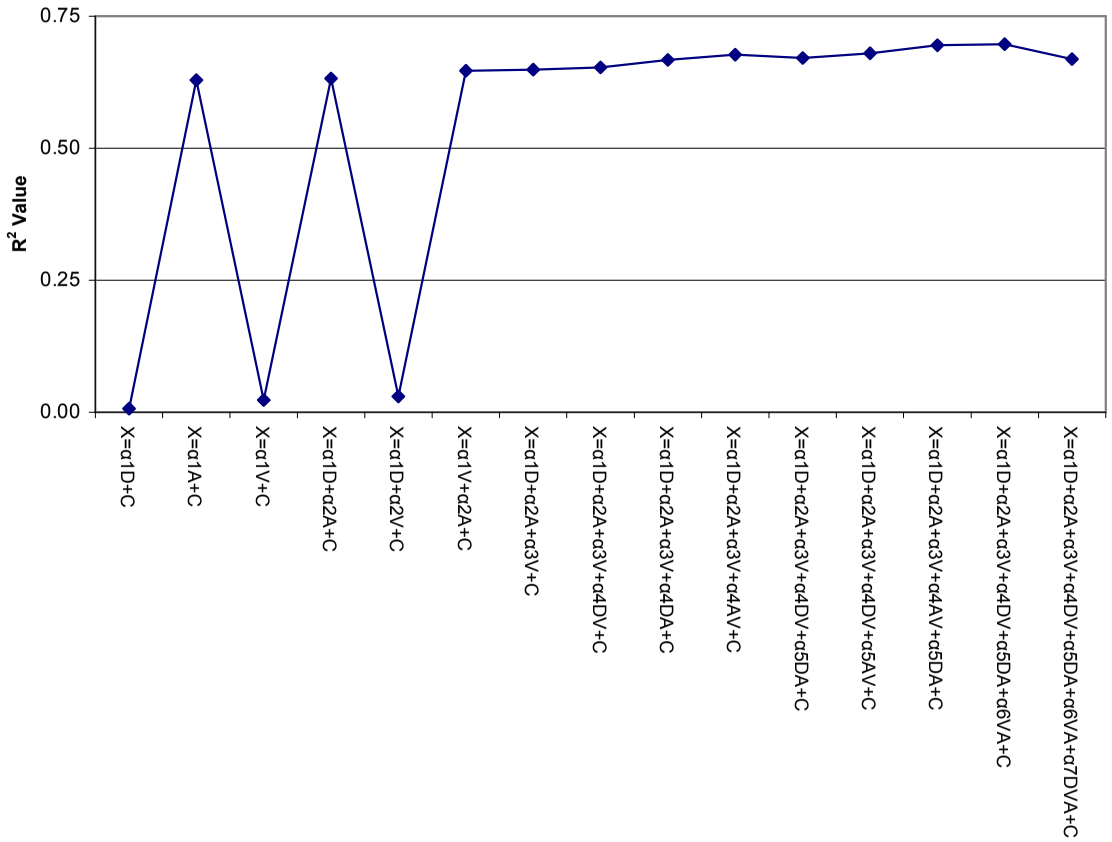

Figure 7.15: Graph of the coefficient of determination for the equations of the forces on the bearing mounts.

Table 7.19: ANOVA tables of the equations for the forces on the bearing mounts.

ANOVA

1 Model		Sum of Squares	df	Mean Square	F	Sig.
1	Regression	65686804.01	1	65686804.01	35.6461183	6.32E-06
	Residual	38697702.57	21	1842747.741		
	Total	104384506.6	22			

a Predictors: (Constant), Angle

b Dependent Variable: S

ANOVA

2 Model		Sum of Squares	df	Mean Square	F	Sig.
1	Regression	70643821.38	4	17660955.35	9.42177654	0.000273125
	Residual	33740685.2	18	1874482.511		
	Total	104384506.6	22			

a Predictors: (Constant), AxS, Depth , SPEED, Angle

b Dependent Variable: S

ANOVA

3 Model		Sum of Squares	df	Mean Square	F	Sig.
1.00	Regression	72512132.63	5	14502426.53	7.73526476	0.000592259
	Residual	31872373.95	17	1874845.526		
	Total	104384506.58	22			

a Predictors: (Constant), DxA, SPEED, Depth , AxS, Angle

b Dependent Variable: S

Model Comparison

Model 1 vs 2

Model		Sum of Squares	df	Mean Square	F	Sig.
1	Regression	65686804.01	1	65686804.01	35.6461183	6.32E-06
	Departure	4957017.371	3	1652339.124	0.88149082	Not significant to 0.05
	Residual	33740685.2	18	1874482.511		
	Total	104384506.6	22			

Model 1 vs 2

Model		Sum of Squares	df	Mean Square	F	Sig.
1	Regression	65686804.01	1	65686804.01	35.6461183	6.32E-06
	Departure	6825328.62	4	1706332.155	0.9101188	Not significant to 0.05
	Residual	31872373.95	17	1874845.526		
	Total	104384506.58	22			